AD-A064 977 MALLORY (P R) AND CO INC BURLINGTON MASS LAB FOR PH--ETC F/G 10/3
ANALYSIS OF PRESSURE PRODUCING REACTIONS IN LITHIUM-SULFUR DIOX--ETC(U)
FEB 79 A N DEY, R W HOLMES DAAB07-77-C-0472
UNCLASSIFIED DELET-TR-77-0472-1 NL

1 OF 2
AD A064977

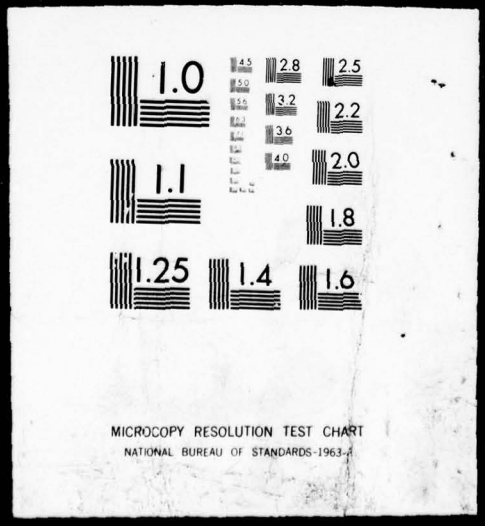

(12) LEVEL II

Research and Development Technical Report

DELET-TR-77-0472-1

ANALYSIS OF PRESSURE PRODUCING REACTIONS IN LITHIUM-SULFUR DIOXIDE CELLS

A.N. DEY and R.W. HOLMES

P.R. MALLORY & CO., INC.
LABORATORY FOR PHYSICAL SCIENCE
BURLINGTON, MA 01803

FEBRUARY 1979

INTERIM REPORT FOR PERIOD 15 SEPT. 1977 TO 30 SEPT. 1978

DISTRIBUTION STATEMENT
APPROVED FOR PUBLIC RELEASE ; DISTRIBUTION UNLIMITED

PREPARED FOR :
US ARMY ELECTRONICS TECHNOLOGY AND DEVICES LABORATORY

ERADCOM

US ARMY ELECTRONICS RESEARCH AND DEVELOPMENT COMMAND
FORT MONMOUTH, NEW JERSEY 07703

NOTICES

Disclaimers

The citation of trade names and names of manufacturers in this report is not to be construed as official Government indorsement or approval of commercial products or services referenced herein.

Disposition

Destroy this report when it is no longer needed. Do not return it to the originator.

Unclassified

SECURITY CLASSIFICATION OF THIS PAGE (When Data Entered)

REPORT DOCUMENTATION PAGE	READ INSTRUCTIONS BEFORE COMPLETING FORM
1. REPORT NUMBER: DELET-TR-77-0472-1	2. GOVT ACCESSION NO. / 3. RECIPIENT'S CATALOG NUMBER
4. TITLE (and Subtitle): Analysis of Pressure Producing Reactions in Lithium-Sulfur Dioxide Cells.	5. TYPE OF REPORT & PERIOD COVERED: 1st Interim Report 9/15/77 to 9/30/78
	6. PERFORMING ORG. REPORT NUMBER
7. AUTHOR(s): A. N. Dey and R. W. Holmes	8. CONTRACT OR GRANT NUMBER(s): DAAB07-77-C-0472
9. PERFORMING ORGANIZATION NAME AND ADDRESS: 11	10. PROGRAM ELEMENT, PROJECT, TASK AREA & WORK UNIT NUMBERS: 1L162705AH94 11-981
11. CONTROLLING OFFICE NAME AND ADDRESS: U. S. Army Elct Tech & Dvcs Laboratory ATTN: DELET-PR, Fort Monmouth, NJ 07703	12. REPORT DATE: February 1979
	13. NUMBER OF PAGES: 83
14. MONITORING AGENCY NAME & ADDRESS (if different from Controlling Office): 97p.	15. SECURITY CLASS. (of this report): Unclassified
	15a. DECLASSIFICATION/DOWNGRADING SCHEDULE

16. DISTRIBUTION STATEMENT (of this Report)

Approved for Public Release; Distribution Unlimited

Interim rept. no. 1, 15 Sep 77-30 Sep 78,

17. DISTRIBUTION STATEMENT (of the abstract entered in Block 20, if different from Report)

18. SUPPLEMENTARY NOTES

19. KEY WORDS (Continue on reverse side if necessary and identify by block number)

Sulfur Dioxide Battery, Lithium, Organic Electrolyte, Safety, Differential Thermal Analysis (DTA), Energy of Activation, Acetonitrile, Sulfur Dioxide.

20. ABSTRACT (Continue on reverse side if necessary and identify by block number)

Although the State-of-the-Art hermetically sealed high-rate D cells made by P. R. Mallory & Co. Inc. are sufficiently abuse resistant for many applications, this program was initiated to explore the feasibility of improving the intrinsic abuse resistance of the system even further by chemical and/or mechanical means, so that the product may be rendered Safe under all user conditions. The approach that was pursued involved:

over

DD FORM 1 JAN 73 1473 EDITION OF 1 NOV 65 IS OBSOLETE

Unclassified

SECURITY CLASSIFICATION OF THIS PAGE (When Data Entered)

(a) the identification of the chemical reactions responsible for the pressure buildup and/or thermal runaway,

(b) the determination of the sensitivity of these reactions to the various use and abuse variables, and

(c) the development of methods to desensitize these reactions.

We have carried out differential thermal analysis (DTA) of the cell constituents that may be present during the various stages of storage and discharge singly, as well as in binary and multiple combinations in order to accomplish (a) and (b) above. We carried out DTA of miniature Li/SO_2 cells in order to establish the applicability of the results to actual cells. In addition, we carried out kinetic studies of the Li + organic solvent (the most reactive couple) reactions in an effort to find organic solvent additives to quench this reaction.

The DTA results showed the Li + SO_2 couple to be the most stable showing no exothermic transition up to as high a temperature as 370 °C, the upper limit of the DTA run. The Li + AN couple was found to be the least stable and as such, the most important reaction pertaining to safety. Both SO_2 & PC were found to be excellent film-forming agents to protect Li from spontaneous reactions with AN. On the other hand, organic solvents such as MF, DME, DG and THFalthough stable with Li by themselves, were found to enhance the Li + AN reactions most likely due to the enhanced solubilizing property of the mixed solvent towards the lithium film. The DTA results of the miniature Li/SO_2 cells corroborated the DTA results on the separate reactive cell constituents. The results obtained to date provide a sound basis for conducting a thorough cell evaluation program in order to establish the efficacy of several approaches, suggested from this study, in improving the safety of the Li/SO_2 cells and for the determination of the necessary tradeoffs.

CONTENTS

		Page
	List of Figures	ii
	List of Tables	vi
I.	Introduction	1
II.	DTA of Li/SO_2 Cell Constituents	3
	A. Experimental	3
	B. Results and Discussion	4
	C. Conclusions	13
III.	DTA of Spirally-Wound Li/SO_2 Miniature Cells	15
	A. Experimental	15
	B. Results and Discussion	16
	C. Conclusions	21
IV.	Kinetics of Lithium-Organic Solvent Exothermic Reactions	23
	A. Experimental	23
	B. Results and Discussion	24
	C. Conclusions	27
V.	General Conclusions and Future Work	28
VI.	References	29

List of Figures

		Page
Fig. 1.	Cross-Sectional View of the High-Pressure Hermetic Crucible.	35
Fig. 2.	Thermogram of S (0.0240 gm); 5°C/Minute.	36
Fig. 3.	Thermogram of $Na_2S_2O_4$ (0.0333 gm); 5°C/Minute.	37
Fig. 4.	Thermogram of Li (0.0123 gm) + Celgard (0.0634 gm); 5°C/Minute.	38
Fig. 5.	Thermogram of Li (0.0031 gm) + LiBr (0.0799 gm); 5°C/Minute.	39
Fig. 6.	Thermogram of Li (0.008 gm) + Teflon Powder (0.0234 gm); 5°C/Minute.	40
Fig. 7.	Thermogram of Li (0.00029 gm) + SO_2; 5°C/Minute.	41
Fig. 8.	Thermogram of Li (0.0010 gm) + AN (100 µl); 5°C/Minute.	42
Fig. 9.	Thermogram of Li (0.0008 gm) + PC (20 µl); 5°C/Minute.	43
Fig. 10.	Thermogram of Li (0.0003 gm) + AN/PC (50:50) 80 µl; 5°C/Minute.	44
Fig. 11.	Thermogram of Li (0.00085 gm) + Electrolyte (40% SO_2, 40% AN, 20% LiBr) ~ 25µl; 5°C/Minute.	45
Fig. 12.	Thermogram of Cathode Mix (0.0661 gm) from a Discharged Li/SO_2 Cell; 5°C/Minute.	46
Fig. 13.	Thermogram of Cathode Mix (0.0819 gm) from a Discharged Li/SO_2 Cell after Exposure to Air; 5°C/Minute.	47
Fig. 14.	Thermogram of Cathode Mix (0.0624 gm) from a Li/SO_2 Cell Which was Discharged and Then Driven into Reversal for 10% of Its Discharged Capacity; 5°C/Minute.	48

List of Figures (continued)

		Page
Fig. 15.	Thermogram of $Na_2S_2O_4$ (0.01007 gm) + Li Powder (0.00131 gm) + Carbon (0.00284 gm); 5°C/Minute.	49
Fig. 16.	Thermogram of Li (0.0015 gm) + S (0.0079 gm); 5°C/Minute.	50
Fig. 17.	Thermogram of Li (0.00094 gm) + Li_2SO_3 (0.0075 gm) As Received; 5°C/Minute.	51
Fig. 18.	Thermogram of Li (0.00572 gm) + Al (0.00720 gm); 5°C/Minute.	52
Fig. 19.	Thermogram of LiAl Alloy (0.01333 gm) + AN; 5°C/Minute.	53
Fig. 20.	Thermogram of LiAl Alloy + AN/SO_2 (75:25) 20 µl; 5°C/Minute.	54
Fig. 21.	Cross-Sectional View of the Miniature Li/SO_2 Cell.	55
Fig. 22.	Fixtures for DTA of Miniature Cell.	56
Fig. 23.	Thermogram of a Discharged Miniature Li/SO_2 Cell of Standard Construction, Discharge Current 1 mA; Discharge Capacity 193 mAHr.	57
Fig. 24.	Voltage, Differential Temperature and the Block Temperature Profiles of a Li/SO_2 Miniature Cell of Standard Construction During Discharge and Force-Discharge at 25°C at a Current of 90 mA.	58
Fig. 25.	Thermogram of the Force-Discharged Li/SO_2 Miniature Cell of Fig. 24.	59
Fig. 26.	Thermogram of the Repeat DTA Run after the One in Fig. 25.	60
Fig. 27.	Thermogram of a Miniature Li/SO_2 Cell of Standard Construction after being Charged at 25°C for 7 Hours at 90 mA.	61

List of Figures (continued)

		Page
Fig. 28.	Thermogram of a Discharged Miniature Li/SO_2 Cell with PC in the Electrolyte; Discharge Current, 10 mA; Discharge Temperature, 25°C.	62
Fig. 29.	Voltage, Differential Temperature and the Block Temperature Profiles of a Li/SO_2 Miniature Cell with PC in the Electrolyte During Discharge and Force-Discharge at 25°C at a Current of 90 mA.	63
Fig. 30.	Thermogram of the Li/SO_2 Miniature Cell with PC in the Electrolyte after the Force-Discharge as Shown in Fig. 29.	64
Fig. 31.	Thermogram of the Repeat DTA Run after the One in Fig. 30.	65
Fig. 32.	Thermogram of a Li/SO_2 Miniature Cell with PC in the Electrolyte after being Force-Discharged at -30°C for 3 Hours at 90 mA.	66
Fig. 33.	Thermogram of the Repeat DTA Run after the One in Fig. 32.	67
Fig. 34.	Thermogram of an Undischarged Li/SO_2 Miniature Cell with Glass Filter Paper Separator.	68
Fig. 35.	Thermogram of a Discharged Li/SO_2 Miniature Cell with Glass Filter Paper Separator; Discharge Current, 10 mA; Discharge Temperature, 25°C.	69
Fig. 36.	Thermogram of a Li/SO_2 Miniature Cell with Glass Filter Paper Separator after being Force-Discharged at -30°C for 3 Hours at 90 mA; Upper Limit of Temperature was 170°C.	70
Fig. 37.	Thermogram of a Li/SO_2 Miniature Cell with Glass Filter Paper Separator after being Force-Discharged at -30°C for 3 Hours at 90 mA; the Upper Limit of the Temperature was 250°C.	71
Fig. 38.	Thermogram of an Undischarged Li/SO_2 Miniature Cell with $LiAsF_6$ Electrolyte.	72

List of Figures (continued)

		Page
Fig. 39.	Thermogram of the Repeat DTA Run after the One in Fig. 38.	73
Fig. 40.	Thermogram of a Discharged Li/SO_2 Miniature Cell with $LiAsF_6$ Electrolyte; Discharge Current 10 mA; Capacity, 160 mAHr; Temperature, 25°C.	74
Fig. 41.	Thermogram of a Li/SO_2 Miniature Cell with $LiAsF_6$ Electrolyte after being Force-Discharged at 25°C, for 5 Hours with 90 mA.	75
Fig. 42.	Thermogram of a Li/SO_2 Miniature Cell with $LiAsF_6$ Electrolyte after Charging at 25°C for 7 Hours with 90 mA.	76
Fig. 43.	Typical Isothermal DTA Thermograms of Li + AN System at Various Temperatures.	77
Fig. 44.	Arrhenius Plots of the Li + AN System; (1) with Li Discs Aged in Dry Box, (2) Freshly Cut Li Discs (3) with 0.32 M LiBr in AN.	78
Fig. 45.	Arrhenius Plots of the Li + AN + PC System; (1) 0% AN, (2) 50% AN, (3) 80% & 95% AN, (4) 100% AN, and (5) 0% PC and 3% SO_2.	79
Fig. 46.	Arrhenius Plots of Li + AN + MF System; (1) 0% AN, (2) 80% AN, and (3) 95% AN.	80
Fig. 47.	Isothermal DTA Thermograms (a) Normal Runs, (b) for Reactions with Short Induction Periods as with Li + AN/MF (80/20).	81
Fig. 48.	Arrhenius Plots of Li + AN + DME System; (1) 0% DME, (2) 5% DME, and (3) 20 % DME.	82
Fig. 49.	Arrhenius Plots of (1) Li + AN/THF (95/5), and (2) Li + AN/DG (95/5) Systems.	83

List of Tables

		Page
Table 1.	List of Possible Chemicals Present in Li/SO_2 Batteries at the Various Stages and Types of Use and Abuse.	31
Table 2.	Summary of DTA Results of the Various Chemicals and their Combinations from Table 1; Heating Rate 5°C/Minute.	32
Table 3.	The Activation Energy and the Frequency Factor of Various Li-Organic Solvent Heterogeneous Reactions Determined by Isothermal DTA Method.	34

I. Introduction:

The Li/SO_2 battery is the most highly developed high-energy density battery system obtainable today and is available in a growing volume from several manufacturers in response to the rising demand for its use in various applications. The rising demand is motivated by the need for a light-weight power source that has a high-rate capability, a good low temperature performance, and good high temperature storability. The Li/SO_2 system has all these characteristics to a greater extent than does any other battery system and for this reason, it has acquired a dominant position in the emerging new primary battery technology. Improvements made at a rapid pace in the Li/SO_2 technology in the areas of efficient manufacturing technology, product reliability (hermetic structures) and abuse tolerance (ventable structures). In this paper, we address ourselves to the area of abuse tolerance. Although, the State-of-the-Art hermetically sealed high-rate D cells made by P. R. Mallory & Co. Inc. are sufficiently abuse resistant (3-5) for various applications, we have initiated a program for exploring the feasibility of improving the intrinsic abuse resistance of the system even further by chemical and/or mechanical means, if possible, so that the product may be rendered Safe under all user conditions. The approach that we have pursued involves:

(a) the identification of the chemical reactions responsible for the pressure buildup and/or thermal runaway;

(b) the determination of the sensitivity of the above reactions to the various use and abuse variables; and

(c) the development of methods to desensitize the above reactions.

We have carried out differential thermal analysis (DTA) of all the cell constituents that may be present at the various stages of storage and discharge, singly, as well as in binary and multiple combinations in order to accomplish (a) and (b) above. We successfully used this method earlier

for the Safety studies of the $Li/SOCl_2$ cells (6). In addition, we carried out DTA of miniature Li/SO_2 cells in order to establish the applicability of the results from the DTA of individual cell constituents to the actual cells. We also carried out kinetic studies of the Li-organic solvent heterogenious reactions (the most significant reactions affecting the safety) at various temperatures using isothermal DTA method. The purpose was to determine the effectiveness of the various organic solvent additives in reducing the Li-organic solvent reactions for enhanced safety. The experimental details and the results of the above studies are reported here.

II. DTA of Li/SO_2 Cell Constituents:

A. Experimental:

The Mettler TA2000 Differential Thermal Analysis System was used for the DTA experiments. High-pressure crucibles made of a corrosion resistant alloy (Nemonic) and having a gold diaphragm capable of withstanding pressures of 1000 PSI were used for most of the experiments. A cross-sectional view of the crucible is shown in Fig. 1. The sealing of the crucible was accomplished by means of the screw cap which when tightened, cuts into the gold diaphragm providing a hermetic seal. In certain experiments with reactive liquids, the crucible was sealed by means of a septum made of viton rubber and the liquid reactants were injected into the crucible. The corrosive gaseous samples were first prepared in a Kovar tube which was hermetically sealed by means of welding and then placed inside the crucible which was sealed by means of the screw-cap and the gold diaphragm as above.

The DTA System was calibrated with indium metal samples in order to obtain quantitative data on the caloric output of the reactions. Thus, the DTA thermograms were useful in determining both the temperature at which a thermal transition (exothermic and/or endothermic) occurred as well as the total heat of such transitions.

All the chemicals were used as received. Since a majority of the above chemicals, shown in Table 2, were moisture sensitive, the transfer of the materials to the high-pressure crucible and the sealing of the crucible were carried out in an argon filled dry box.

The DTA runs were carried out at heating rates of 5°C/minute, from room temperature to approximately 450°C and back. Thermograms were recorded for both the heating and the cooling modes, the latter was occasionally useful in identifying the reaction products generated during the heating mode.

B. Results and Discussion:

Li/SO_2 organic electrolyte cells contain Li anode, Teflon (polytetrafluoroethylene) bonded carbon cathode on expanded aluminum grid, LiBr electrolyte salt, acetonitrile organic solvent and liquid SO_2 depolarizer. Porous polypropylene has been most commonly used for separator. Electrolyte salts such as $LiAsF_6$ (8) and organic solvents such as propylene carbonate and methyl formate have also been used. The cell container is made of nickel-plated cold-rolled steel with glass-to-metal seal electrical feedthrough comprising tantalum or molybdenum positive terminal. The cell case is the negative terminal. A list of all the possible chemicals that may be present in a Li/SO_2 battery at the various stages of use and abuse is provided in Table 1. The list includes (a) the possible starting materials mentioned above, (b) the possible impurities and (c) the possible chemicals generated during the various use and abuse regimes. Lithium dithionite is the main discharge product according to the cell reaction,

$$2\ Li + 2\ SO_2 \longrightarrow Li_2S_2O_4 \qquad [1]$$

The formation of Li_2SO_3, Li_2SO_4, Br_2, $SOBr_2$ and S_2Br_2 as a result of prolonged high temperature storage has been postulated (7, 8) to be due to the reactions between LiBr and SO_2,

$$8\ LiBr + 8\ SO_2 \longrightarrow 4\ Li_2SO_3 + 4\ SOBr_2 \qquad [2]$$

$$4\ SOBr_2 \longrightarrow 2\ SO_2 + S_2Br_2 + 3\ Br_2 \qquad [3]$$

$$4\ Li_2SO_3 + 2\ Br_2 \longrightarrow 2\ Li_2SO_4 + 4\ LiBr + 2\ SO_2 \qquad [4]$$

$$4\ LiBr + 4\ SO_2 \longrightarrow 2\ Li_2SO_4 + S_2Br_2 + Br_2 \qquad [5]$$

The formation of CH_4 and LiCN during reversal of an unbalanced Li/SO_2 cell has been reported (9). The formation of CS_2, H_2S and CO_2 from the reactions between CH_4 and SO_2 was predicted from thermodynamic considerations (10).

The list in Table 1 contains only the stable chemical species known to be present in Li/SO_2 cell. There are unstable species which may be formed during the electrochemical and chemical reactions that occur during storage, use and abuse of the cell. Both the nature of and the effect of these species in the abuse resistance of the cells are uncertain. Since all these stable and unstable chemicals may be present simultaneously in the cell, any and all of these may be important in determining the abuse resistance of the Li/SO_2 cells. In this report, we have attempted to identify the chemicals and the chemical combination which contribute to the unsafe behavior (thermal runaway, etc.) of the cell from the DTA of the chemicals and their combinations shown in Table 1. Chemical combinations which produce exothermic transitions at ambient temperatures may be responsible for the initiation of a thermal runaway, whereas the chemicals and/or combinations thereof that produce exothermic transitions at elevated temperatures, may sustain a thermal runaway once initiated by other means.

The DTA results are summarized in Table 2. All the runs were made at a heating rate of 5 °C/minute. The thermograms of some important chemicals and their combinations are discussed below.

Single Components:

Lithium: The thermogram of Li consists of one sharp endotherm at 188 °C corresponding to the melting of Li. The difference between the melting point of Li (179 °C) and the above temperature indicates the thermal lag of the crucible at the heating rate of 5 °C/minute.

The lag would be expected to depend upon both the temperature and the heating rate. All the temperatures reported in Table 2 are the furnace temperatures, the actual sample temperatures corresponding to the furnace temperature can be approximated by subtracting 8 °C from the furnace temperature. On cooling mode, the Li thermogram showed an exotherm corresponding to the freezing of Li. The identical caloric output corresponding to melting and freezing, indicated the lack of reaction of Li and the crucible.

Carbon Black: The thermogram of Shawinigan black, the major constituent of the carbon cathode showed no transitions.

Separator: The thermogram of Celgard 2400, the porous polypropylene separator material, showed an endothermic transition at 156°C corresponding to the melting of polypropylene and an exotherm on cooling mode for freezing of polypropylene, with identical caloric output.

Acetonitrile (AN): The thermograms of both AN and PC showed no characteristic transitions within the temperature range (25° to 350°C) examined.

Teflon: The thermogram of Teflon powder (TL-120) showed a small gradual endothermic transition at 250°C most likely indicating the sintering of Teflon powder. The Teflon is used as a binder for the carbon cathode.

Sulfur: The thermogram of elemental S is shown in Fig. 2. The two overlapping endothermic transitions at 112° and 120°C correspond to the melting of two crystalline forms (rhombic and monoclinic) of sulfur and the sharp exotherm on cooling mode represents the crystallization of one type of sulfur since one form changes to the other on melting. The absence of any other transtions indicate the inertness of the crucible to sulfur.

Sodium Dithionite: Lithium dithionite, $Li_2S_2O_4$, the primary cell reaction product of the Li/SO_2 battery, was not commercially available. Therefore, we used commercially available $Na_2S_2O_4$ which is chemically similar to $Li_2S_2O_4$;the $Na_2S_2O_4$ was approximately 90% pure, having sulfite and thiosulfate as major impurities. The DTA thermogram of $Na_2S_2O_4$ is shown in Fig. 3. The material showed several strong exothermic transitions above 100°C on heating. The absence of endothermic transitions on cooling indicates that the above transitions represent irreversible decomposition of $Na_2S_2O_4$. The thermogram on cooling showed an exothermic transition corresponding to the freezing of elemental S. The repeat run (not shown)

shows another endothermic transition corresponding to the melting of elemental S; thus, confirming that one of the product of the decomposition of $Na_2S_2O_4$ is S. The quantity of S formed was estimated (using the DTA thermogram of elemental S shown in Fig. 2) to be 0.0056 gm. The amount of S expected based on the decomposition reactions such as

$$2\ Na_2S_2O_4 \longrightarrow 2\ Na_2SO_3 + SO_2 + S \qquad [6]$$

or $$2\ Na_2S_2O_4 \longrightarrow 2\ Na_2O + 3\ SO_2 + S \qquad [7]$$

is 0.0055 gm. The agreement is reasonable.

The total caloric output of the exothermic decomposition was determined by integrating the area under the three major peaks (two major peaks in the case of pre-dried material) and it turned out to be approximately -14.4 K.Cal/mole as the heat of decomposition of $Na_2S_2O_4$. Assuming reaction [6] as the decomposition reaction, the heat of formation of $Na_2S_2O_4$ was calculated using the known heats of formation of Na_2SO_3 (-260.6 K.Cal/mole, and SO_2 (-70.96 K.Cal/mole). This turned out to be -290 K.Cal/mole. The heat of formation of $Na_2S_2O_4$ calculated (11) from the data in aqueous ammonia was 296 K.Cal/mole. The agreement is reasonable. Thus, the heat of decomposition of -14 K.Cal/mole for $Na_2S_2O_4$ as determined from the DTA thermogram is probably reasonable.

Lithium Bromide: The thermogram of anhydrous LiBr as used in the electrolyte for the Li/SO_2 batteries was found to be completely featureless.

Combinations:

Li + Celgard: The thermogram of Li and the porous polypropylene separator (Celgard) which remains in contact with Li in the cell, is shown in Fig. 4. The endothermic transitions corresponding to melting of polypropylene and Li during heating mode and the identical exothermic peaks during the cooling mode, indicate the absence of chemical activity between the two.

Li + LiBr: The thermogram of a mixture of Li and LiBr, as shown in Fig. 5, consists of one exothermic peak at 124°C prior to Li melting. The exothermic peak most likely represents the reaction between Li and some trace impurities in LiBr.

Li + Teflon: The thermogram of Li + Teflon powder is shown in Fig. 6. The strong exothermic peak, at 279°C, beyond the lithium melting most likely represents the following reaction:

$$4\ Li + \frac{1}{n}(C_2F_4)_n \longrightarrow 4\ LiF + 2\ C \qquad [8]$$

$$\Delta H_o = -96\ K.\ Cal/g\ atom\ of\ Li.$$

The caloric output determined by integrating the exothermic peak was 88 K. Cal/gm atom of Li which is in reasonable agreement with the literature value. In all these experiments, the weight of Li used was very small, viz, 0.0008 gm or less and errors in the Li weight may lead to the above deviations of the experimental values from the literature values.

Li + SO_2: The mixture of Li and liquid SO_2 was prepared by taking a small piece of Li in a Kovar tube which was then cooled in liquid N_2 and SO_2 was condensed in the tube which was then sealed by welding. This sealed tube was placed in the crucible shown in Fig. 1 and DTA run was taken. A typical thermogram is shown in Fig. 7. The endotherm at 190°C corresponding to the melting of Li indicated that the sensitivity of the system was not altered significantly by the use of the Kovar tube. The thermogram is very striking in that there was no exothermic transition below 320°C, the highest temperature used, indicating the absence of chemical reaction between molten Li and liquid SO_2. The runs were repeated with new samples and the above results were confirmed. Also, the Kovar tubes were opened at the end of the run and the presence of unreacted Li and liquid SO_2 was confirmed. The results demonstrate the exceptional chemical stability of Li towards SO_2. The film is sufficiently protective even when the Li is in a molten state, thus indicating continuous regeneration of the film.

Li + AN: Li and AN were found to react exothermically at room temperature. For this reason, the DTA crucible (Fig. 1) was modified slightly to incorporate a septum top through which AN was injected and the DTA runs were started immediately after such injection. The exothermic reaction was accelerated at higher temperatures as shown in the thermogram in Fig. 8. AN was found to be one of the most reactive agents towards Li. We examined the kinetics of this heterogeneous reaction in some detail using the DTA. The results will be reported later.

Li + PC: PC was used as a co-solvent along with AN in Li/SO_2 cells. Li was found to be quite inert in PC probably due to the formation of a protective film (12) of Li_2CO_3. The thermogram shown in Fig. 9 indicate strong exothermic reactions at 270°C. In this respect, Li is more stable in SO_2 than in PC.

Li + PC + AN: AN and PC were mixed in equal volumes and injected through the septum of the crucible containing Li. The thermogram is shown in Fig. 10. The exothermic peak represents Li + AN reaction. Note that the temperature at which the exothermic reactions occurred was increased to 180°C from 80°C (Fig. 8). The results indicate the protective nature of PC. In similar runs with AN:PC volume rations of 95:5 , the exothermic peaks occurred at 98°C. Thus, the extent of protection is dependent upon the concentration of PC. In this analysis, the relative stabilities of the various materials are judged by the temperature at which they react, the higher the temperature, the more stable the materials at ambient temperature.

Li + SO_2 + AN + LiBr: The SO_2, AN and LiBr mixture used represents an electrolyte for the Li/SO_2 battery having a pressure of one atmosphere and consists of approximately 40% SO_2, 40% AN, and 20% LiBr by weight. The thermogram is shown in Fig. 11. The exothermic transition occurring at 180° prior to the melting of Li most likely represent the Li + AN reactions. SO_2 acts as a protective agent for Li as did the PC above.

The results indicate that the spontaneous reactions between Li and AN can be mitigated by the addition of either SO_2 or PC. The use of a mixture of AN and PC as the organic co-solvent may thus be beneficial in preventing spontaneous exothermic reaction of Li and AN in a completely discharged Li/SO_2 cell which has SO_2 as the capacity limiting component. The efficacy of this approach will be reported later.

$Na_2S_2O_4$ + C: The thermogram of a mixture of $Na_2S_2O_4$ (analogous to $Li_2S_2O_4$) and carbon black was found to be similar to the thermogram of $Na_2S_2O_4$ alone as shown in Fig. 3, thus indicating the absence of any significant effect of carbon black.

Cathode Mix: The thermogram of the cathode mix consisting of carbon and Teflon did not show any transitions in the sealed crucible. However, the dried cathode mix obtained from a discharged Li/SO_2 cell, containing the cell discharge product, $Li_2S_2O_4$, and the electrolyte salt, LiBr in addition to carbon and Teflon did. A thermogram of such a discharged cathode mix is shown in Fig. 12. The exothermic transition at 180°C is similar to that observed with dry $Na_2S_2O_4$. The caloric output was approximately 13 Cal/gm of carbon mix. The thermogram of the cathode mix (from the same discharged cell) which was exposed to air is shown in Fig. 13. Note the additional exothermic peaks similar to those on the thermogram of as received $Na_2S_2O_4$ (Fig. 3). The caloric output was found to be 38 K Cal/gm of cathode mix. Another thermogram of the cathode mix from a cell which was discharged into reversal, so that the cell voltage was negative for approximately 10% of its normal capacity is shown in Fig. 14. The cathode mix was inadvertently exposed to air prior to the DTA run. The thermogram looked very similar to the previous one, except the caloric output was increased to 112 Cal/gm of the cathode mix. Thus, the behavior of the discharged cathode was very similar to the behavior of $Na_2S_2O_4$. Moisture appeared to enhance the exothermic decomposition. The presence of Li in the discharged cathode (from the cell reversal) enhanced the heat output of the decomposition reactions. Carbon and Teflon did not appear to have any significant effect.

Li + $Na_2S_2O_4$ + C: The thermogram of a physical mixture of powdered Li, powdered $Na_2S_2O_4$ and carbon black (simulating a cathode mix of a Li/SO_2 cell which was in reversal) is shown in Fig. 15. Note that the thermogram is very similar to that in Fig. 14, except for the endotherm corresponding to Li melting. The slight differences in the temperature at which the two major exotherms occurred are most likely due to the differences in the size of the sample. We found that the exothermic transitions occur at higher temperatures for the smaller samples. The first peak at 198°C most likely represents the decomposition of $Na_2S_2O_4$ (Figs. 3, 12) and the second strong peak at 290°C most likely represents the reaction between Li and the decomposition products of $Na_2S_2O_4$ such as S and Na_2SO_3 according to reaction [6] or [7]. The striking similarity of the thermograms shown in Figs. 14 and 15, indirectly supports the assumed similarity of $Na_2S_2O_4$ and $Li_2S_2O_4$ insofar as their thermochemical characteristics are concerned.

Li + S: The thermogram, shown in Fig. 16, indicates a very strong exotherm after the melting of two forms of sulfur, corresponding to the exothermic formation of Li_2S according to,

$$2\ Li + S \longrightarrow Li_2S \qquad [9]$$

The similarity of the strong exotherm to that observed in the thermogram of Li + $Na_2S_2O_4$ (in Fig. 15) suggests that the latter was due to Li + S reactions. The higher temperature of the strong exotherm in Fig. 15, is most likely due to the poor physical distributions of the trace amounts of S (formed as a result of the decomposition of $Na_2S_2O_4$) which may have to be in a vapor form to react with the molten Li in view of the trace amounts of S involved.

Li + Li_2SO_3: Li_2SO_3 may be a product of decomposition of $Li_2S_2O_4$ according to reaction [6]. The thermogram of as-received Li_2SO_3 is shown in Fig. 17. There are strong exothermic reactions prior to the melting of Li. However, with dehydrated Li_2SO_3, the thermogram of Li + Li_2SO_3 showed only the endothermic transition due to the melting of Li, but no exothermic transition. This demonstrates the important effect of moisture (as impurity) in the various cell components on the thermal characteristics of the cell constituents.

Li + Al: Expanded Al was used as a current collector for the carbon cathode. During cell reversal, Li deposition may occur on Al and spontaneous alloying (13) may ensue leading to the formation of LiAl. The thermogram shown in Fig. 18 indicates a strong exothermic reaction at the melting point of Li corresponding to the formation of Li-Al alloys. The two endotherms at higher temperatures correspond to the melting of two types of Li-rich alloys of Al. On cooling mode, three exotherms correspond to the freezing of the above two alloys and the excess Li. X-ray diffraction of the products indicated the presence of Li_9Al_4 and LiAl which remained in a solid state during the DTA run since the melting point (718°C) is much higher than the upper temperature limit of the DTA run. DTA runs with excess Al also had similar characteristics as shown in Fig. 18, except that there was no exotherm corresponding to Li freezing during cooling.

LiAl + AN: LiAl alloy prepared with excess Al was used for this run. The thermogram is shown in Fig. 19. The strong exotherm at 154°C represents the Li and AN reaction since DTA runs with Al + AN showed no significant reactivity. A comparison of the thermograms in Fig. 19 with the Li + AN thermogram in Fig. 8 shows that the reactivity as judged by the temperature of the exotherm is significantly reduced by the alloying of Li with Al. With pure Li (Fig. 8) AN reacted vigorously even at room temperature, whereas with the LiAl alloy, the reaction started at 154°C.

LiAl + SO_2: The thermogram showed no exothermic transitions up to 470°C, only endothermic transitions corresponding to the melting of lithium-rich alloys.

LiAl + AN + SO_2: AN and SO_2 were used in the volume ratio of 75:25. The thermogram is shown in Fig. 20. The major exothermic peak corresponding to the Li + AN reaction occurred at 420°C, instead of occurring at 180°C, as in the case of pure Li (Fig. 11). Furthermore,

addition of SO_2 increased the temperature of the exotherm from 154°C as in the case of LiAl + AN (Fig. 19) to 420°C. Thus, the reactivity of the most reactive components of the Li/SO_2 batteries viz Li and AN can be reduced by both the addition of SO_2 (film forming agent) and the alloying of Li and there appears to be a significant synergism when both are used together.

In addition to the above, DTA of other mixtures of various chamicals that may be formed in Li/SO_2 cells, were carried out and the results are summarized in Table 2. The DTA of Li with some organic solvents other than AN and with mixtures of AN and other solvents were carried out in an effort to find alternate less reactive solvents or solvent mixtures. DME (dimethoxy ethane) appears to be a good substitute for AN. However, the performance characteristics of cells with this solvent and other prospective solvent mixtures, need to be established in order to determine the tradeoffs between cell performance and Safety.

C. Conclusions:

DTA has been found to be an effective tool in the identification of the cell constituents responsible for the thermal runaway of the Li/SO_2 cells. The method was also useful in the development of approaches to deactivate the above active cell constituents. The specific conclusions from the DTA Studies are listed below.

1. The cell discharge product $Li_2S_2O_4$ and analogous $Na_2S_2O_4$ undergoes exothermic decomposition producing S as one of the products.

2. The presence of Li in a discharged cathode containing $Li_2S_2O_4$ leads to a stronger exothermic reaction most likely due to the exothermic reaction of Li and S formed from the decomposition of $Li_2S_2O_4$.

3. Moisture in the cell parts particularly in the cathode may lead to the production of additional heat due to its exothermic reaction with $Li_2S_2O_4$ and Li which is formed in the cathode during cell reversal.

4. Li and AN are the most reactive components of the Li/SO_2 cells, from the standpoint of internal heat generation at ambient temperatures.

5. Li and SO_2 are extremely inert even at temperatures as high as 320°C. This unexpected stability has been attributed to the formation of a protective film on Li.

6. PC is less reactive to Li than AN and the reactions of PC and AN mixtures is dependent upon the concentration of PC in the mixture.

7. Li alloys with Al exothermically near the melting point of Li producing primarily LiAl.

8. The reactivity of alloyed lithium with AN is significantly less than that of pure lithium.

9. The alloying of Li (to form LiAl) and the addition of SO_2 both reduce the reactivity of Li towards AN, but when used together, there is a synergistic effect which reduces the reactivity of Li towards AN to such an extent that the reaction occurred at 420°C instead of at 150°C.

10. The above DTA results indicate that the following approaches may be useful in improving the abuse resistance of Li/SO_2 cells:

(a) Use of excess SO_2 in the cell to ensure its presence at all stages of use, storage and abuse.

(b) Use of mixtures of AN + PC instead of pure AN.

(c) Use of alternate solvents instead of AN and mixtures of solvents.

(d) Control of moisture levels in the cell components.

The efficacy of the above approaches in improving the safety of the Li/SO_2 cell and the necessary tradeoffs will be reported later.

III. DTA of Spirally Wound Li/SO_2 Miniature Cell

We augmented the DTA studies of the cell constituents by DTA studies on actual Li/SO_2 cells. We chose to use a miniature spirally wound Li/SO_2 cell instead of the LO26 cells (D size). The design of the miniature cell was such that it reflected the behavior of the larger D size cell insofar as the heat generation characteristics are concerned. The purpose of these DTA studies are to determine the heat generation characteristics of the actual Li/SO_2 cells and compare them with the behavior predicted from the DTA studies of the cell constituents as well as to determine the effect of some of the cell design variables on the heat generation characteristics of the Li/SO_2 cells. The cell design variables studied were: separator material (porous polyethylene and glass) electrolyte salt (LiBr and $LiAsF_6$) and organic solvent (AN and PC + AN). The experimental details and the results are presented here.

A. Experimental

(a) Miniature Li/SO_2 Cell: The cross sectional view of the miniature Li/SO_2 cell is shown in Fig. 21. The cell was made in a nickel plated cold rolled steel can, 0.302 inch diameter and approximately 1.5 inch high. The cell top consists of a G/M seal having a tantalum tube feed through which serves both as the positive terminal and as electrolyte fill port. The G/M seal was welded to the cell can. The cell bottom has a thermocouple well for the measurement of internal temperature. The cell was made with spirally wound electrodes: 1.2 inch x 1.3 inch x 0.012 inch cathode; 1.2 inch x 1.4 inch x 0.005 inch Li anode. The carbon cathode had expanded aluminum current collector but the Li anode did not have any current collector. The cells were filled with electrolyte having 70% SO_2 by weight. The fill tube was welded shut after the cell filling. The cells were made with the following variables:

Separator:	porous polypropylene, (celgard) (standard)
	glass filter paper.
Electrolyte Salt:	LiBr (standard)
	$LiAsF_6$
Organic Solvent:	AN (standard)
	PC + AN (1:1)

(b) DTA Fixture: A cross sectional view of the DTA fixture is shown in Fig. 22. It consists of an aluminum heating block having two cavities for the reference and the sample miniature cells. The differential thermocouples are inserted into the thermocouple wells (of the cells) by means of heat transfer compounds. The heating elements were wrapped around the aluminum black which was insulated all around by means of fiber glass. The heating block itself served as the negative terminal of the sample cell and the positive terminal was carefully insulated from the aluminum heating block. The DTA runs consisted of heating the aluminum block at a fixed rate from room temperature to a maximum of 250°C and monitoring both the block temperature as well as the differential temperature on a strip chart recorder. The open circuit voltages of the cells were also monitored during the DTA run. In some experiments the differential temperature of the cell was monitored during discharge, reversal and charging of a cell.

B. Results and Discussion

The miniature cell was designed to reflect the thermal characteristics of the larger LO26S (D size) cells with the exception that the potential explosive energies involved would be substantially lower and hence less destructive of the available DTA fixtures. The electrochemical heat evolved per unit volume, as measured by the current density (i), over voltage (η) and the cell volume, turned out to be 9.1 $(i\eta)_L$ watts/cm^3 for the LO26S cells and 11.5 $(i\eta)_S$ watts/cm^3 for the miniature cell. Thus, if the cells are discharged at comparable current densities where they would experience comparable overvoltages, the heat evolution per unit volume would be approximately the same for the two cells and so would their thermal excursions under adiabatic conditions.

The miniature cells delivered 227 mA.Hr at 1mA and 180, 210, 180 and 180 mA.Hr at 10 mA when discharged at 25°C. At -30°C, the cells delivered 90, 83 and 97 mA.Hr at 90 mA to a cutoff voltage of 2.0 volts. 90 mA current for the miniature cell corresponds to approximately 2A for the LO26S cells, in terms of equivalent current density.

DTA runs with two empty cell cans and with two cell cans filled with Al_2O_3 showed no transitions as expected. DTA runs with two fresh cells also showed no transitions. Cell cans filled with Al_2O_3 were chosen as a reference for all further DTA runs.

Altogether four different types of cells were tested. These will be referred to as (a) standard cells, (b) cells with PC (propylene carbonate), (c) cells with glass filter paper separator, and (d) cells with $LiAsF_6$ electrolyte salt.

Almost all the DTA experiments were done in triplicate and the results were found to be quite reproducible.

(a) Standard Cells: The standard cells contained 0.005 inch thick Li anode, 70% SO_2 + 7% AN (acetonitrile) + 23% LiBr electrolyte and porous polypropylene (celgard) separator. The stoichiometric ratio of Li:SO_2 was approximately 1:1.3 based on the cell reaction

$$2\,Li + 2SO_2 \longrightarrow Li_2S_2O_4 \qquad [10]$$

The cells were discharged at currents of 1, 10 and 90 mA at 25°C and then these were subjected to DTA runs by heating from 25°C to 170°C. The differential thermocouple showed one small exothermic transition starting at temperatures of 150°C. A typical thermogram is shown in Fig. 23. There was no significant effect of the discharge current on the size of this exotherm, although the exothermic transition was somewhat smaller for a partially discharged cell. The exothermic transition is attributed to the exothermic decomposition of the discharge product $Li_2S_2O_4$. However the upper limit of the temperature of the DTA run was too low for most of the other exothermic reaction. The sharp lowering of the open circuit voltage of the cell at temperatures of 140°C was

probably due to the formation of shorts in the cell after melting of the polypropylene separator.

Miniature cells were force-discharged to reversal at 25° and -30°C in triplicate. One typical plot of the cell voltage, differential temperature and the aluminum block temperature during the cell discharge is shown in Fig. 24. The differential temperature increased sharply at the point of the cell polarization. The block temperature was increased only slightly. The cell was at reversal for only 0.75 hr corresponding to a capacity of 67.5 mA.Hr. There was no cell venting or explosion. The cell was then subjected to a DTA run. The thermogram, as shown in Fig. 25, has two strong exothermic peaks very similar to those observed in thermograms of mixtures of powdered Li and $Na_2S_2O_4$ (analogous to $Li_2S_2O_4$). The first exotherm was attributed to the decomposition of $Li_2S_2O_4$ to produce S and the second one was most likely due to the Li + S reaction. Li + AN reaction may also occur simultaneously in view of the lower concentration of SO_2. The similarity of the thermograms of actual cells with that of the synthetic mixtures of chemicals, done earlier, supports our conclusions regarding the identification of chemicals responsible for thermal runaway of Li/SO_2 cells. In the cell, $Li_2S_2O_4$ is formed during discharge and Li is formed during the reversal in the cathode. The presence of Li enhanced the exothermic caloric output of $Li_2S_2O_4$ as observed earlier in DTA experiments with cathodes as well as in synthetic mixtures. A second DTA run (Fig. 26) with the same cell showed virtually no exothermic transition indicating that the active constituents (Li and $Li_2S_2O_4$) had reacted almost completely during the first DTA run, similar to our observations on $Li/SOCl_2$ cells (14).

The intensity of the exothermic transitions of the cells which were reversed appeared to be independent of the temperature at which the reversal occurred but dependent on the extent of reversal. Prolonged reversal produces more Li in the cathode than a short reversal and this leads to the increased caloric output as observed in the thermograms of mixtures of Li + $Na_2S_2O_4$.

Miniature cells were also charged at 90 mA for 7 hours without any cell explosion. The DTA thermogram of the charged cell is shown in Fig. 27. Note that there is a small endotherm at 180°C most likely indicating the melting of Li. The strong exotherm above 200°C indicate the Li + AN reaction in the presence of excess SO_2 which protects Li from reaction with AN at a lower temperature. Since, the cell was not discharged, there was no strong exotherms corresponding to the decomposition of $Li_2S_2O_4$, although some $Li_2S_2O_4$ may have formed by chemical reaction with the dendritic Li formed on the anode during charging. Again, the thermograms of the cells appeared to be interpretable based on the DTA results of the individual chemicals. A repeat DTA run of the above cell showed considerably reduced exothermic transitions indicating the consumption of the active materials during the first run.

(b) Cells with PC: These cells have the same size electrodes as the standard cells, only the electrolyte consists of 70% SO_2 + 23% mixture of AN and PC (3:1) + 7% LiBr. The thermogram of a discharged cell, as shown in Fig. 28 was found to be identical to that of the standard cell. Note that the upper limit of the temperature was only 170°C. The voltage and the differential temperature profile during discharge and reversal at 25°C at 90 mA for 3 hours as shown in Fig. 29 also are very similar to those of the standard cell. However the DTA thermogram of the above reversed cell, as shown in Fig. 30, is interesting. Note that the upper limit of the temperature was 250°C. It shows three exothermic transitions prior to a very sharp exotherm occurring during the cooling cycle of the DTA. The repeat DTA run (Fig. 31) shows no significant exotherms. The thermogram of another cell force discharged at -30°C for 3 hours at 90 mA, is shown in Fig. 32. Note that it shows only the three exothermic peaks. But on the repeat run, the fourth strong exothermic peak appears as shown in Fig. 33. The above experiment was repeated and the DTA thermograms were found to be identical to the above. We believe that the three peaks are due to the following three reactions, viz Li + AN, decomposition of $Li_2S_2O_4$ and Li + PC. The fourth sharp peak in Fig. 30 is most likely due to the Li + S reaction. We found earlier that Li + S reaction produced the sharpest exothermic transitions indicating a very fast reaction.

All the DTA experiments were carried out at least one day after the discharge and reversal of the cells; thus the exothermic transitions reflect

reactions of relatively stable species and not transient species.

(c) Cells with Glass Filter Paper Separator: These cells are similar to the standard cells in every respect except the separator is made of glass filter paper. The thermogram of a fresh cell heated to 170°C is shown in Fig. 34. Note that the OCV remained unchanged during the run indicating the absence of shorting that occurred in cells with celgard separator which melts at approximately 140°C causing shorting. Also, there was no significant transitions as expected. The thermogram of a completely discharged cell, as shown in Fig. 35, showed a small exotherm very similar to that of the standard cells, most likely because the upper limit of the temperature was 170°C. Note also that the OCV of the cell did not drop to zero; indicating lack of cell shorting. The repeat run did not show any transition as before.

The DTA thermogram of a cell which was force-discharged at -30°C at 90 mA showed only a small exotherm (as shown in Fig. 36) when the upper limit of the DTA run was kept at 170°C. However, when the upper limit of the DTA temperature was increased to 250°C of a similarly force-discharged cell, stronger exothermic transitions were observed again (Fig. 37) very similar to those of the standard cells.

The efficacy of the glass separator in preventing cell shorting at elevated temperatures is demonstrated from the above experiments. However, the exothermic reactions at 150°C is not thus preventable, as expected.

(d) Cells with $LiAsF_6$ Electrolyte Salt: These cells are identical to the standard cells except the electrolyte salt is $LiAsF_6$ instead of LiBr. The electrolyte consisted of 70% SO_2 + 21% AN + 9% $LiAsF_6$. The thermogram of a fresh cell is shown in Fig. 38. The open circuit voltage of the cell curiously increased above 132°C from 2.95 volt to 3.66 volt. We found this phenomenon to be quite reproducible. There is a small exotherm in the thermogram corresponding to this increase in OCV. Our earlier DTA studies were incomplete insofar as this electrolyte salt is concerned and as such the reason for this increased OCV is not quite clear. The thermogram showed an endotherm corresponding to the melting of Li. Curiously, the cell did not short in spite of the fact that the cell temperature exceeded the melting point of the celgard separator. It is possible

that the electrode assembly was not tight enough to create a short when the separator melted. The thermogram then showed a sharp exothermic transition corresponding to the shorting of the cell as indicated by the sudden drop of OCV. This cell did not explode at this point although another cell did in a subsequent run. A repeat run of the same cell showed no significant transitions as shown in Fig. 39, indicating complete decomposition of any electrochemically and thermally active materials including $Li_2S_2O_4$ formed during shorting. The temperature of the cell must have been high enough to complete all the thermally active processes discussed earlier.

The thermograms of discharged cells showed relatively smaller exotherms (Fig. 40) compared to those of a force-discharged cell (Fig. 41) as observed earlier with the standard cells. The thermogram of a charged cell (Fig. 42) was similar to that of a fresh cell with the exception that the OCV was higher initially (3.44 volts) and it was reduced to 2.85 volts prior to shorting which resulted in a very large exotherm corresponding to both electrochemical and chemical heats. Note that the cell shorting occurred after the lithium melting as indicated by the small endotherm prior to the sharp drop of OCV. Repeat run showed no transitions as before.

The above results demonstrate the applicability of the cell DTA technique, in resolving the chemical processes occurring in cells during thermal excursions, and this method, in conjunction with the DTA of cell constituents, provides a useful tool for studying the thermal runaway processes of Li/SO_2 and other cells.

C. Conclusions

The differential thermal analysis (DTA) of miniature Li/SO_2 cells was found to be a useful tool in elucidating the chemical processes that occur in a cell during thermal excursions, as in thermal runaways. The DTA data of cell constituents were particularly useful for the identification of the various processes occurring in the cell by comparing the nature of the transitions of the cell with those of synthetic mixtures of cell constituents. The effect of the cell construction variables such as glass filter paper separator on the DTA thermograms of the

miniature cells was found to be predictable in most cases based on the DTA data of the cell constituents. The major reactions which contribute to the thermal runaway processes are the Li-organic solvent reaction and the decomposition of $Li_2S_2O_4$ as well as the Li + S reaction, where S was produced from $Li_2S_2O_4$. The cell reversal results in stronger exothermic transitions due to the formation of Li in the cathode containing $Li_2S_2O_4$.

IV. Kinetics of Lithium-Organic Solvent Exothermic Reactions

From the DTA studies we have shown that the reactions most likely to initiate a thermal runaway are the Li-organic solvent reactions, particularly the exothermic Li-acetonitrile reaction which occurs at room temperature. For this reason, we chose to concentrate on the study of the kinetics of this reaction in an effort to find ways and means of quenching it. We also carried out kinetic study of several other organic solvents in an effort to find suitable candidates for replacing acetonitrile in the electrolyte of the Li/SO_2 cells or adding to it, if possible. The extent of the reaction is proportional to the heat evolved and the rate of the reactions is proportional to the rate of the heat evolution at a constant temperature and at a constant surface area of the Li. Therefore, an isothermal DTA technique was used to study these reactions. The experimental details and the results are reported here.

A. Experimental:

The Mettler TA2000 Differential Thermal Analysis System with the high pressure hermetic crucibles, described earlier, was used for the isothermal DTA runs. A 0.098 inch diameter piece of 0.005 inch thick Li foil weighing 0.00029 gm was placed in the DTA sample crucible in an argon filled dry box. 20 microliters of the appropriate organic solvent was injected into the crucible and the crucible sealed. The Li disc size, weight and the location inside the sample container as well as the volume of the organic solvent were kept as constant as possible from run to run. The mixtures were then heated very quickly to various temperatures in the DTA furnace and maintained at those temperatures while the differential temperatures were recorded as a function of time yielding isothermal DTA thermograms at the various temperatures.

All the organic solvents used were of the highest purity available from Eastman Kodak and were used as received except for PC which was vacuum distilled over Li foil prior to use.

The Li foils were used as received from the Foote Mineral Co. and contained 1% Na as impurity. The foils were shiny in appearance and all the

experiments were carried out using freshly punched Li from one roll except for some preliminary experiments with AN for which the Li discs were punched several days prior to the experiments. Although the Li foil was shiny in appearance it is reasonable to assume that it has a thin protective film and the freshly punched areas of the discs are probably most active towards the organic solvents. Therefore, the duration between the punching of a Li disc and the isothermal run was kept constant from run to run in order to reduce any variation of the activity of the Li surface from run to run.

B. Results and Discussion:

Some typical isothermal DTA thermograms at various temperatures for the Li + AN system are shown in Fig. 43. It can be shown that the slopes of the rising portion of the DTA thermogram at the point of inflection of the temperature-time curve can be expressed as

$$\frac{d \Delta T}{dt} = k \left(\frac{\Delta H}{L + S}\right) \qquad [11]$$

where ΔH = heat of the reaction
k = zeroth order rate constant
L = heat capacity of reaction mixture
S = heat capacity of container

when the DTA furnace is maintained at a constant temperature and the chemical reaction obeys zeroth order kinetics.

Since ΔH, L and S are constants, the slope is proportional to the rate constant of the Li + solvent reaction which is controlled by the reaction temperature and the surface area of the Li disc which were kept constant for all the runs.

An Arrhenius plot of the above slopes as a function of the reaction temperature for the Li + AN system with Li discs cut several days prior to the experiment is shown in Fig. 44. The plot is linear and the energy of activation, as determined from the least square slope (excluding the point at the lowest temperature) was 13 K.cal mole^{-1} with a frequency factor of 8. A similar plot

of the same system with freshly cut Li discs as shown in Fig. 44 was also linear and had a higher reaction rate and a slightly lower activation energy; 10 K.cal $mole^{-1}$. This probably reflects the effect of the Li film (formed during storage in the dry box) on the kinetics of the Li + AN reaction.

The effect of LiBr on the kinetics of the Li + AN reaction was studied and the Arrhenius plot is also shown in Fig. 44. The activation energy of the reaction was reduced further to 6 K.cal $mole^{-1}$ possibly indicating the catalytic effect of Li^+ (15) on the Li + AN reaction.

Although PC was found to be rather inert towards Li at room temperature, it reacted with Li at higher temperatures. The energy of activation as determined from the linear Arrhenius plot, shown in Fig. 45, was 22 K.cal $mole^{-1}$.

The effect of addition of PC on the Li and AN reactivity was studied. The results are shown in Fig. 45. The addition of PC, up to 20%, resulted in a lowering of the reaction rates without altering the energy of activation significantly. This probably indicates that the Li + AN reaction is occurring through a film which only lowers the reaction rates without altering the activation energy. PC is known (12) to form an insoluble film of Li_2CO_3 on Li thus protecting it from further attack. With 50% PC, the reaction rates were reduced drastically, and the Arrhenius plots showed two linear regions corresponding to activation energies of 22 and 113 K.cal $mole^{-1}$ for the lower and the upper region respectively. In this mixture, the reaction temperatures are very high and as such complex reactions may occur to give rise to this type of behavior.

The addition of small amounts of SO_2 (3%) to the AN resulted in a sharp reduction of the reaction rates as shown in Fig. 45, without altering the energy of activation. This demonstrates the excellent film forming ability of small amounts of SO_2 and its efficacy in reducing the Li + AN reactivity, the key element in the safety of the Li/SO_2 cells.

Li was found to be stable in MF (methyl formate) at ambient temperature and reacted only at very high temperatures. Surprisingly, the reaction rates were found to be considerably lower than those of the Li + PC. Also the

energy of activation, as determined from the Arrhenius plot shown in Fig. 46 was almost twice that of the Li + PC, viz 43K.cal $mole^{-1}$.

The effect of MF on the Li + AN reaction was studied. The reaction rates increased significantly with 5% MF present giving rise to a non-linear plot as shown in Fig. 46. At higher concentration of MF, the reaction was too rapid, particularly at the higher temperature, so that it was not possible to measure the rates by the isothermal DTA method. A substantial part of the reaction was completed during the heating period so that the slopes were not representative of the reaction rates. The Arrhenius plots with 20% MF were found to be meaningless as shown in Fig. 46. In a normal isothermal DTA run, as shown in Fig. 47 (a), the first short peak represents the difference in temperature between the sample and the reference during the short heating period. Note that the differential temperature reached the base line before it shot up as a result of the exothermic reaction. Also the area under this major peak representing the heat released, is very similar for all the runs at various temperature for a particular system, indicating the correctness of our assumptions regarding reasonable adiabaticity. The abnormal isothermal runs with the Li + AN + MF system, is shown in Fig. 47 (b). Note that the differential temperature does not reach the base line after the first short peak (corresponding to the heating of the sample) prior to the reaction exotherm, indicating that the reaction was already initiated during the heating up period. Also, the areas under these exothermic peaks are different from run to run. These results demonstrate the limitation of this technique which is applicable to only those heterogeneous reactions which have a sufficiently long induction period during which the samples may be heated without any substantial reactions. In systems such as Li + AN + MF, the induction periods are too short, most likely due to the increased solubility of the reaction products in the mixed solvents. Thus, although MF by itself is less reactive to Li, addition of it to AN increased the Li solvent reactivity to a greater extent than the reactivity with the individual solvents. The above results indicate that although pure MF may be used by itself in Li/SO_2 cells, the mixture of MF and AN may be deleterious from a safety stand point. The reported (5) unsafe behavior of Li/SO_2 cells with MF in the electrolyte may be due to the presence of other impurities which may act as

cosolvent with MF to dissolve the protective lithium film.

The Li + DME (dimethoxyethane) reaction was found to be extremely slow at the moderate to high temperatures used in our studies. However, the reactivities of AN + DME mixtures to Li were examined successfully. The Arrhenius plots, shown in Fig. 48 were found to be linear. The reaction rates were increased significantly by the addition of DME to AN and the activation energies were reduced. The results again point to a solubilizing effect of the AN + DME mixed solvents towards the lithium film formed as a result of the Li-solvent reaction.

Similar runs with AN + DG (diglyme) and AN + THF (tetrahydrofuran) systems (Fig. 49) also showed enhanced reactivity.

The energy of activation and the frequency factors of all the above reactions are presented in Table 3.

C. Conclusions:

The isothermal DTA technique developed for studying the kinetics of the heterogeneous reactions involving Li and organic solvents at various temperatures provided an effective tool to assess the usefulness of solvent additives to the Li/SO_2 electrolyte in improving the safety of the Li/SO_2 cells. The results show that whereas SO_2 and PC are effective in reducing the Li + AN reactivity, organic solvents such as MF, DME, THF and DG enhance the Li + AN reactivity and are unsuitable electrolyte additives for safety, although these may be used in place of AN in the electrolyte.

V. General Conclusions and Future Work

We have shown that Li reacts very slowly with SO_2 even in the molten state up to the maximum temperature (370°C) examined in this study. The excellent stability of lithium is due to the kinetic effect of the protective film on the lithium. The DTA results corroborate the observed excellent shelf life and the relative safety of the Li/SO_2 batteries under various conditions of use and abuse.

The organic solvent AN was found to be the most reactive constituent of the cell. The cell discharge product, $Li_2S_2O_4$ was found to decompose exothermally producing S and as such could contribute in sustaining a thermal runaway (initiated by other means) but could not initiate one since the decomposition temperature is above 100°C.

The DTA results on the miniature Li/SO_2 cells corroborated our conclusions from the DTA of individual cell constituents and it was found to be a useful tool for studying the thermal runaway process.

The kinetic studies of the Li-organic solvent reactions were useful in determining the effectiveness of the organic solvent additive (to AN) in reducing the Li and AN reactivity for increased safety. The results show that the solvents MF, DME, DG and THF, although stable by themselves, were unsuitable as additives since they enhance the Li and AN reactivity; most likely due to an enhanced solubilizing effect of the mixed solvent on the Li film. PC was found to be a beneficial solvent in that respect.

We plan to continue some of the above studies. In addition, we plan to do calorimetry of LO26S cells under use and abuse conditions in order to obtain a quantitative measure of the heat released. We also plan to establish the efficacy of some of the approaches developed from the DTA studies, using hermetic Li/SO_2 D size (LO26) cells. The DTA results discussed in this report provide a sound basis for conducting a thorough cell evaluation program in order to establish the possible tradeoffs (in performance and cost) for increased safety of the Li/SO_2 cells.

VI. References

1. P. Bro, R. Holmes, N. Marincic and H. Taylor, Paper No. 45, Proc. Intl. Power Sources Symposium, Brighton, England, 1974.

2. P. Bro, H. Y. Kang, C. Schlaikjer and H. Taylor, Tenth Intersociety Energy Conversion Engineering Conference, Newark, Delaware, p. 432 (1975).

3. H. Taylor and B. McDonald, p. 66, Proc. 27th Power Sources Symposium, Atlantic City, 1976.

4. E. S. Brooks, p. 42 Proc. 26th Power Sources Symposium, Atlantic City, 1974.

5. H. F. Hunger, and J. A. Christopulos, R&D Technical Report ECOM-4292, February 1975.

6. A. N. Dey, Proc. 28th Power Sources Symposium, Atlantic City, 1978.

7. W. Behne, G. Jander, and H. Hecht, Z. Anorg. Allegem. Chem. 269, 249 (1952).

8. P. Shah, p. 59, Proc. 27th Power Sources Symposium, Atlantic City, 1976.

9. G. DiMasi, p. 75, ibid.

10. J. J. Helstrom and G. A. Atwood, Ind. Eng. Chem. Process Res. Dev., 16, 148 (1977).

11. D. D. Wagman, National Bureau of Standard, (Private Communication).

12. A. N. Dey, Thin Solid Films 43, 131 (1977).

13. A. N. Dey, J. Electrochem. Soc. 118, 1547 (1971).

14. A. N. Dey, Paper No. 23, Proc. ECS Symp. on Design and Optimization, Pittsburg Meeting, October 1978.

15. A. Soffer and E. Yeager, Abstract No. 548, Proceedings ECS Meeting Seattle, May 1978.

TABLE 1

List of Possible Chemicals Present in Li/SO_2 Batteries at the Various Stages and Types of Use and Abuse

(a) Starting Materials

1. Li
2. SO_2
3. Carbon black
4. Teflon
5. Aluminum
6. Nickel plated cold rolled steel: Ni, Fe
7. Polypropylene
8. LiBr
9. Acetonitrile
10. Propylene carbonate
11. $LiAsF_6$
12. Methyl formate
13. Other prospective organic solvents such as THF, γ-BL, DME, Dioxolane, etc.
14. Tantalum

(b) Possible Impurities

1. H_2O
2. Mg
3. Na
4. LiOH
5. Propylene glycol
6. CH_3COOH
7. Ni, Fe, Ta salts, heavy trace metals
8. Acrylonitrile
9. Acetamide
10. Propylene
11. Li_2CO_3
12. Li_3N
13. Li_2O

(c) Chemicals Generated

1. Li_2SO_4
2. Br_2
3. Li_2SO_3
4. S
5. S_2Br_2
6. $SOBr_2$
7. Undefined polymers of AN, PC
8. $Li_2S_2O_4$
9. CH_4
10. CS_2
11. H_2S
12. CO_2
13. LiCN

TABLE 2

Summary of DTA Results of the Various Chemicals
And Their Combinations From Table 1; Heating Rate 5 °C/minute

	Chemicals	Temperature of Transitions °C	
		Exothermic	Endothermic
1.	Li	--	188
2.	Carbon	--	--
3.	Celgard (Porous Polypropylene)	--	156
4.	Acetonitrile (AN)	--	--
5.	Propylene Carbonate (PC)	--	--
6.	Teflon powder	--	245
7.	Sulfur	--	112, 120
8.	$Na_2S_2O_4$ (sodium dithionite)	91, 125, 211, 284	--
9.	LiBr	--	--
10.	Li + Celgard	--	152, 191
11.	Li - LiBr	124	188
12.	Li + Teflon powder	279	191
13.	Li + SO_2	--	192
14.	Li + AN	89, 149	--
15.	Li + PC	264, 306	189
16.	Li + AN/PC (50:50)	180, 226	--
17.	Li + AN/PC (95:5)	98	--
18.	Li + SO_2/AN/LiBr (40:40:20)	182, 211	--
19.	Cathode mix from discharged cell	179	--
20.	Above after exposure to air	64, 159, 210	--
21.	Cathode mix from a reversed (force-discharged) cell	58, 177, 237	--
22.	Li + Carbon + $Na_2S_2O_4$	198, 292	184
23.	Li + S	160	110, 121
24.	Li + Li_2SO_3 (as received)	126, 151, 190	187
25.	Li + Li_2SO_3 (dried)	--	189
26.	Li + Al	188	281, 346
27.	LiAl alloy + AN	157, 327	--
28.	Al + AN	--	--
29.	LiAl alloy + SO_2	--	--

TABLE 2 (continued)

Chemicals	Temperature of Transitions °C	
	Exothermic	Endothermic
30. LiAl alloy + AN/SO_2 (75:25)	424	345
31. PC + Br_2	68,150,200,247	--
32. $Na_2S_2O_4$ + Br_2	143, 204	--
33. Br_2 + AN/SO_2/LiBr (40:40:20)	119, 173	--
34. CH_4 + Br_2	324	--
35. Li + CH_4	--	191
36. Li + Diglyme	187, 280, 374	--
37. Li + AN/PC (95:5)	103	--
38. Li + AN/PC (80:20)	86,114,148,190	--
39. Li + DME	432	188
40. Li + AN/DME (95:5)	30	--
41. Li + AN/MF (95:5)	78	--
42. Li + AN/MF (80:20)	102	--
43. Li + AN/MF (50:50)	148	--
44. Li + AN/THF (95:5)	34	--
45. Li + THF	--	188
46. Li + MF	184, 318	--
47. Li + MF/PC (50:50)	184, 235	--
48. Li + AN + Napthalene	75	--
49. Li + $LiAsF_6$	282	190, 269
50. Li + $LiAsF_6$ + AN	189	--
51. Li + S_2Br_2	362, 386, 400	--

TABLE 3

The Activation Energy and the Frequency Factor of Various Li-Organic Solvent Heterogeneous Reactions Determined by Isothermal DTA Method.

	Reactions	Activation Energy K.Cal Mole^{-1}	Frequency Factor
1.	Li + AN	13.1 ± 0.5	8.3
2.	Li (freshly cut) + AN	10.3 ± 0.3	7.1
3.	Li + 0.32 M LiBr, AN	5.9 ± 0.6	4.3
4.	Li + PC	22.3 ± 3.2	9.8
5.	Li + AN/PC (95/5)	15.0 ± 0.6	8.8
6.	Li + AN/PC (80/20)	11.1 ± 0.6	6.6
7.	Li + AN/PC (50/50)	{ 21.7 ± 2.5 { 112.9 ± 22.6	10.8 56.8
8.	Li + AN/SO_2 (97/3)	12.5 ± 2.1	7.0
9.	Li + MF	42.7 ± 5.2	16.7
10.	Li + AN/DME (95/5)	5.9 ± 0.5	3.9
11.	Li + AN/DME (80/20)	9.1 ± 0.9	6.4
12.	Li + AN/DG (95/5)	9.5 ± 0.3	6.6
13.	Li + AN/THF (95/5)	9.6 ± 0.8	6.6

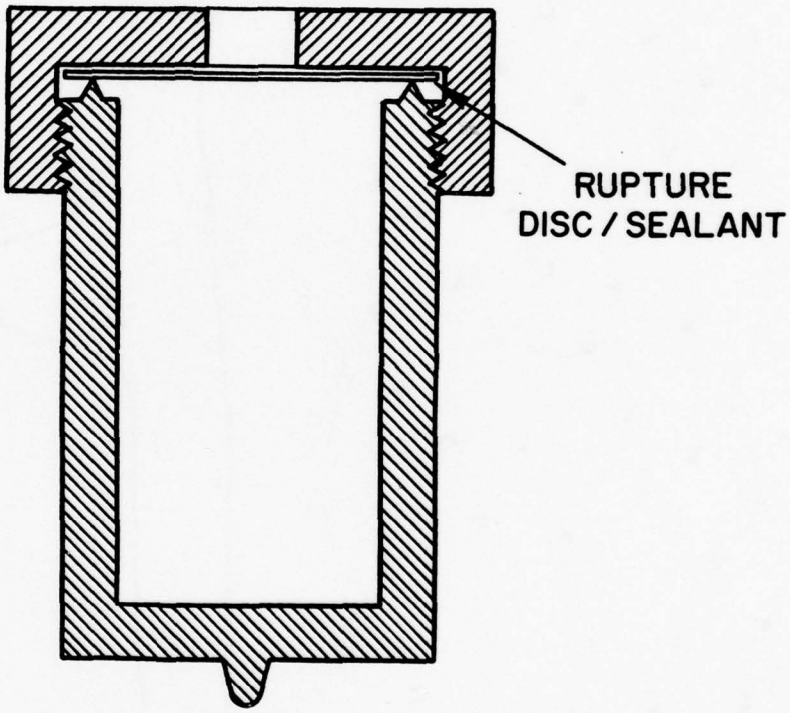

Fig. 1. Cross-Sectional View of the High-Pressure Hermetic Crucible.

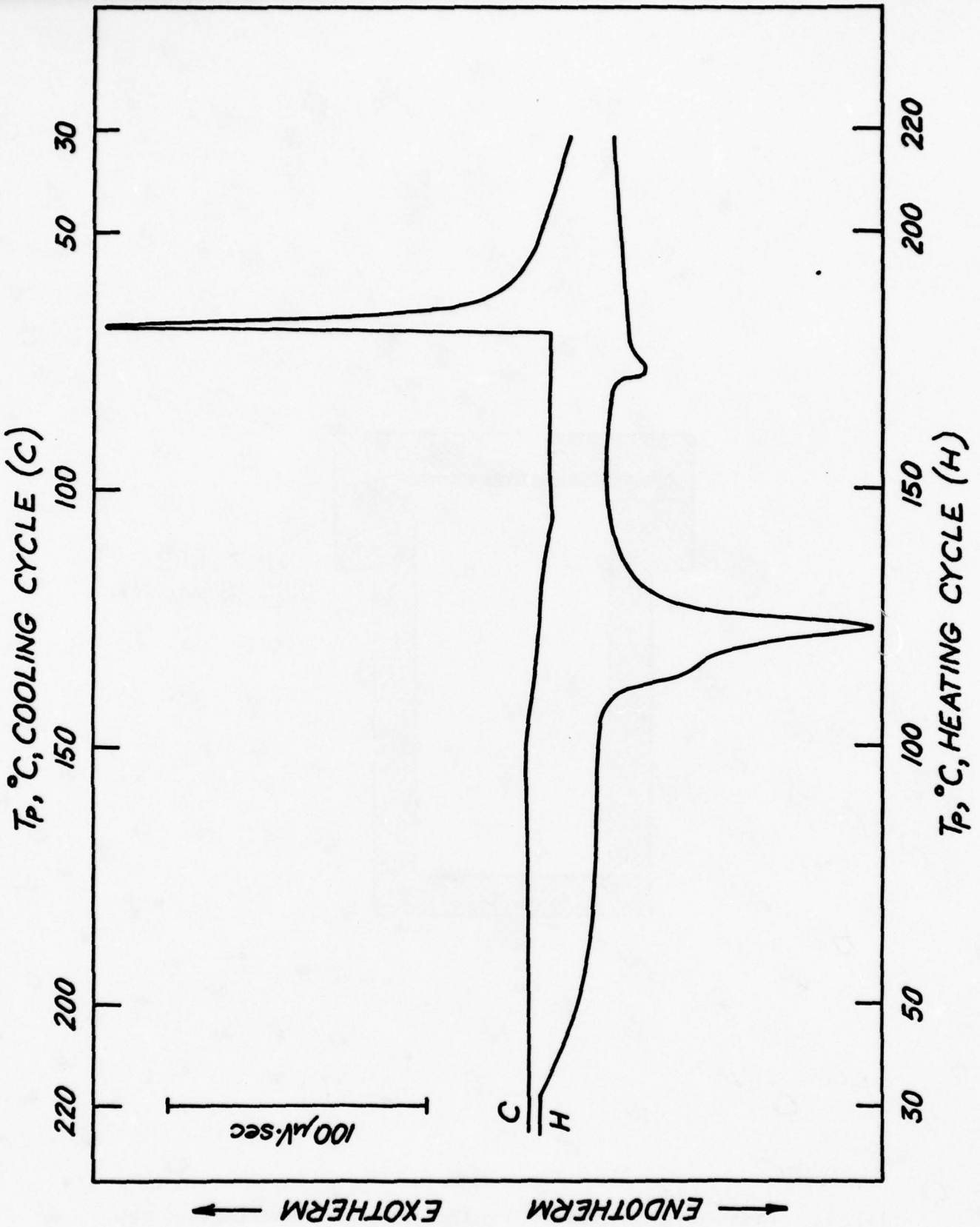

Fig. 2. Thermogram of S (0.0240 gm); 5°C/Minute.

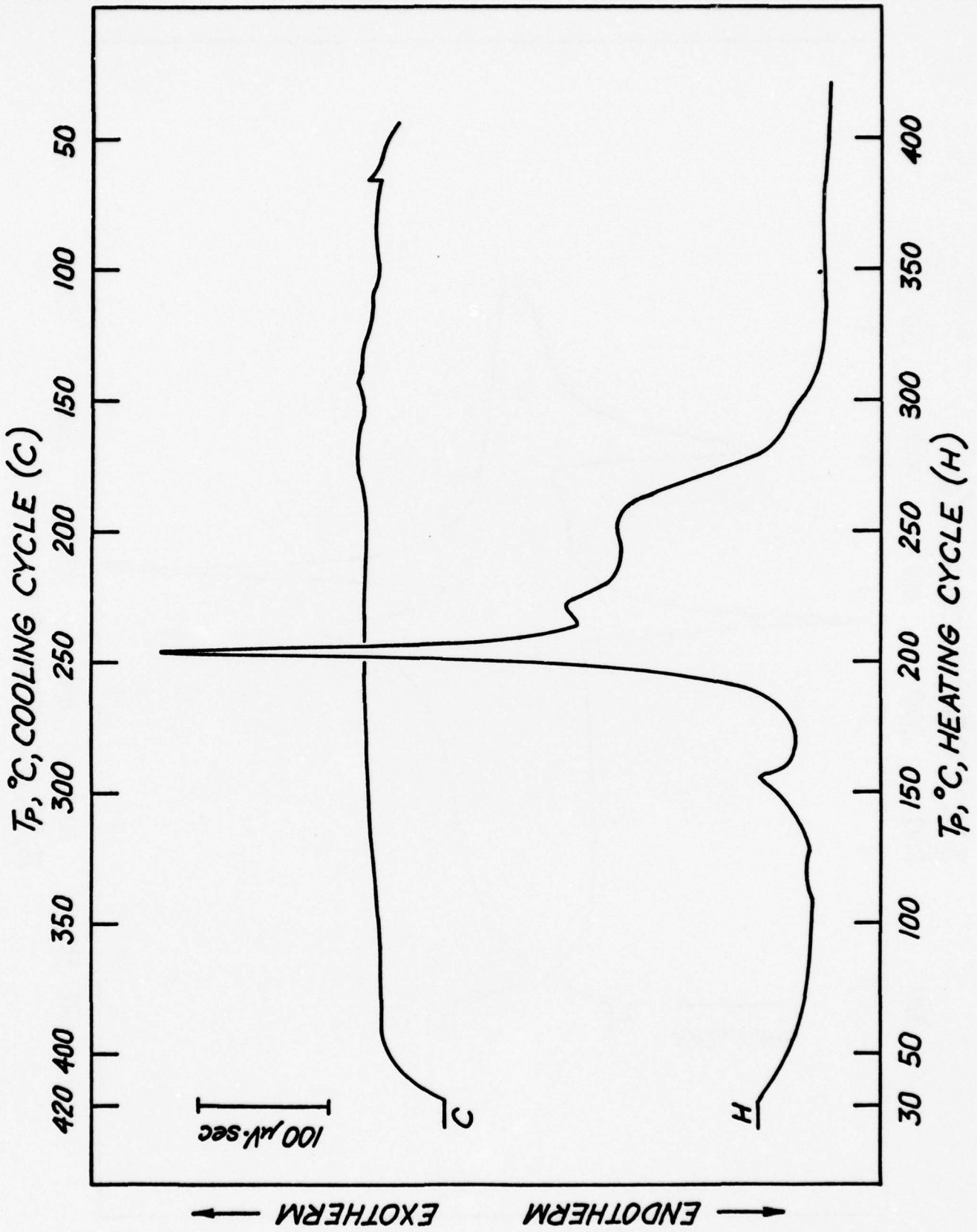

Fig. 3. Thermogram of $Na_2S_2O_4$ (0.333 gm); 5°C/Minute.

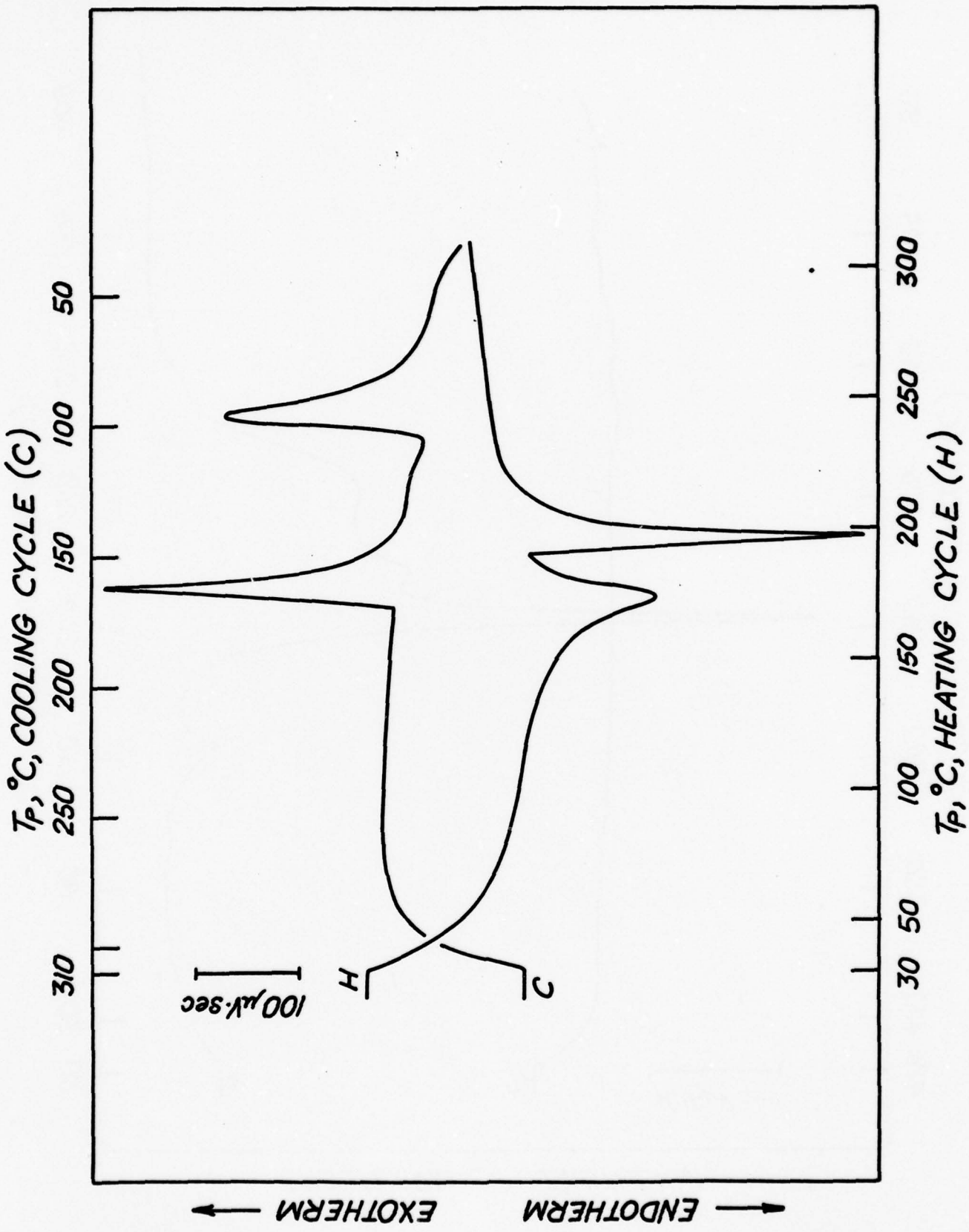

Fig. 4. Thermogram of Li(0.0123 gm) + Celgard (0.0634 gm); 5°C/Minute.

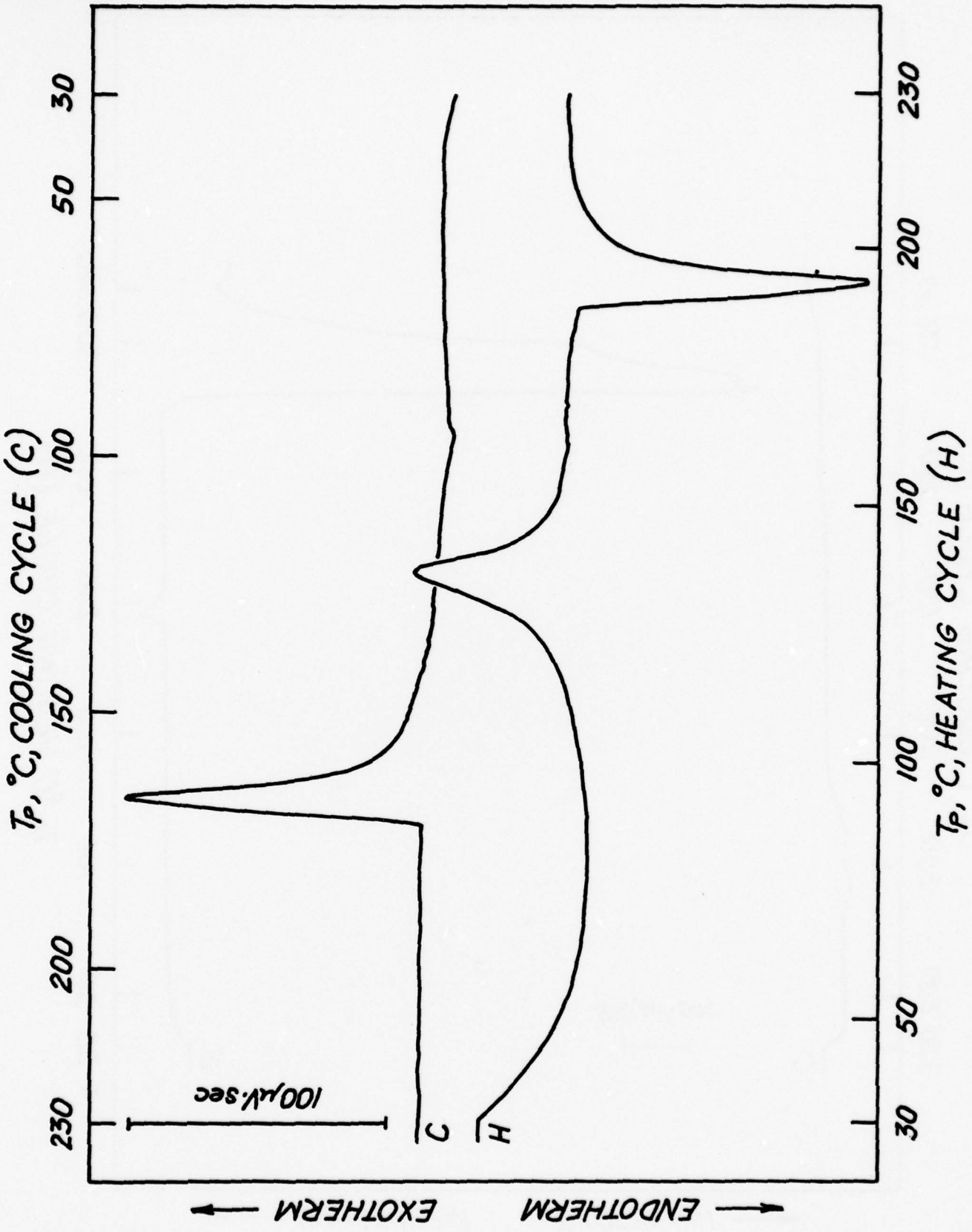

Fig. 5. Thermogram of Li (0.0031 gm) + LiBr (0.0799 gm); 5°C/Minute.

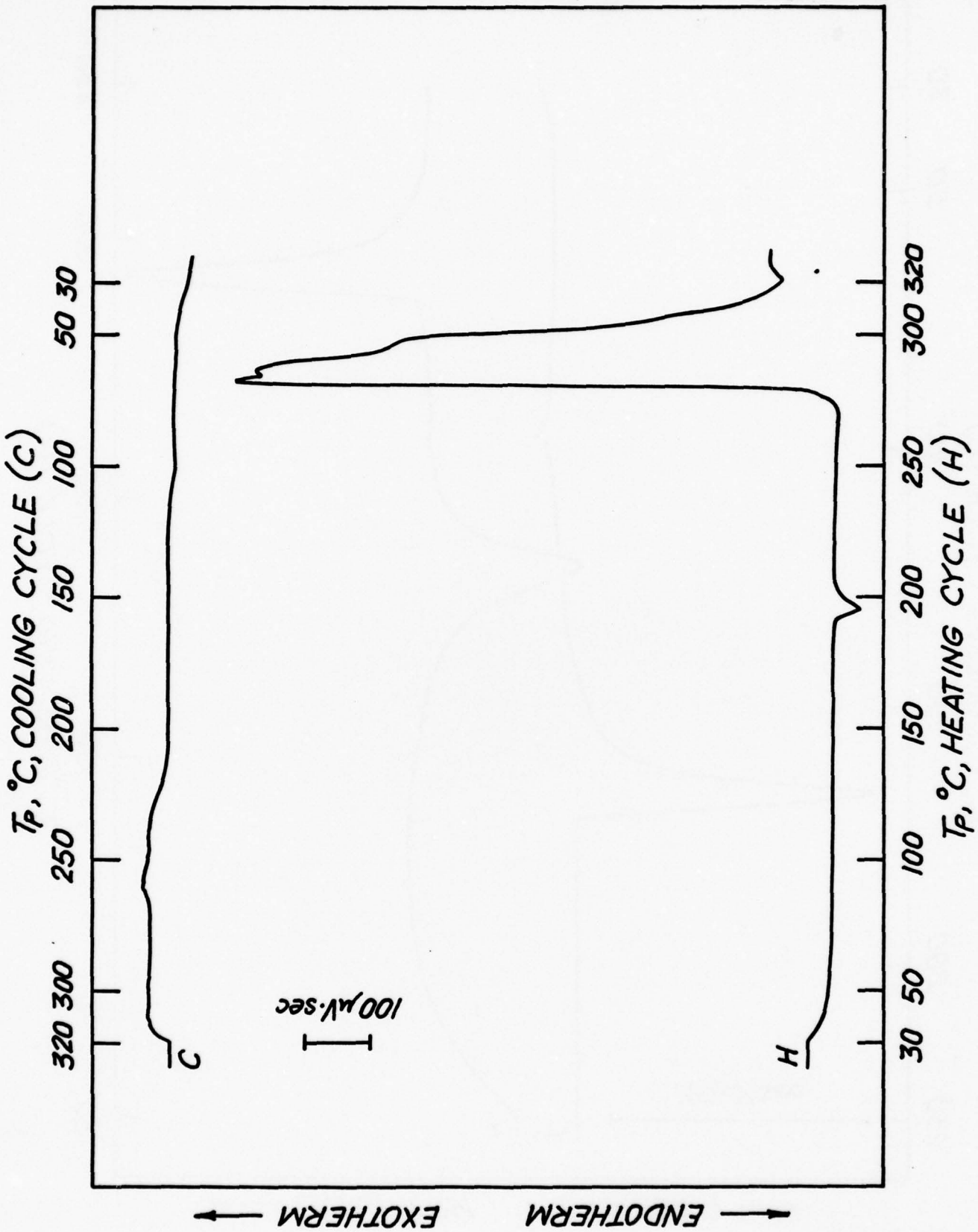

Fig. 6. Thermogram of Li (0.008 gm) + Teflon Powder (0.234 gm); 5°C/Minute.

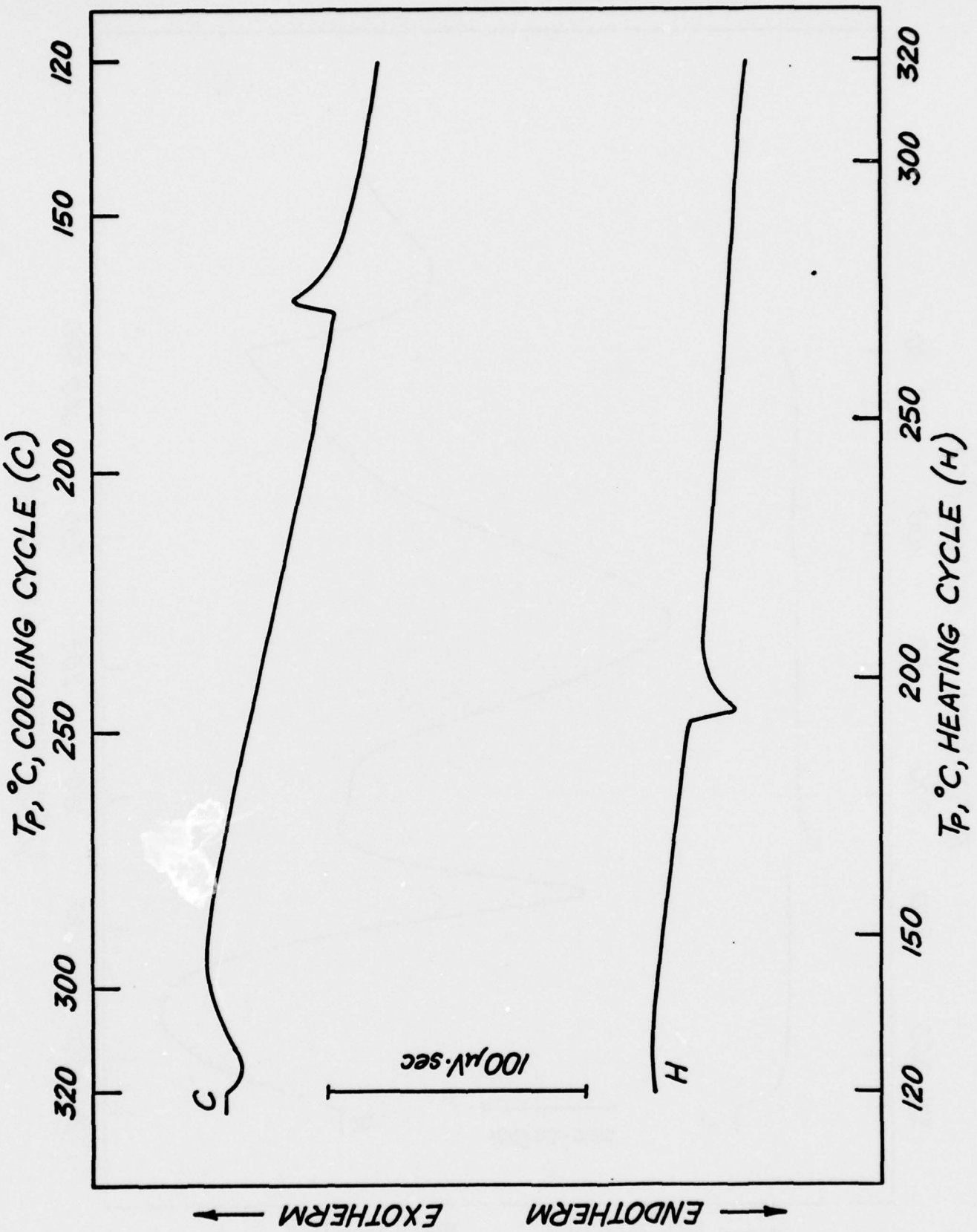

Fig. 7. Thermogram of Li (0.00029 gm) + SO_2; 5°C/Minute.

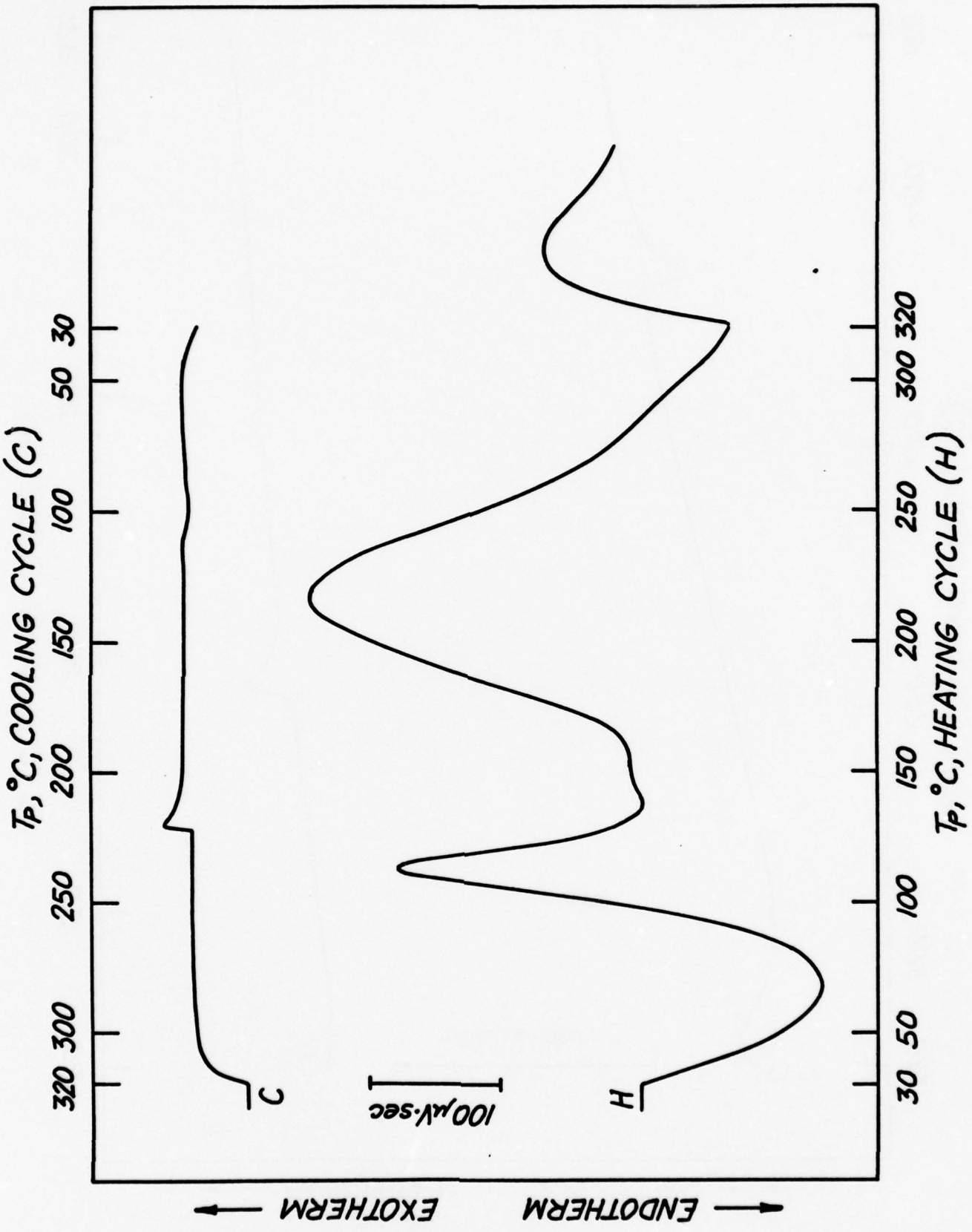

Fig. 8. Thermogram of Li (0.0010 gm) + AN (100 μl); 5°C/Minute.

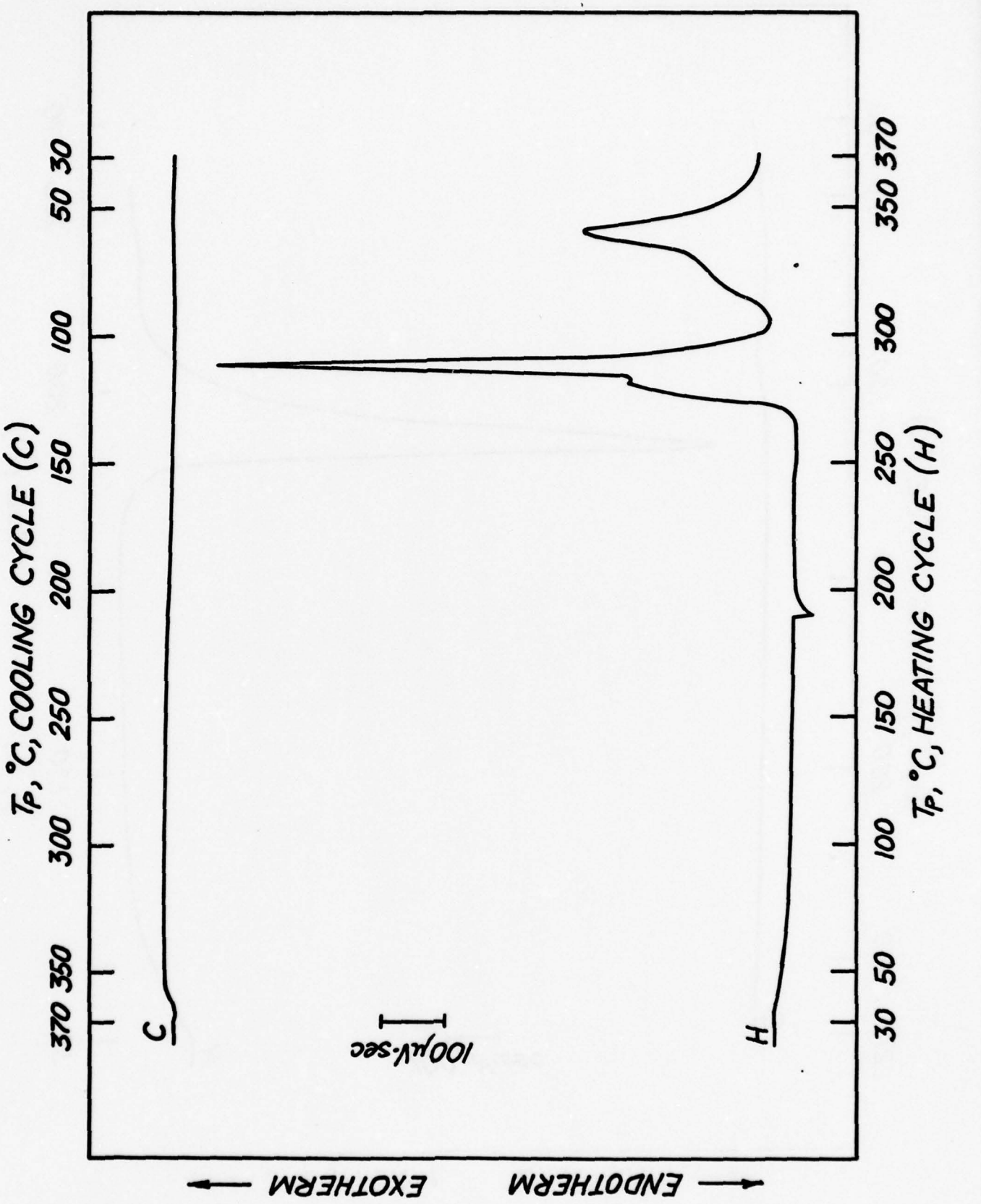

Fig. 9. Thermogram of Li (0.0008 gm) + PC (20 μl); 5°C/Minute.

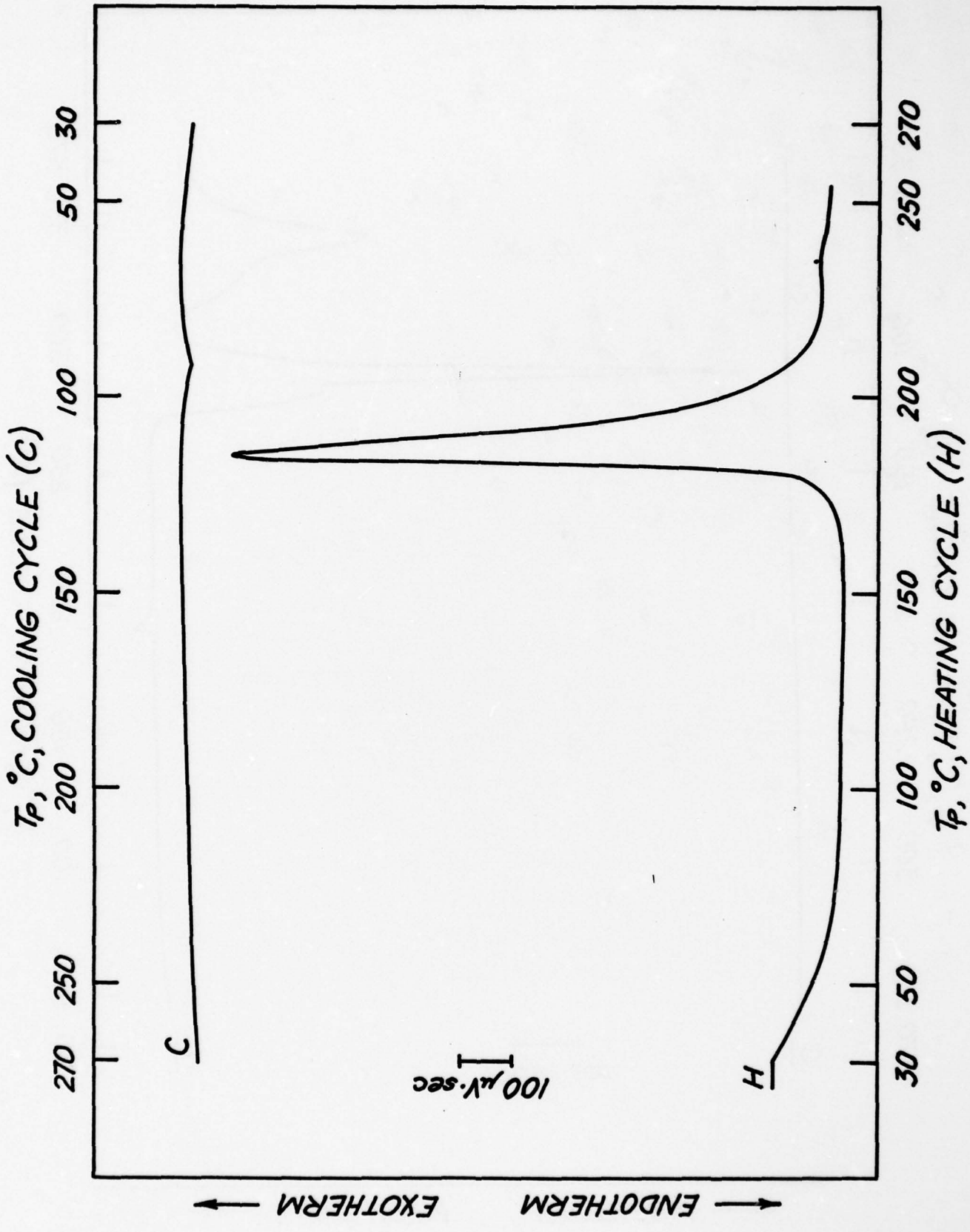

Fig. 10. Thermogram of Li (0.0003 gm) + AN/PC (50:50) 80 μl; 5°C/Minute.

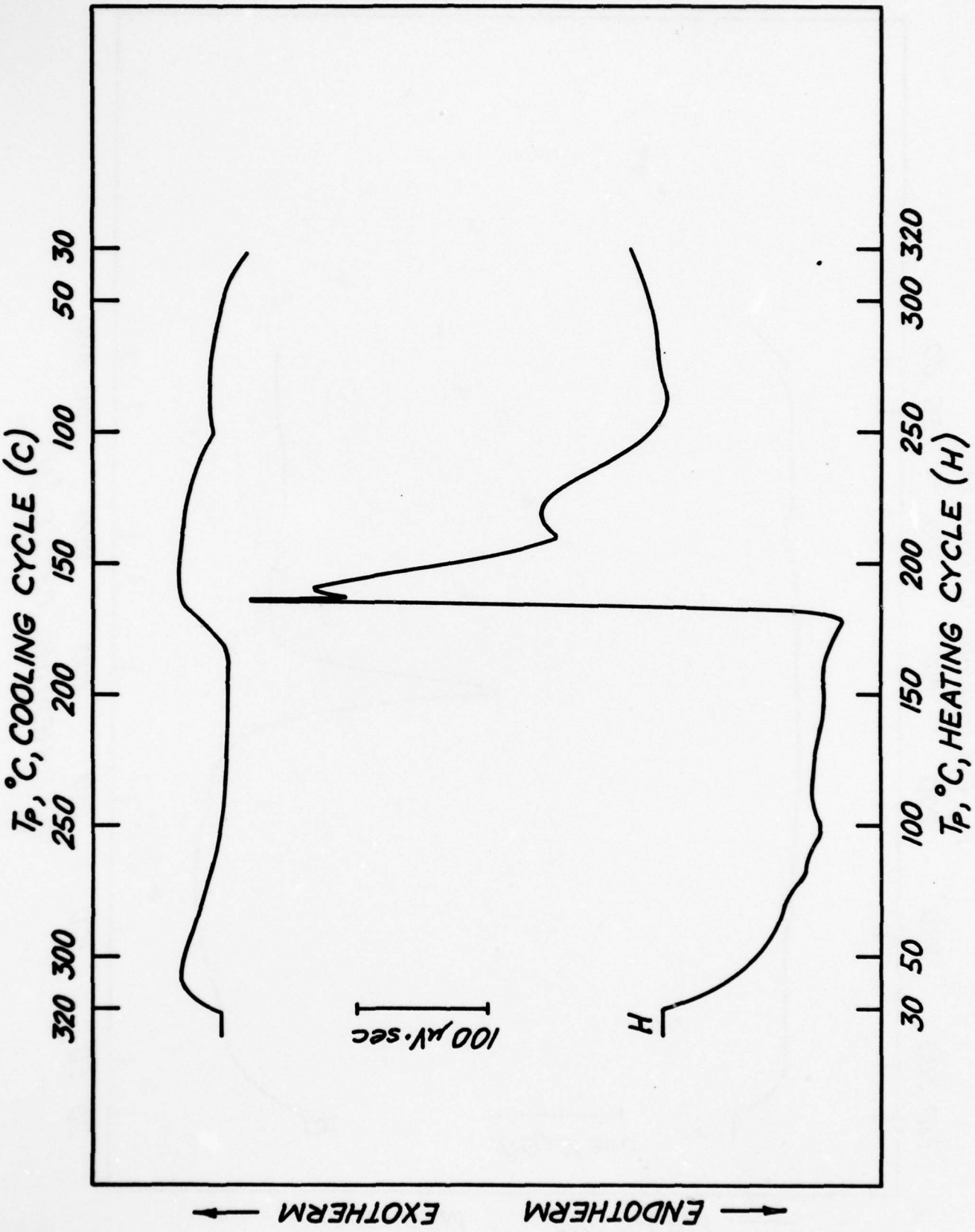

Fig. 11. Thermogram of Li (0.00085 gm) + Electrolyte (40% SO_2, 40% AN, 20% LiBr) ~ 25 μl; 5°C/Minute.

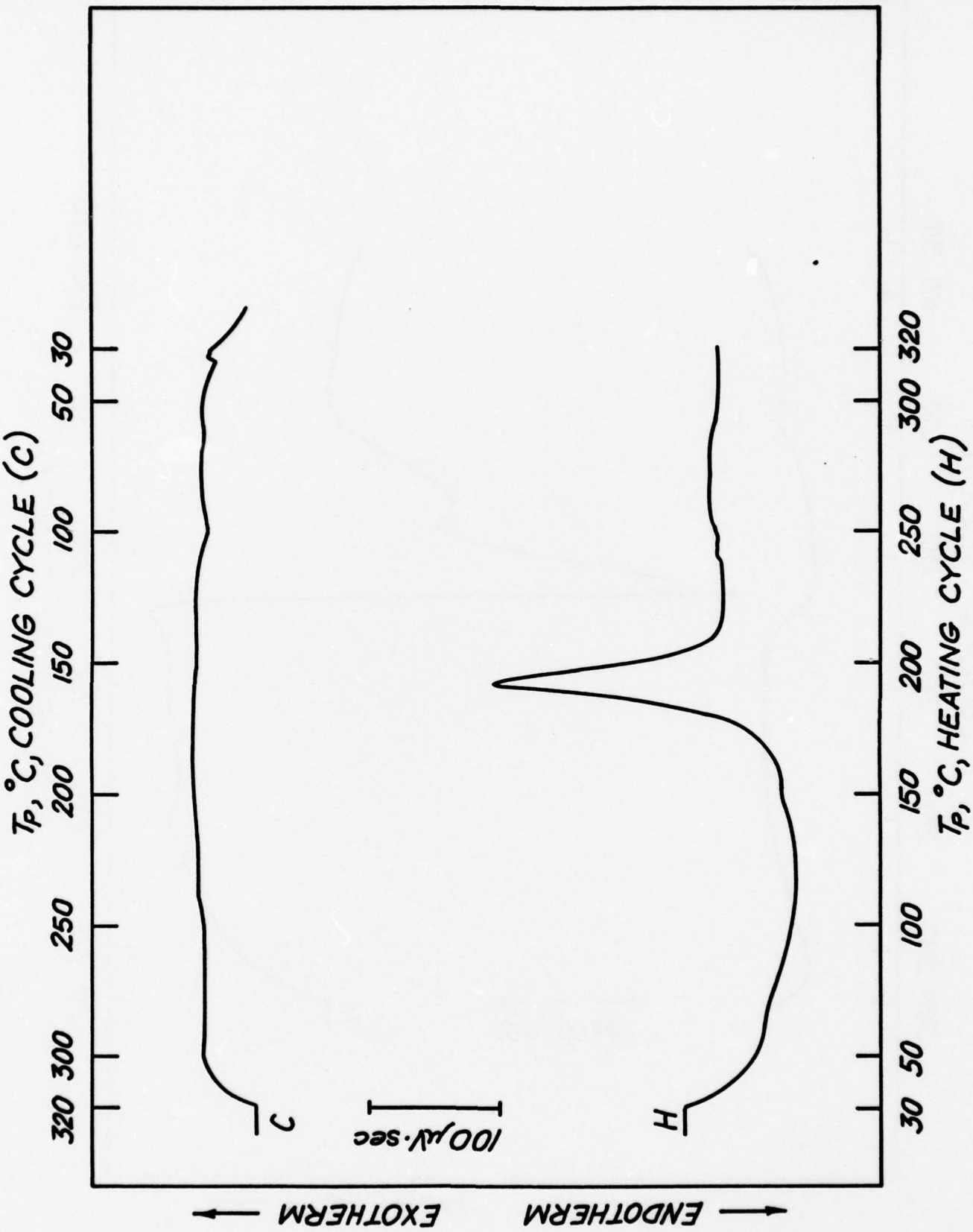

Fig. 12. Thermogram of Cathode Mix (0.0661 gm) from a Discharged Li/SO_2 Cell; 5°C/Minute.

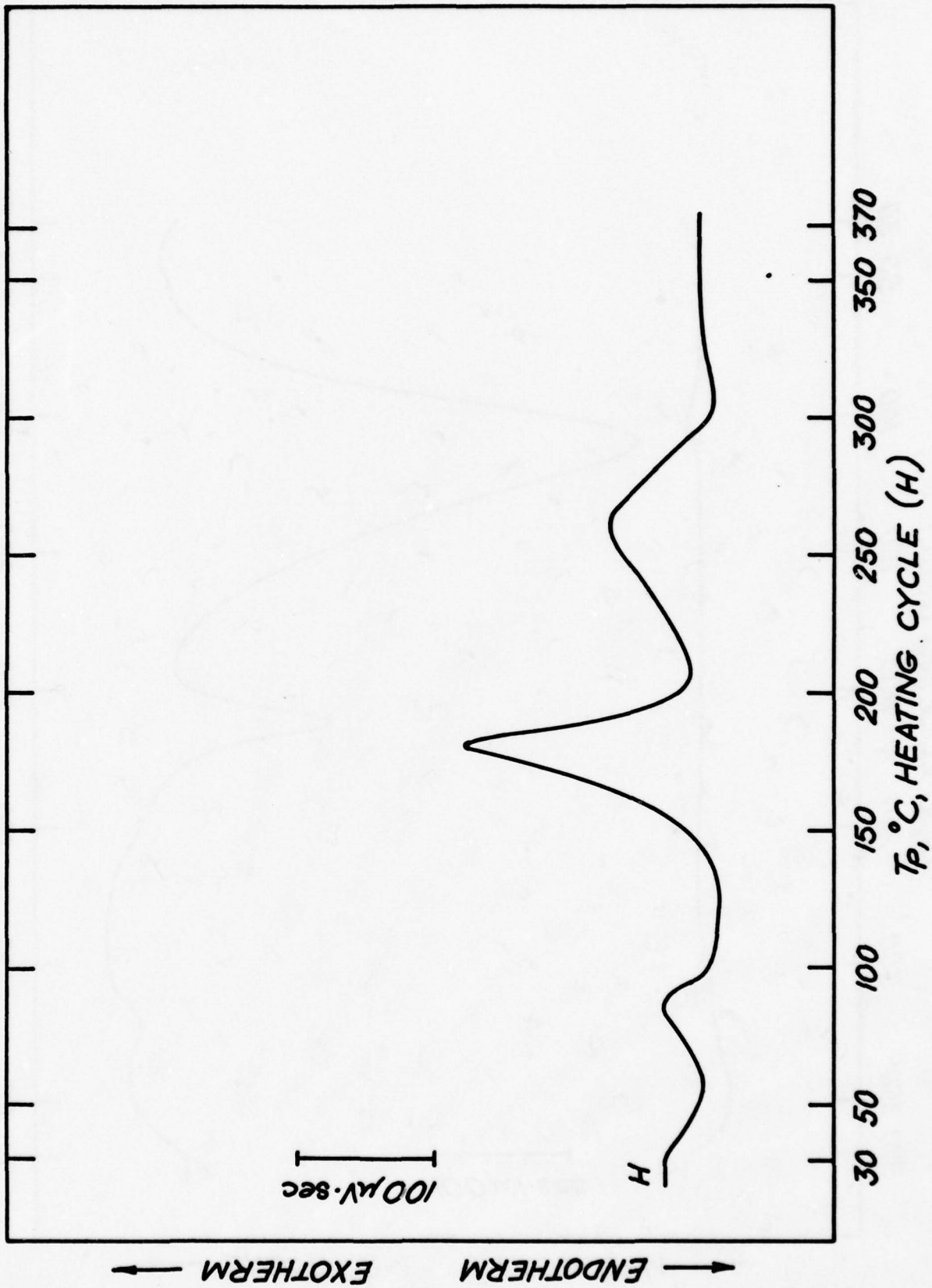

Fig. 13. Thermogram of Cathode Mix (0.819 gm) from a Discharged Li/SO_2 Cell after Exposure to Air; 5°C/Minute.

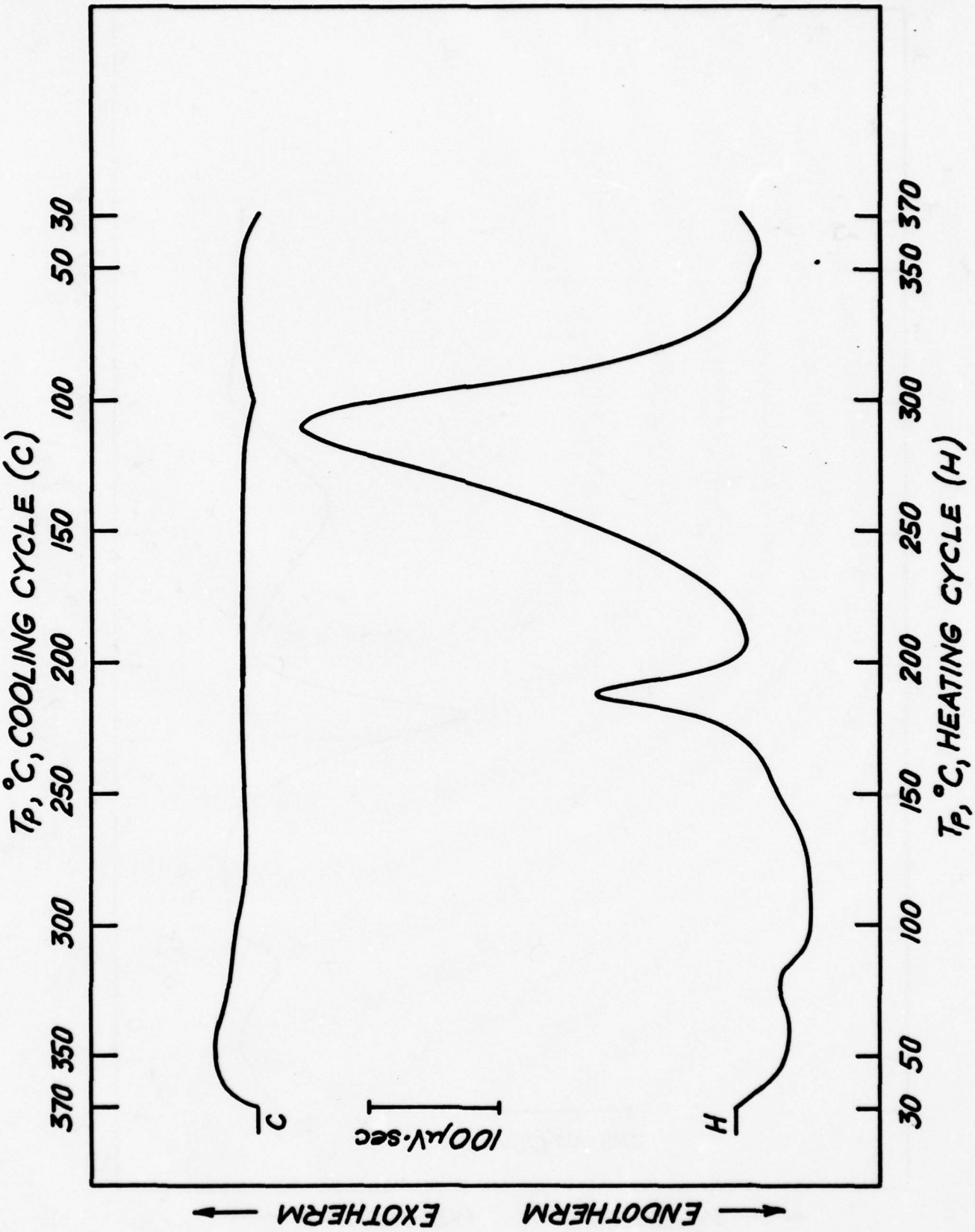

Fig. 14. Thermogram of Cathode Mix (0.0624 gm) from a Li/SO_2 Cell which was Discharged and then Driven into Reversal for 10% of Its Discharged Capacity; 5°C/Minute.

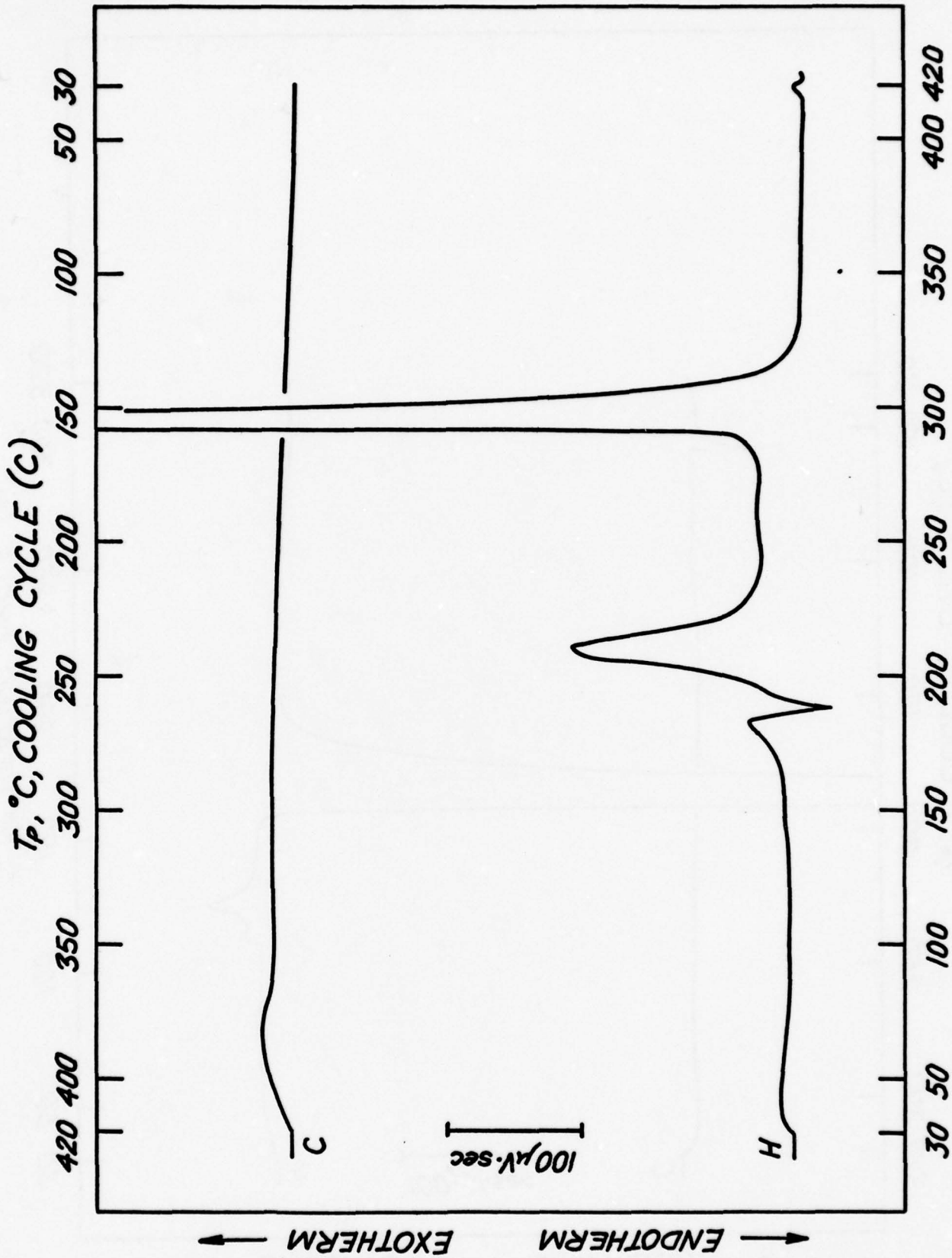

Fig. 15. Thermogram of $Na_2S_2O_4$ (0.01007 gm) + Li Powder (0.00131 gm) + Carbon (0.00284 gm); 5 °C/Minute.

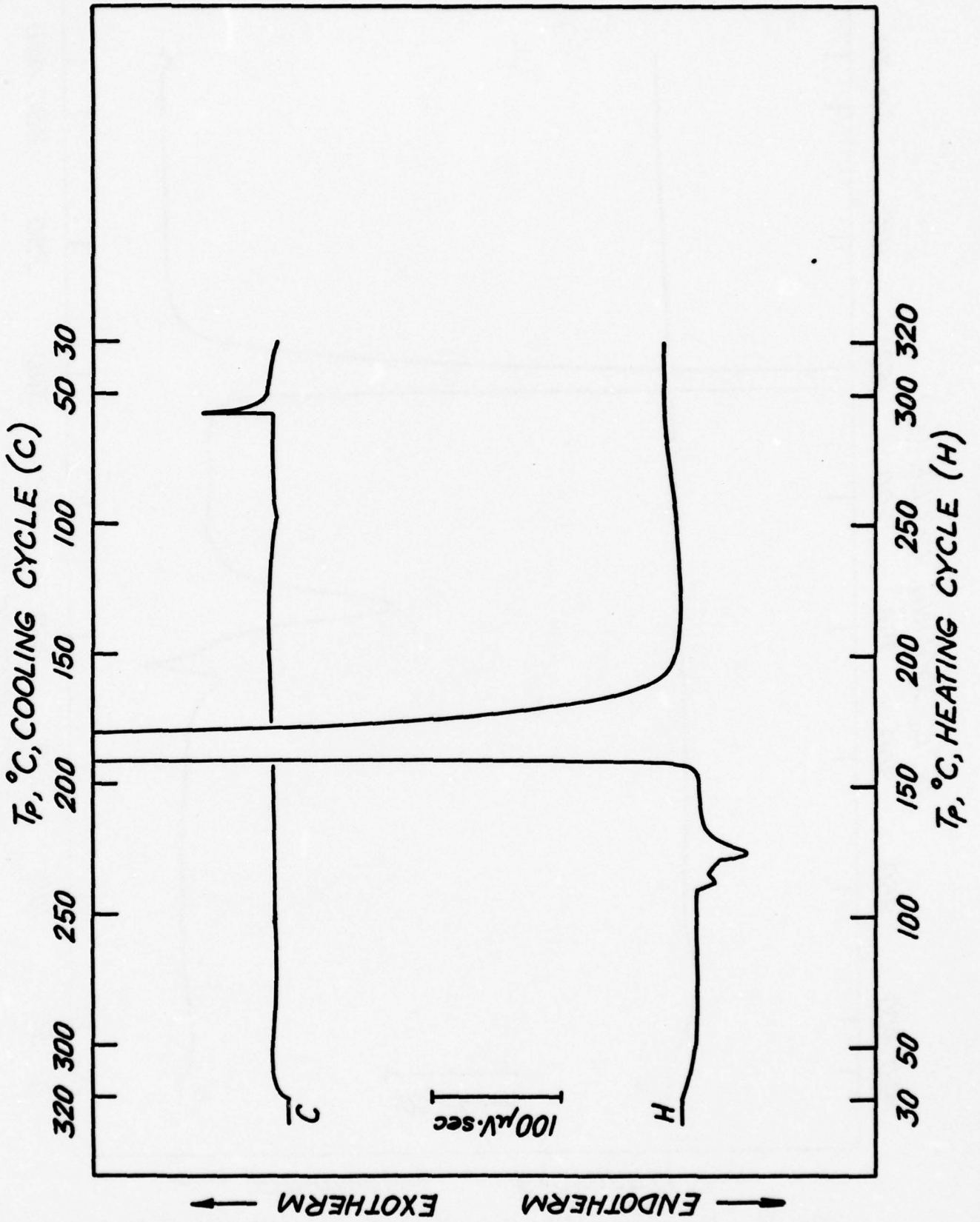

Fig. 16. Thermogram of Li (0.0015 gm)+ S (0.0079 gm); 5°C/Minute.

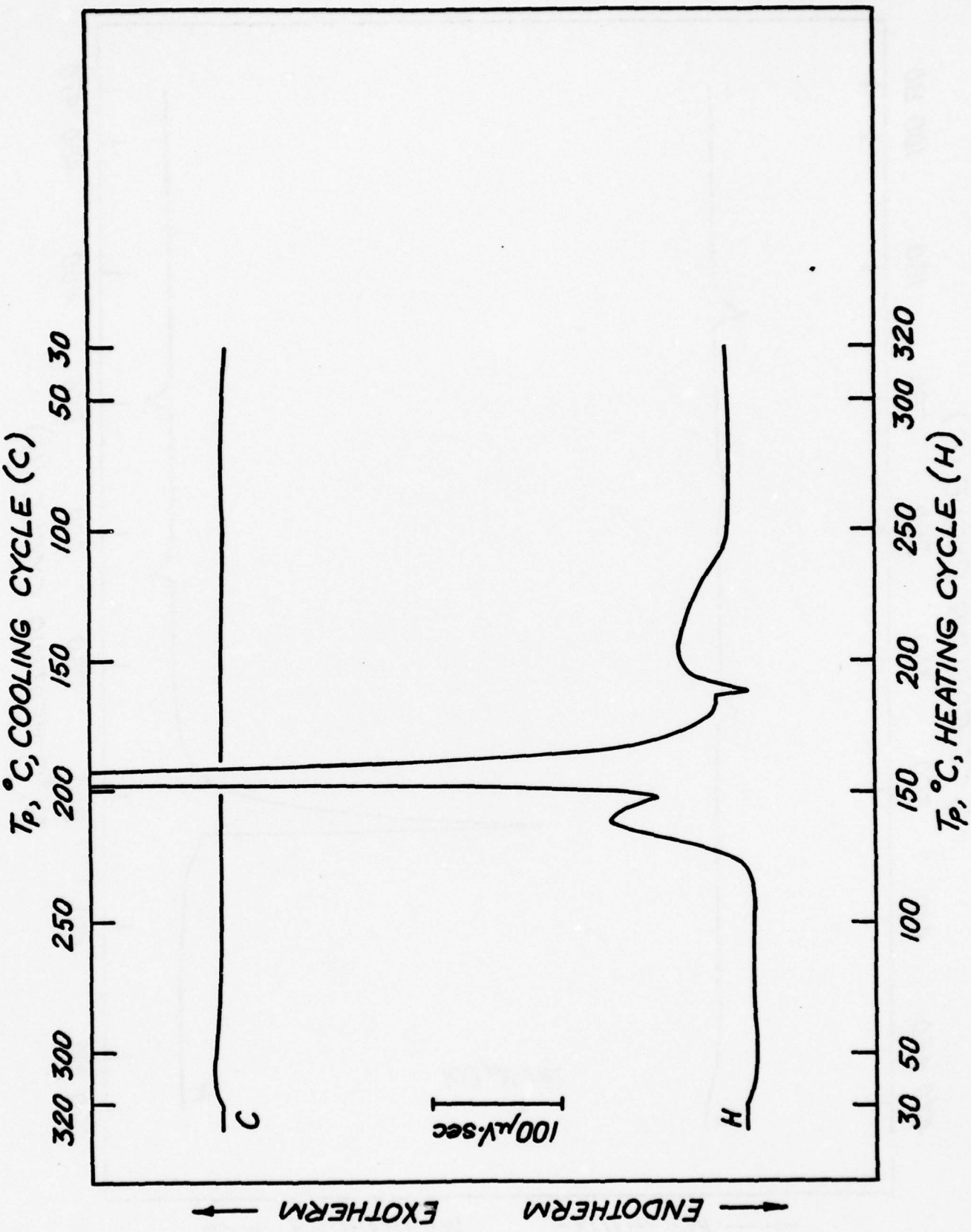

Fig. 17. Thermogram of Li (0.00094 gm) + Li_2SO_3 (0.0075 gm) As-Received; 5°C/Minute.

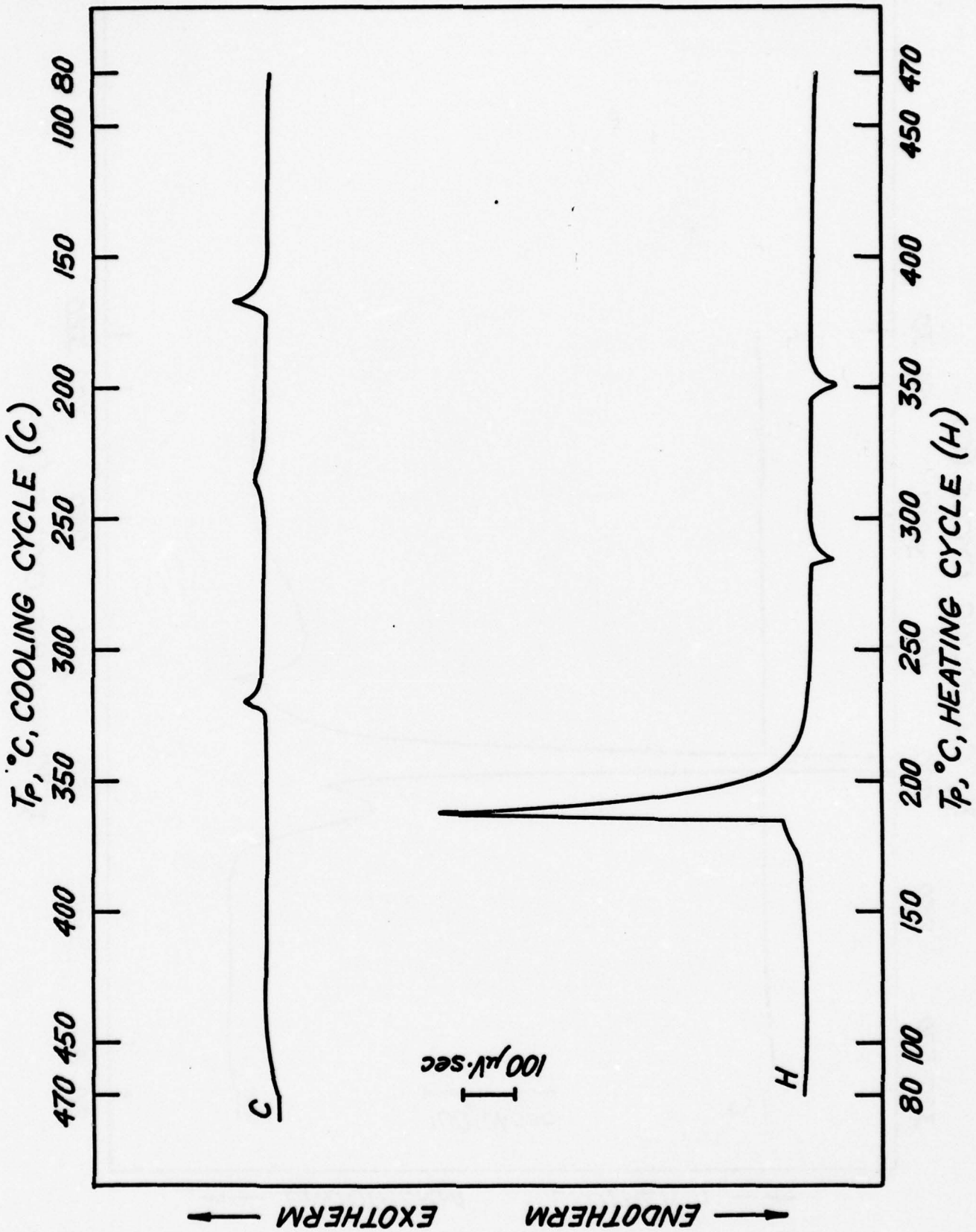

Fig. 18. Thermogram of Li (0.00572 gm) + Al (0.00720 gm); 5°C/Minute.

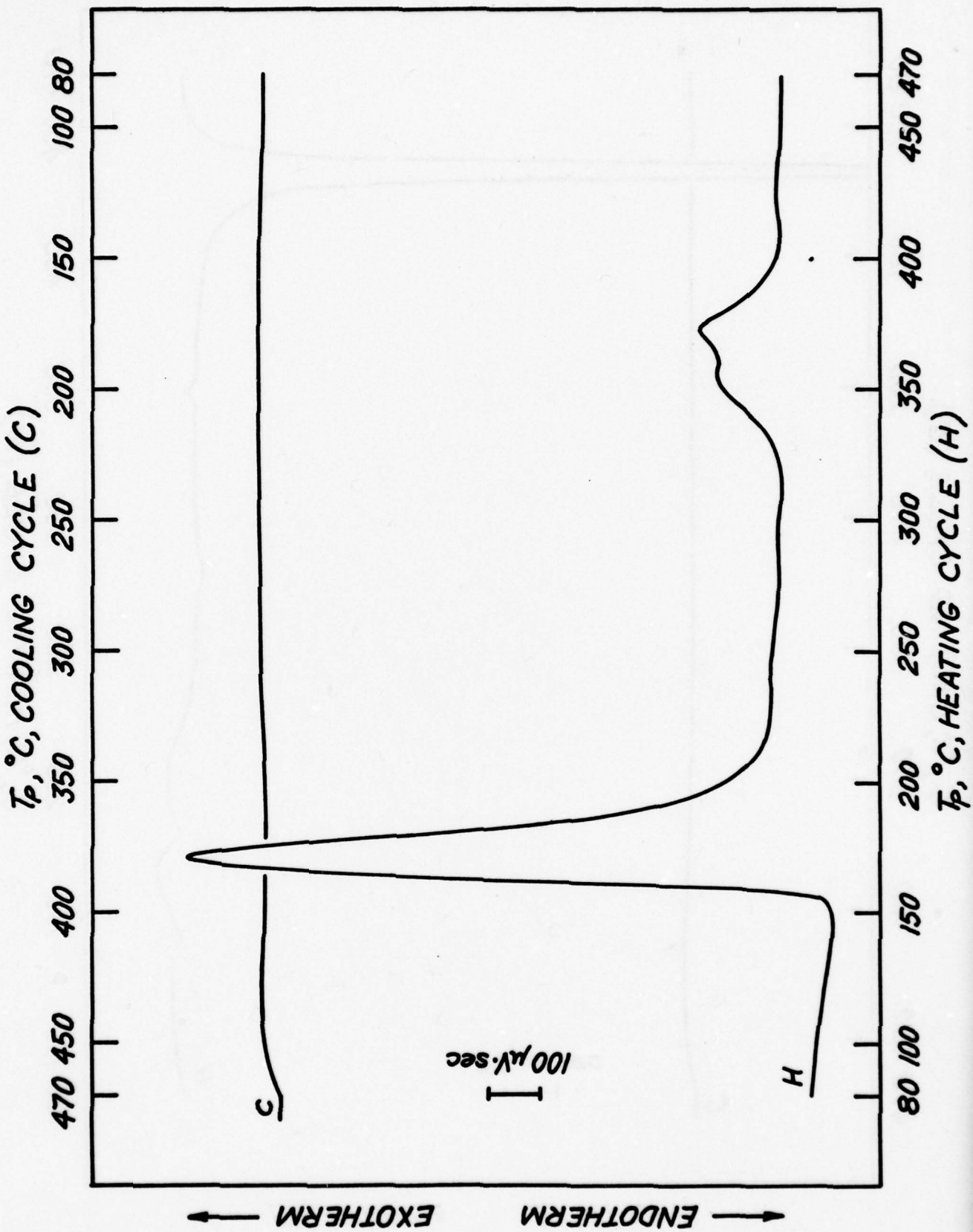

Fig. 19. Thermogram of LiAl Alloy (0.01333 gm) + AN; 5°C/Minute.

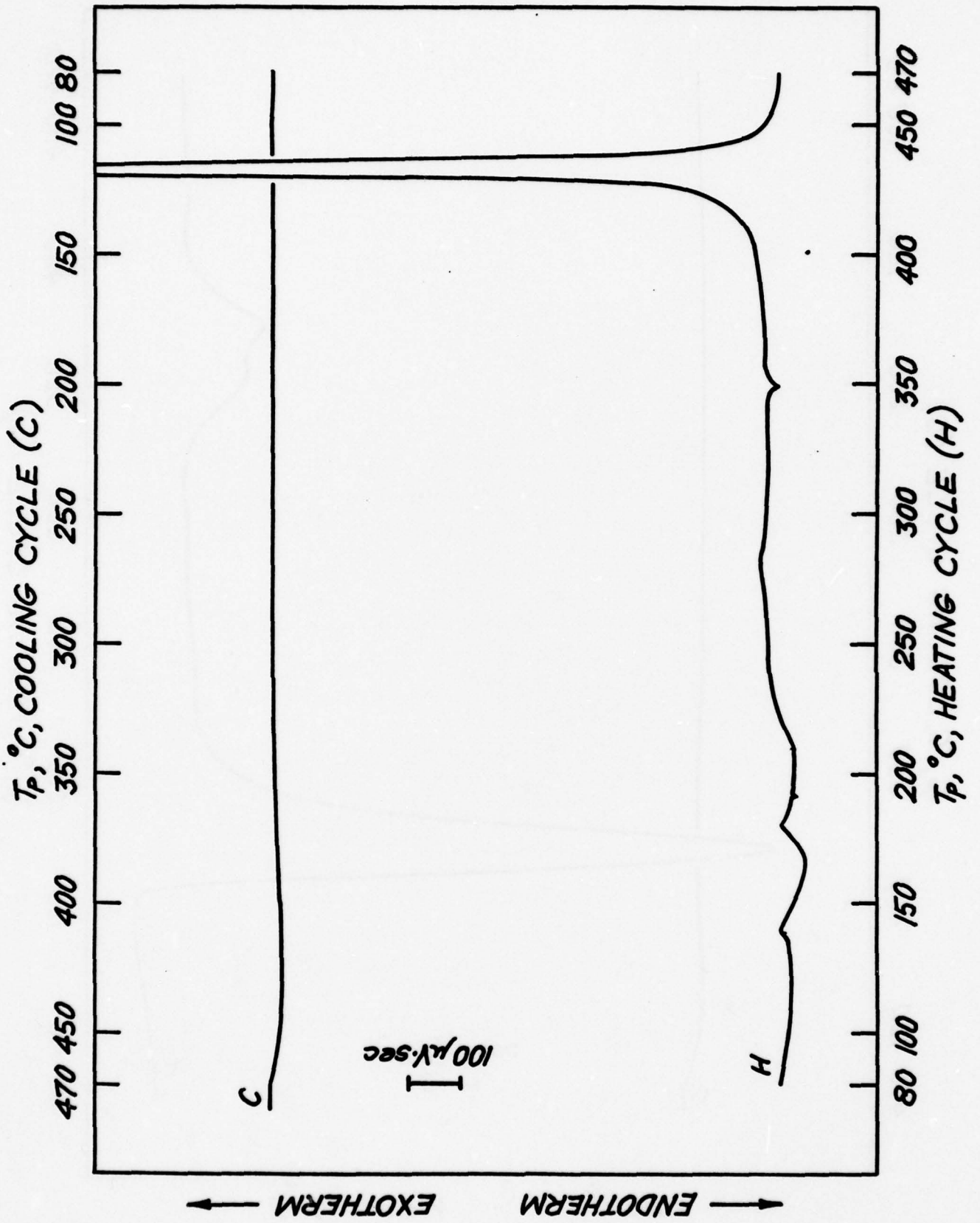

Fig. 20. Thermogram of LiAl Alloy + AN/SO_2 (75:25) 20μl; 5°C/Minute.

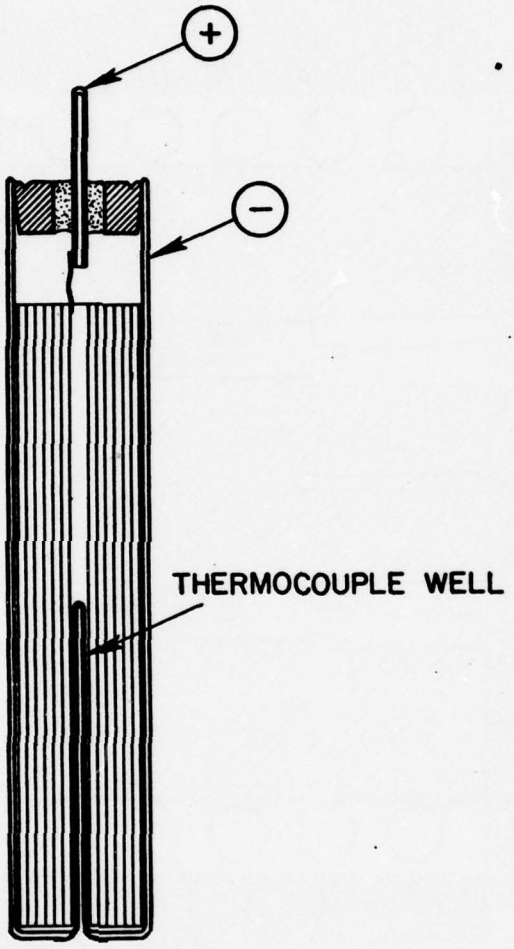

Fig. 21. Cross-Section View of the Miniature Li/SO_2 Cell.

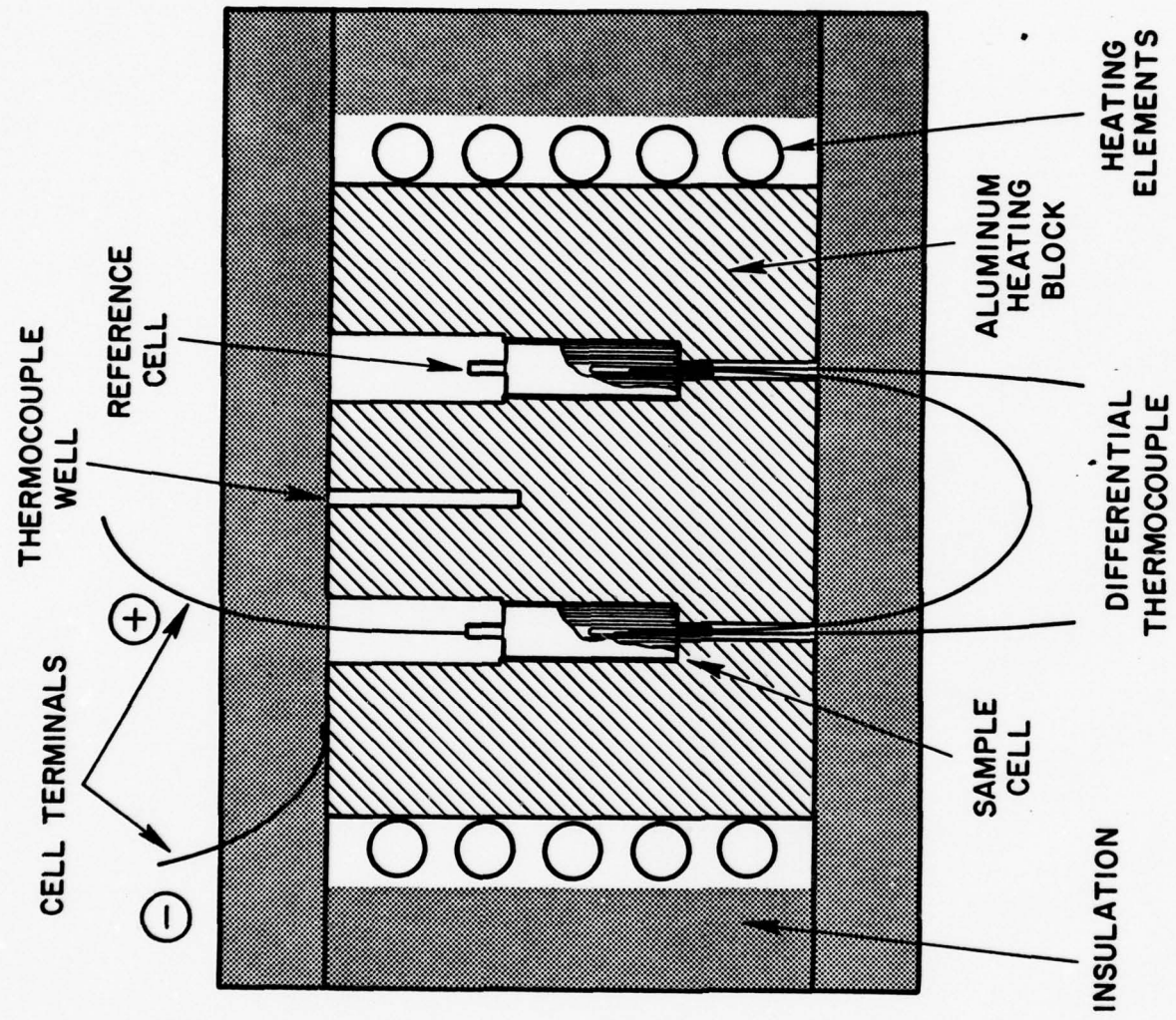

Fig. 22. Fixtures for DTA of Miniature Cell.

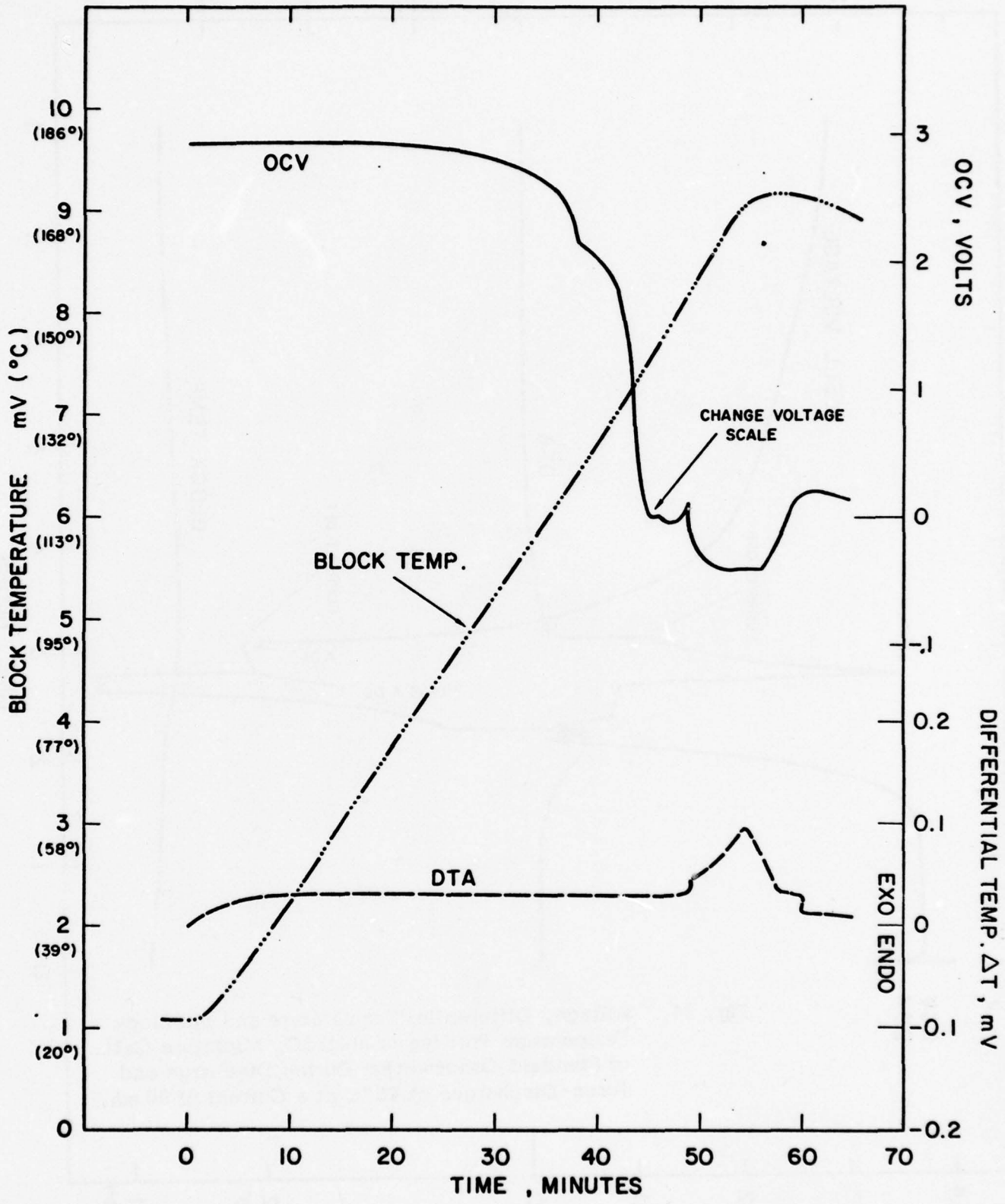

Fig. 23. Thermogram of a Discharged Miniature Li/SO_2 Cell of Standard Construction, Discharge Current 1 mA; Discharge Capacity 193 mAHr.

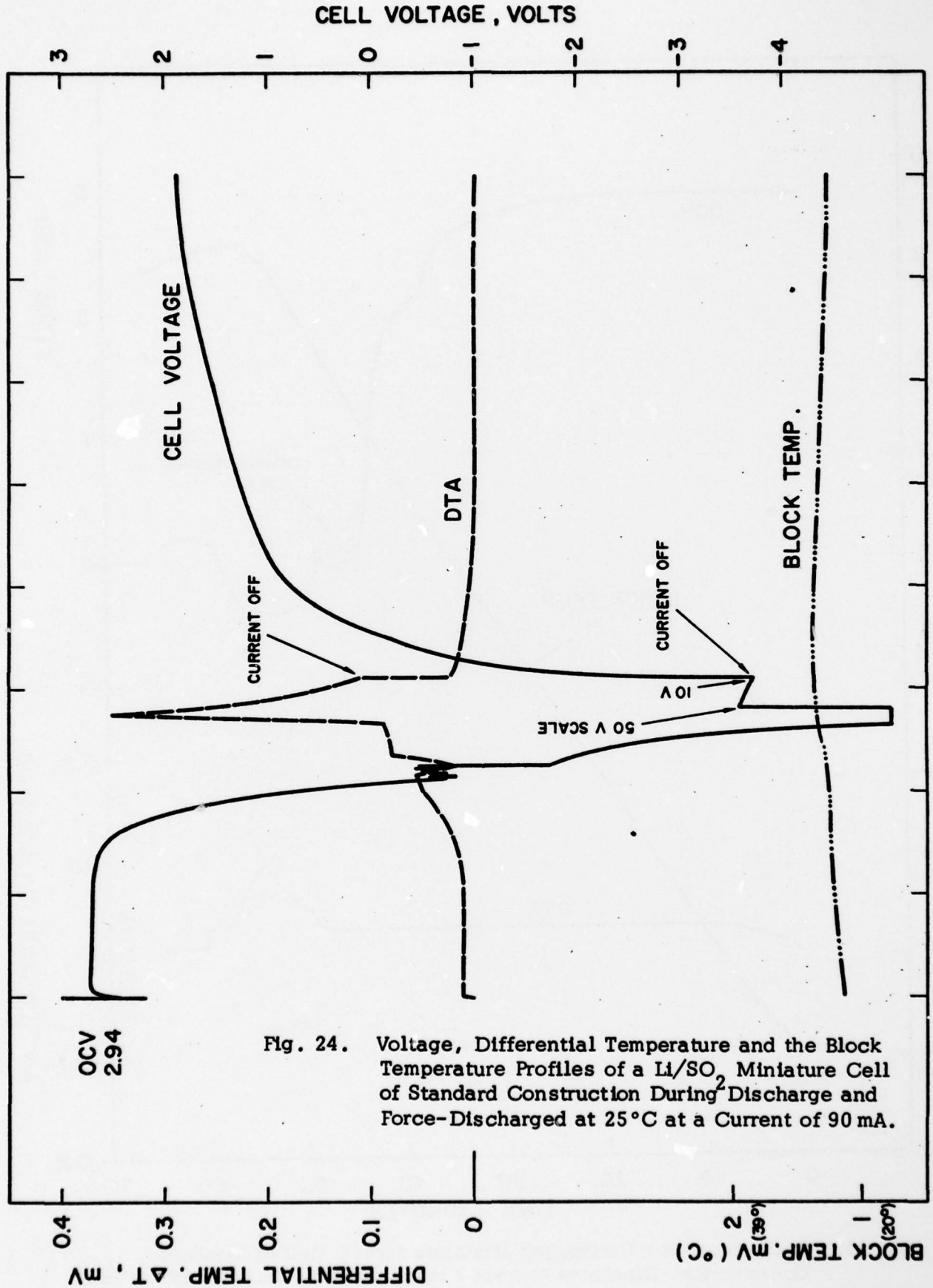

Fig. 24. Voltage, Differential Temperature and the Block Temperature Profiles of a Li/SO_2 Miniature Cell of Standard Construction During Discharge and Force-Discharged at 25°C at a Current of 90 mA.

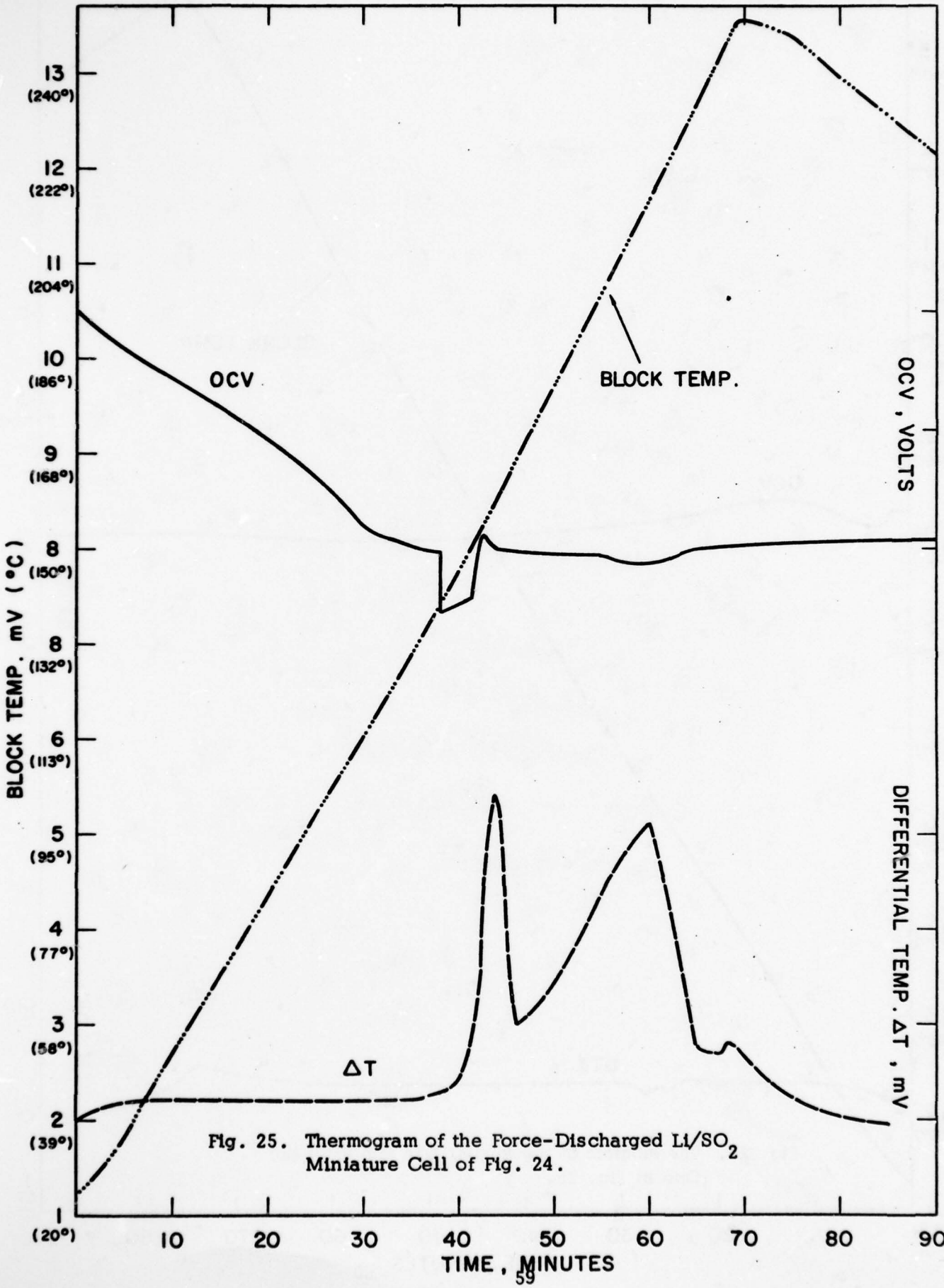

Fig. 25. Thermogram of the Force-Discharged Li/SO_2 Miniature Cell of Fig. 24.

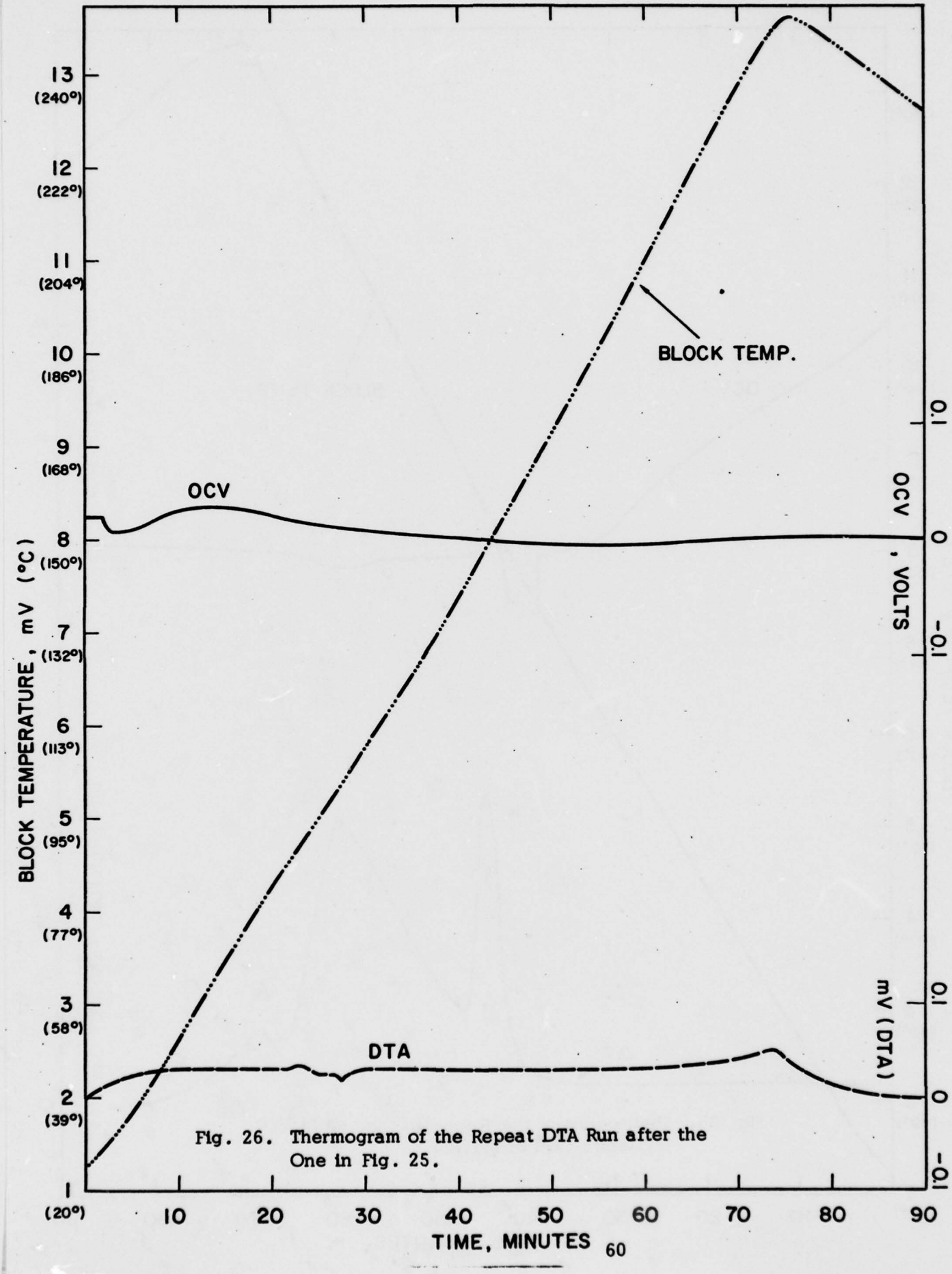

Fig. 26. Thermogram of the Repeat DTA Run after the One in Fig. 25.

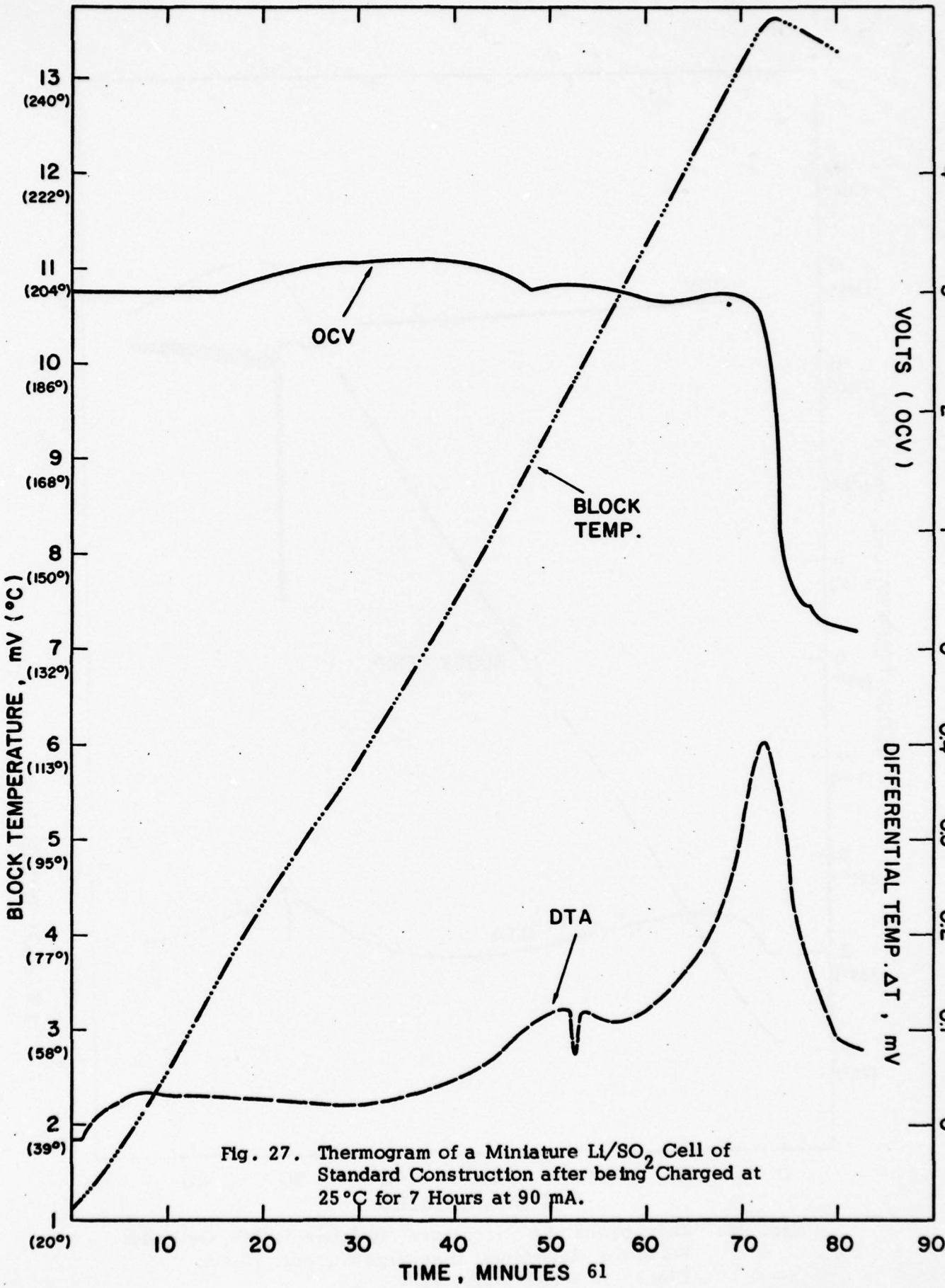

Fig. 27. Thermogram of a Miniature Li/SO_2 Cell of Standard Construction after being Charged at 25°C for 7 Hours at 90 mA.

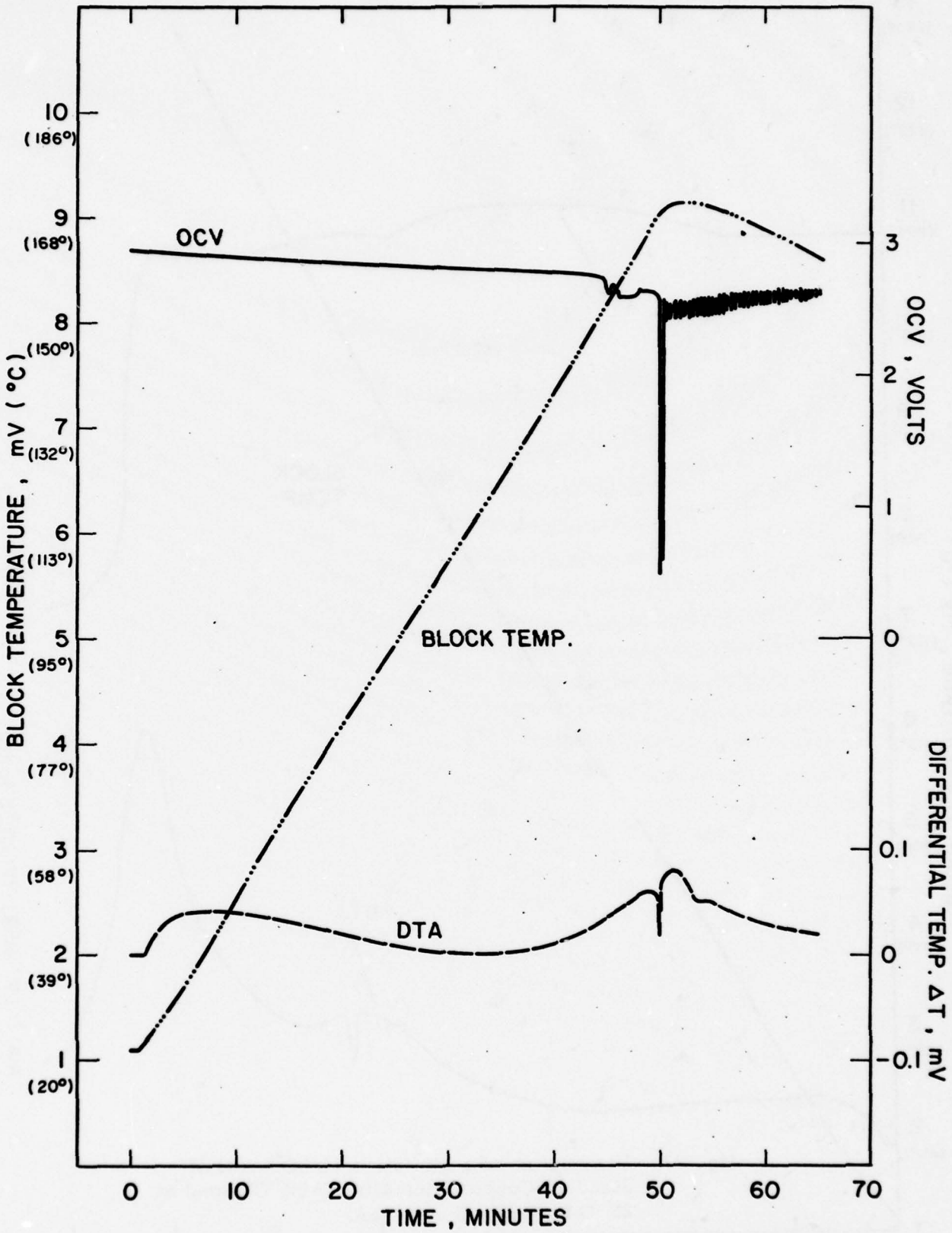

Fig. 28. Thermogram of a Discharged Miniature Li/SO_2 Cell with PC in the Electrolyte; Discharge Current, 10 mA; Discharge Temperature, 25°C.

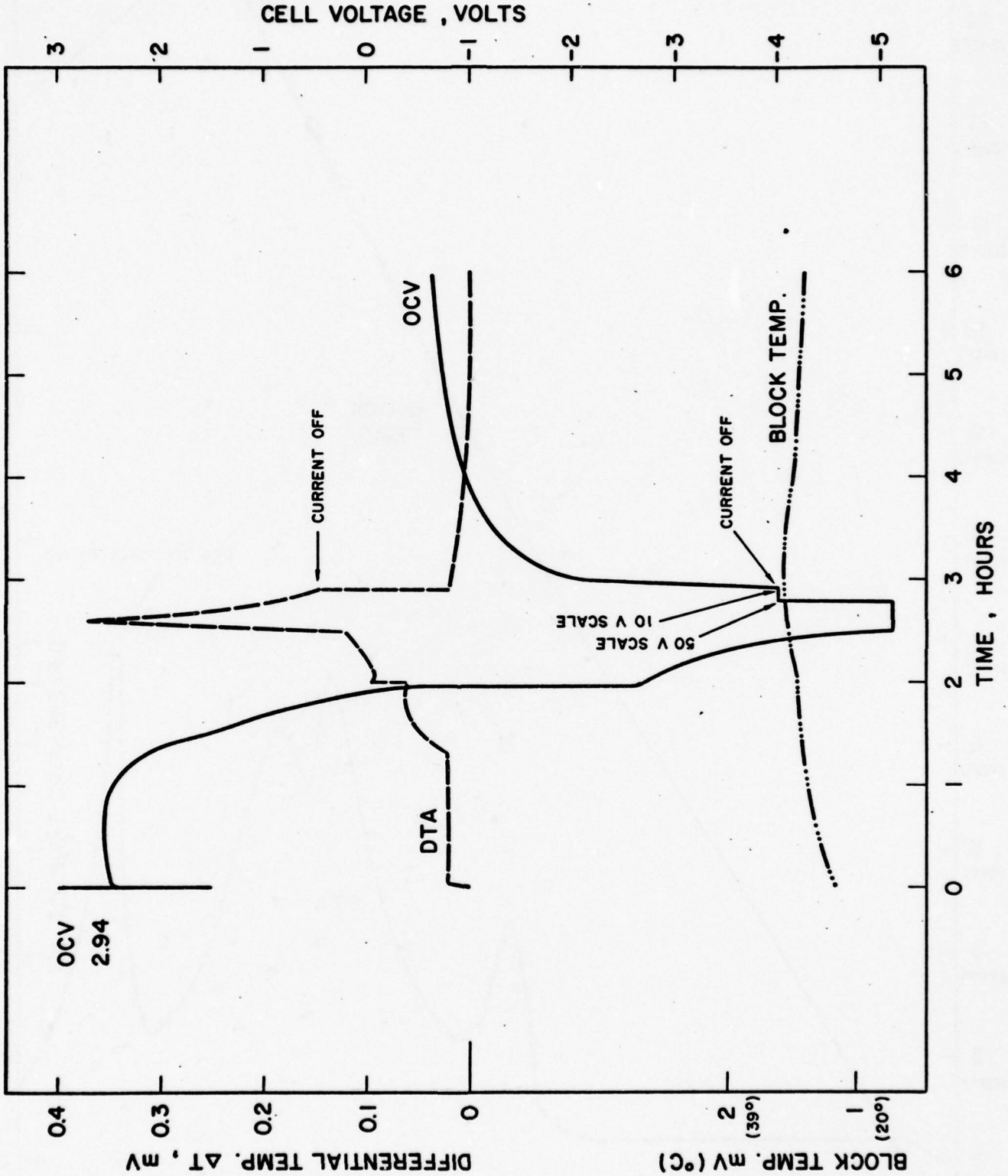

Fig. 29. Voltage, Differential Temperature and the Block Temperature Profiles of a Li/SO_2 Miniature Cell with PC in the Electrolyte During Discharge and Force-Discharge at 25°C at a Current of 90 mA.

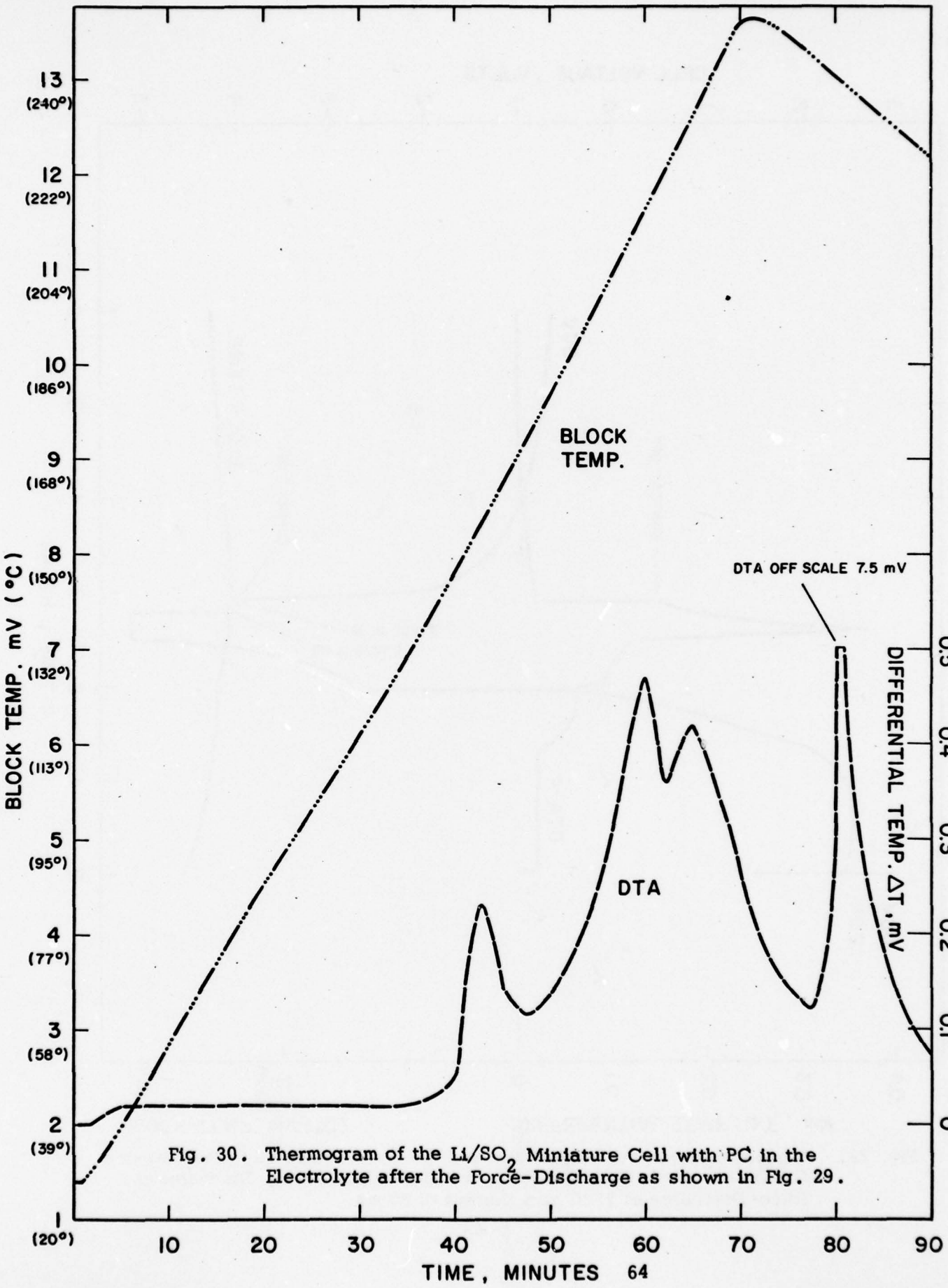

Fig. 30. Thermogram of the Li/SO_2 Miniature Cell with PC in the Electrolyte after the Force-Discharge as shown in Fig. 29.

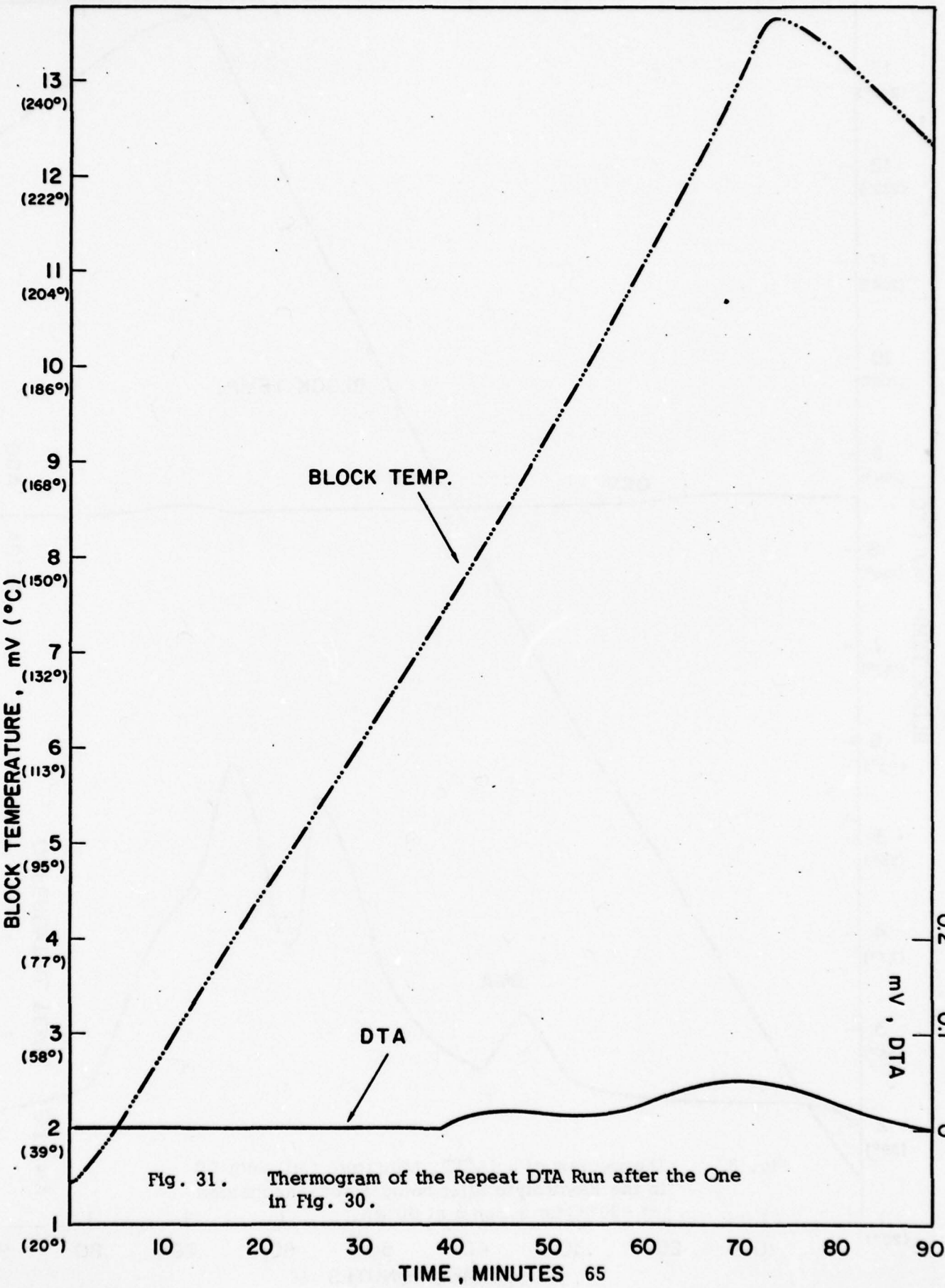

Fig. 31. Thermogram of the Repeat DTA Run after the One in Fig. 30.

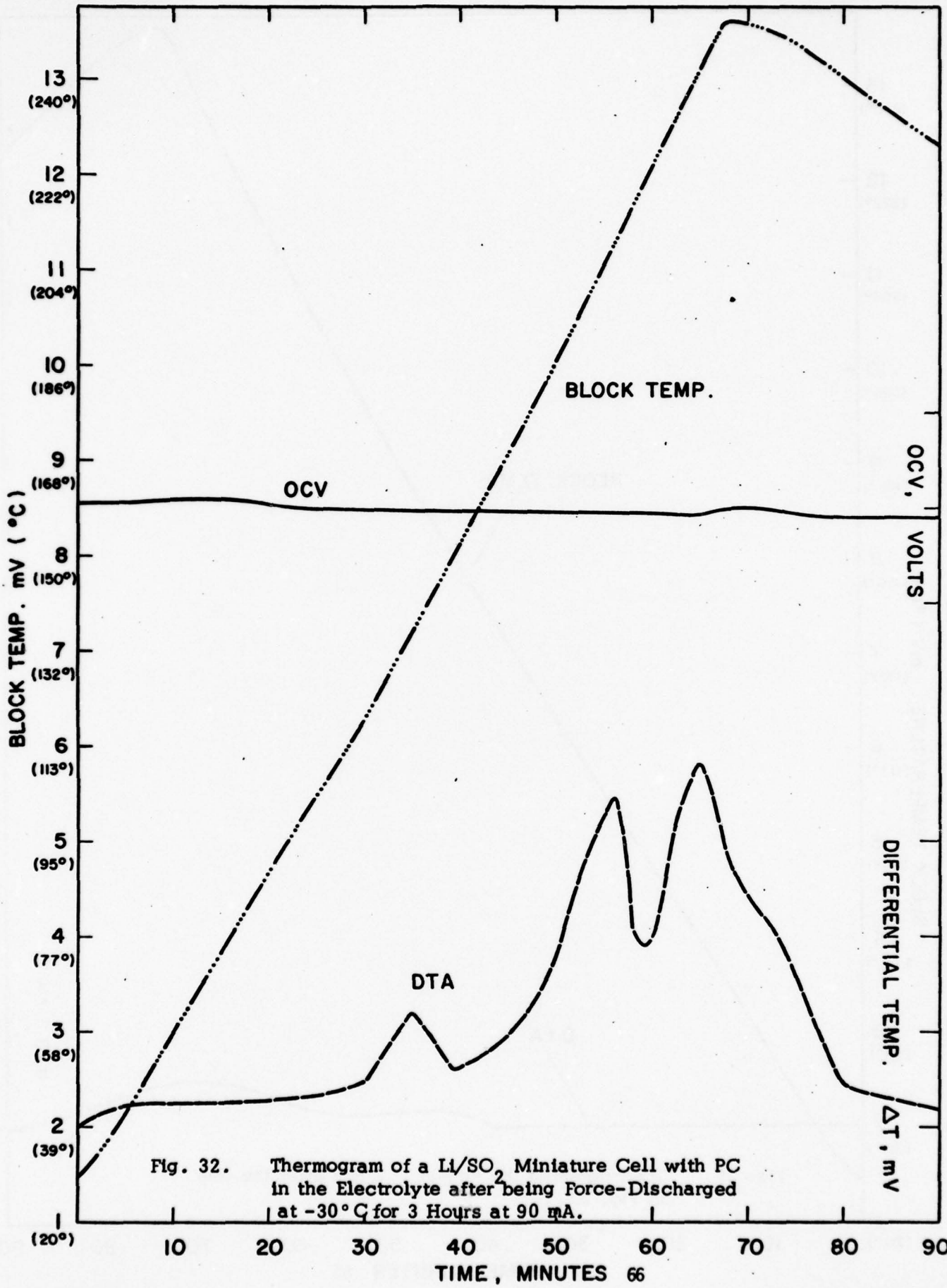

Fig. 32. Thermogram of a Li/SO_2 Miniature Cell with PC in the Electrolyte after being Force-Discharged at -30°C for 3 Hours at 90 mA.

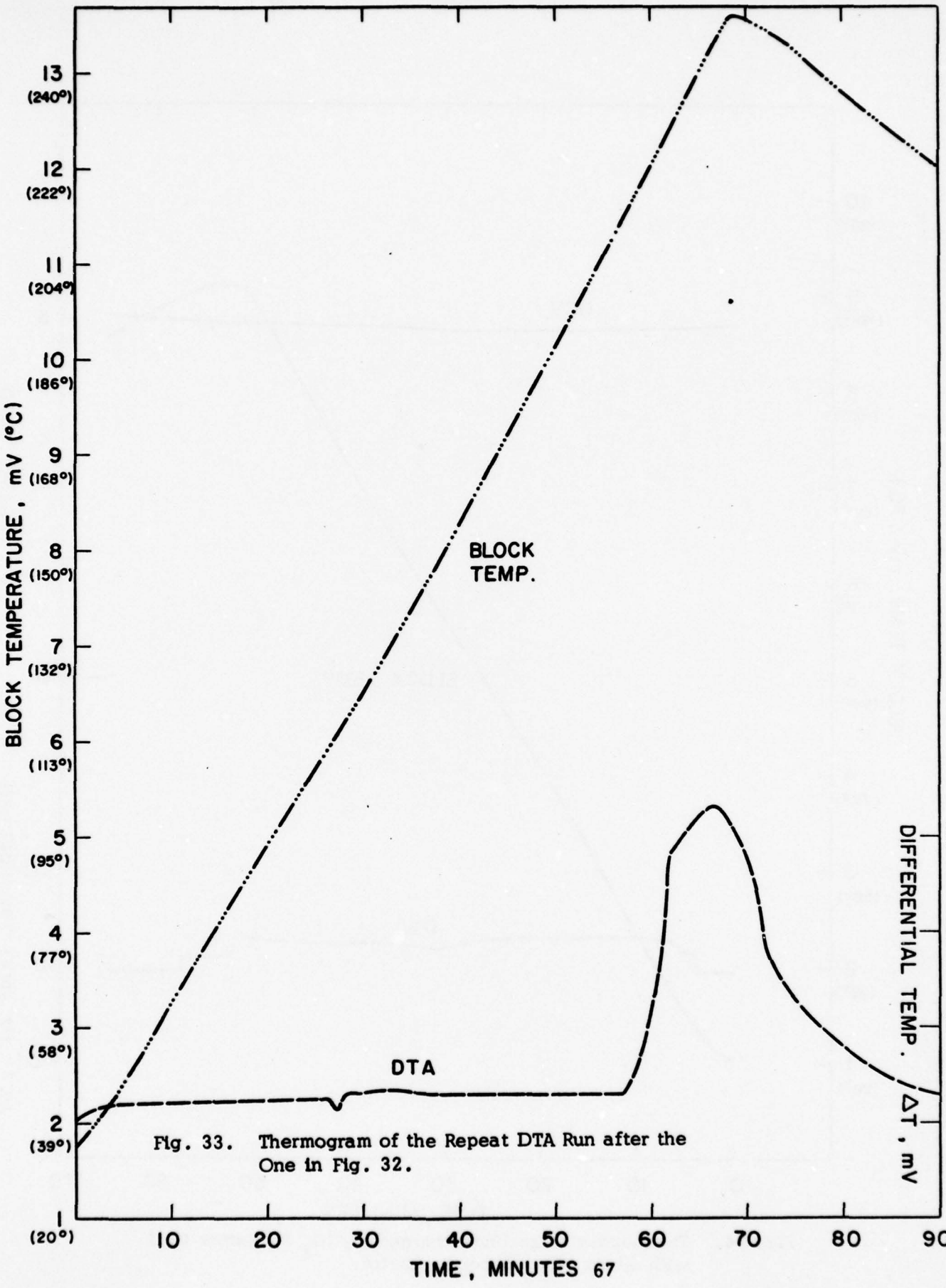

Fig. 33. Thermogram of the Repeat DTA Run after the One in Fig. 32.

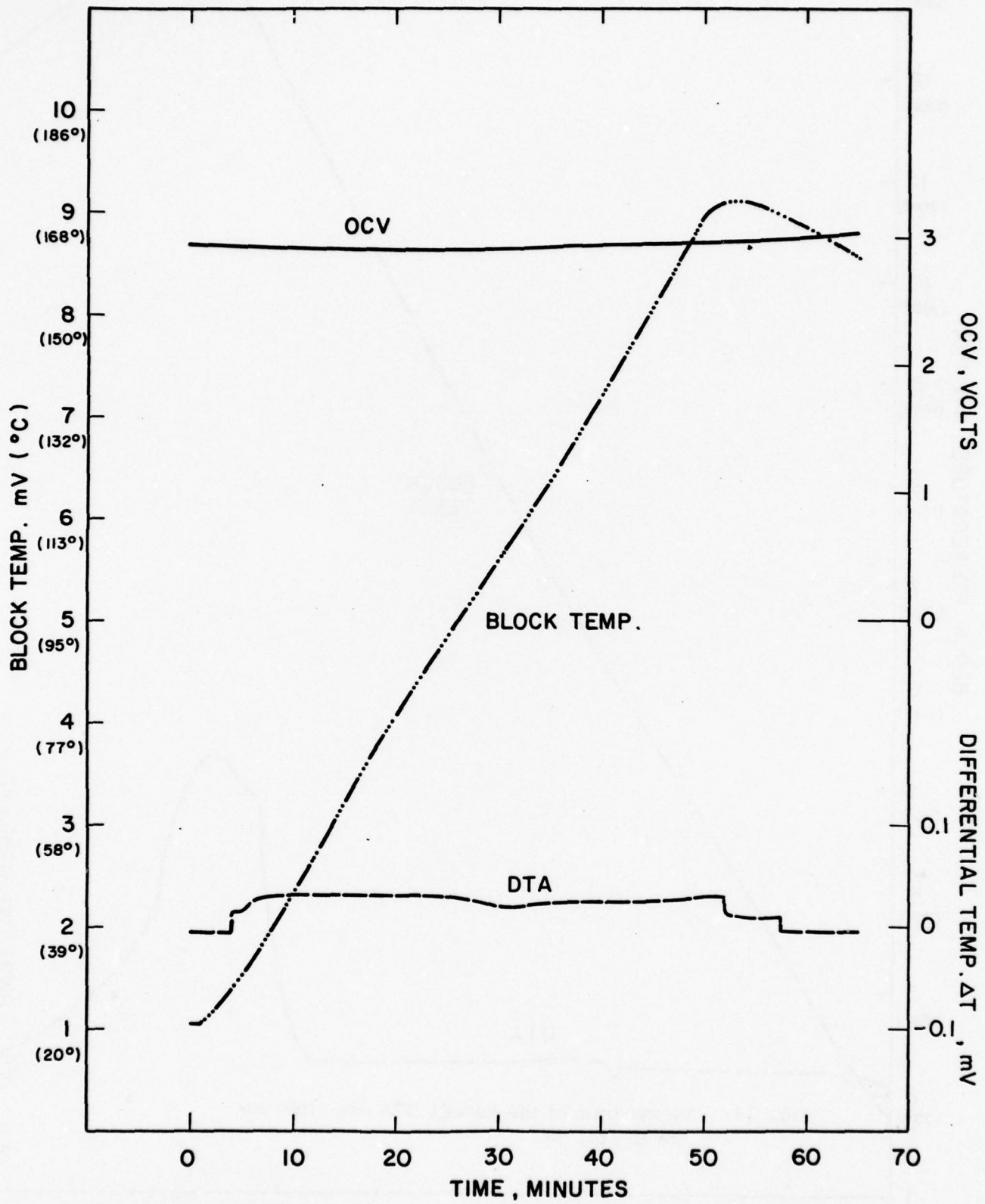

Fig. 34. Thermogram of an Undischarged Li/SO_2 Miniature Cell with Glass Filter Paper Separator.

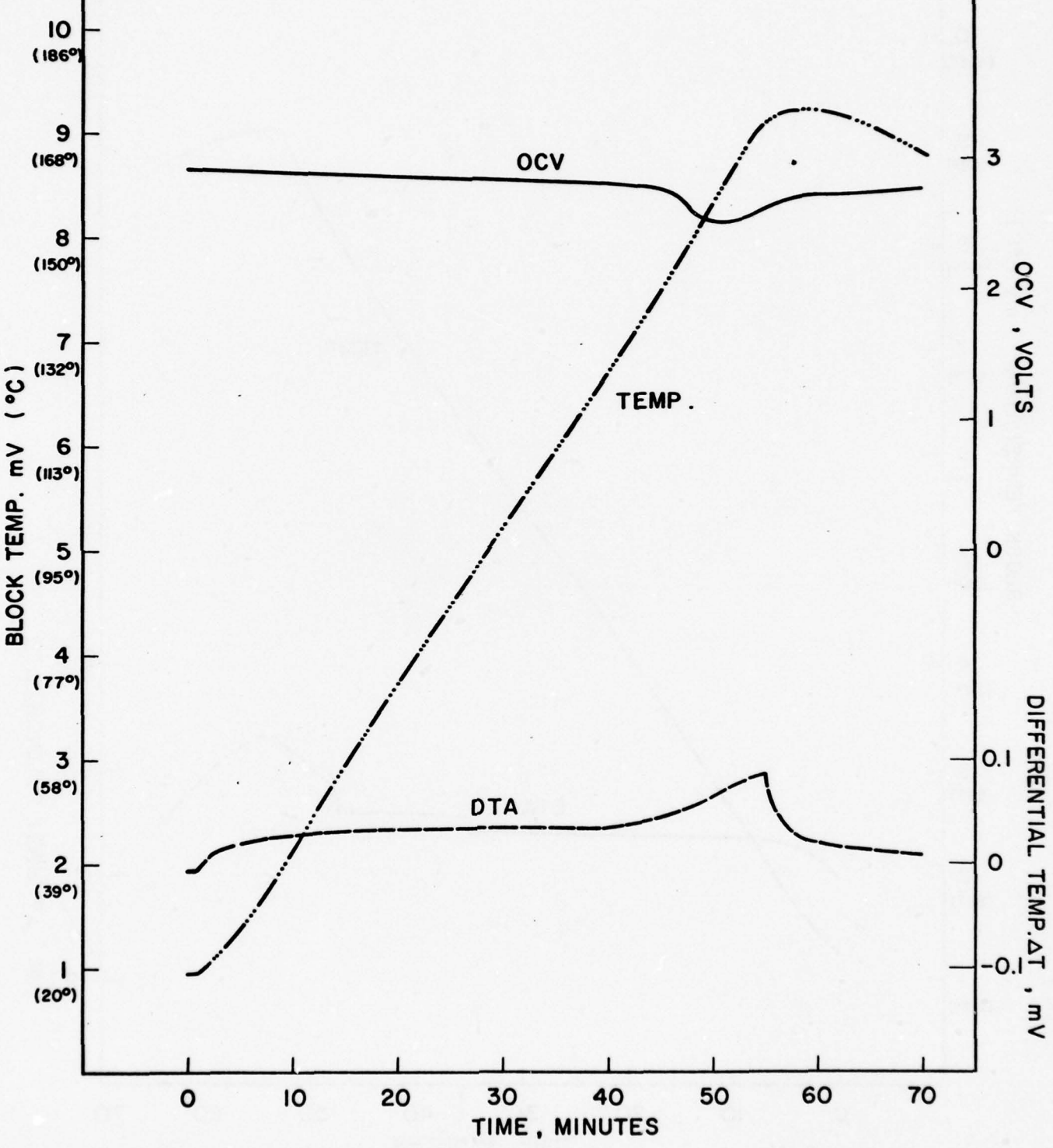

Fig. 35. Thermogram of a Discharged Li/SO_2 Miniature Cell with Glass Filter Paper Separator; Discharge Current, 10 mA; Discharge Temperature, 25°C.

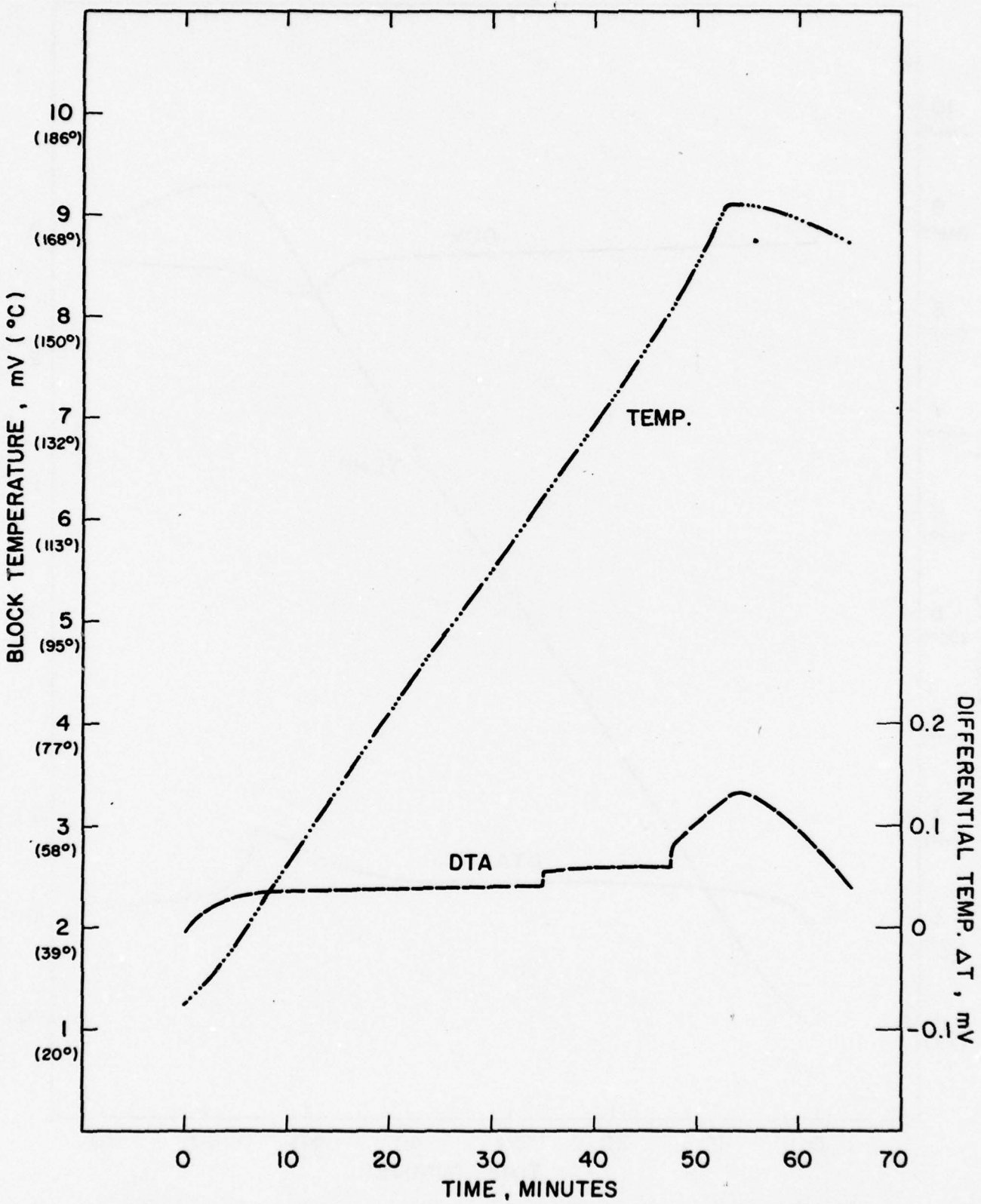

Fig. 36. Thermogram of a Li/SO_2 Miniature Cell with Glass Filter Paper Separator after being Force-Discharged at -30 °C for 3 Hours at 90 mA; Upper Limit of Temperature was 170 °C.

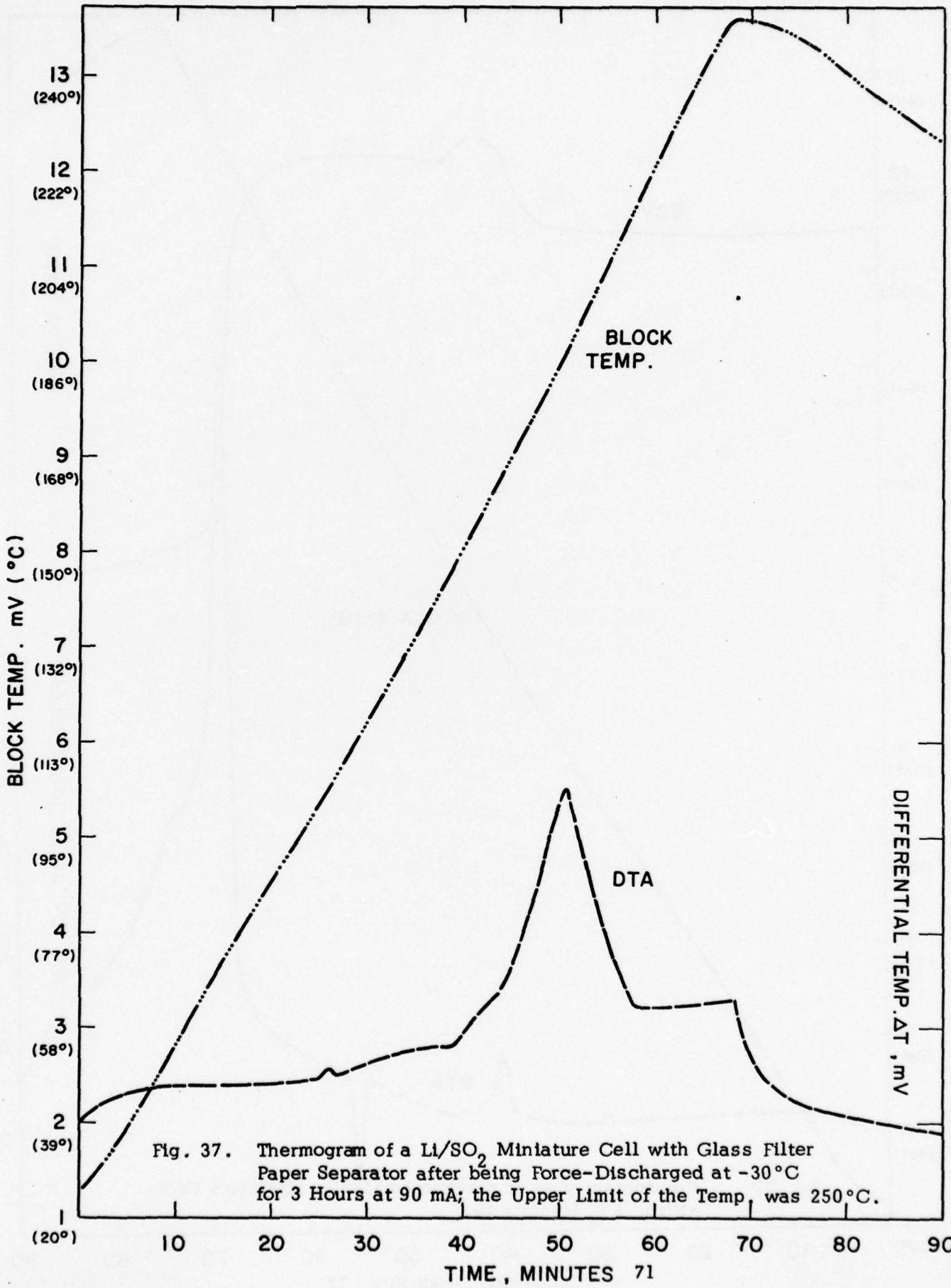

Fig. 37. Thermogram of a Li/SO_2 Miniature Cell with Glass Filter Paper Separator after being Force-Discharged at -30°C for 3 Hours at 90 mA; the Upper Limit of the Temp. was 250°C.

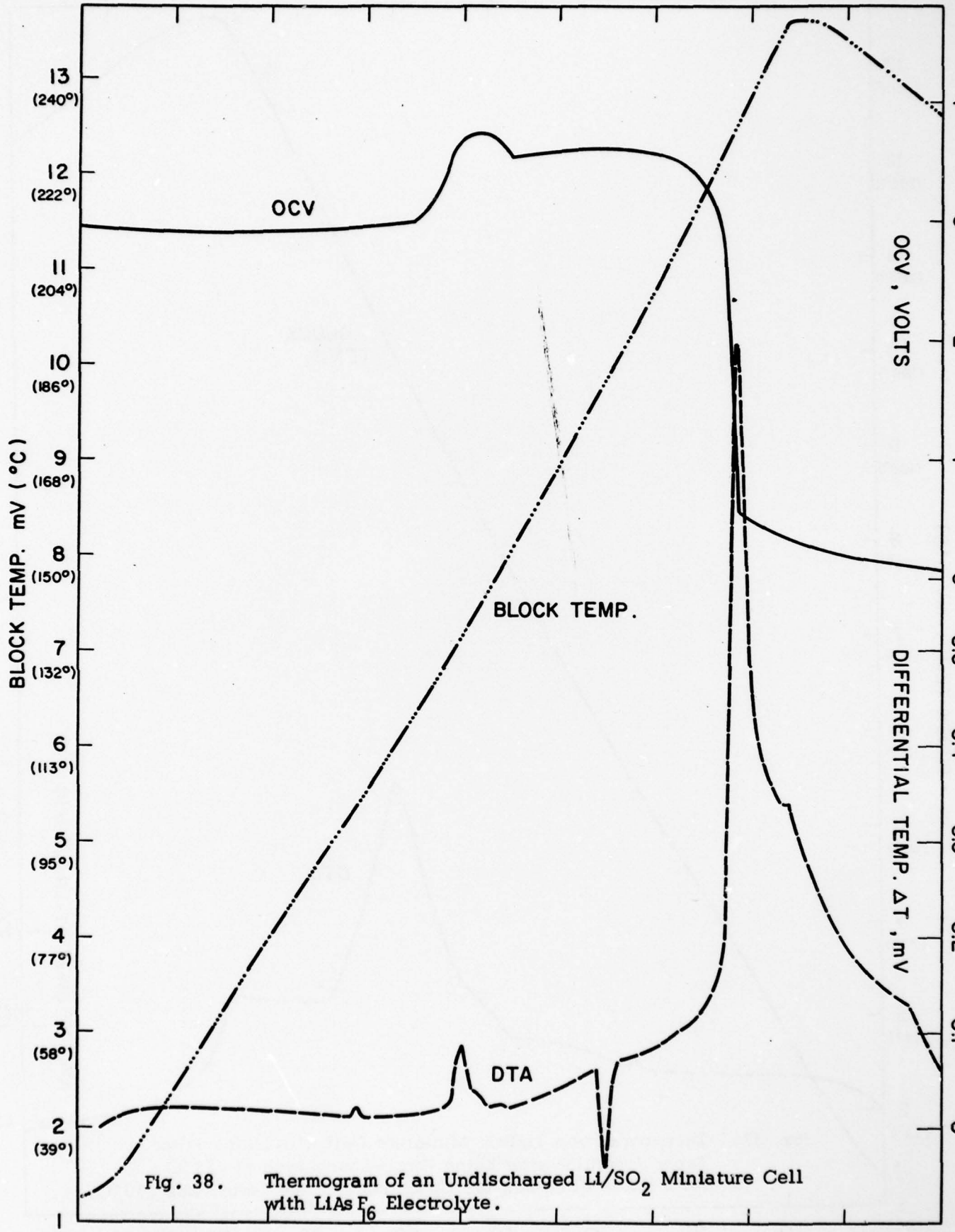

Fig. 38. Thermogram of an Undischarged Li/SO_2 Miniature Cell with $LiAsF_6$ Electrolyte.

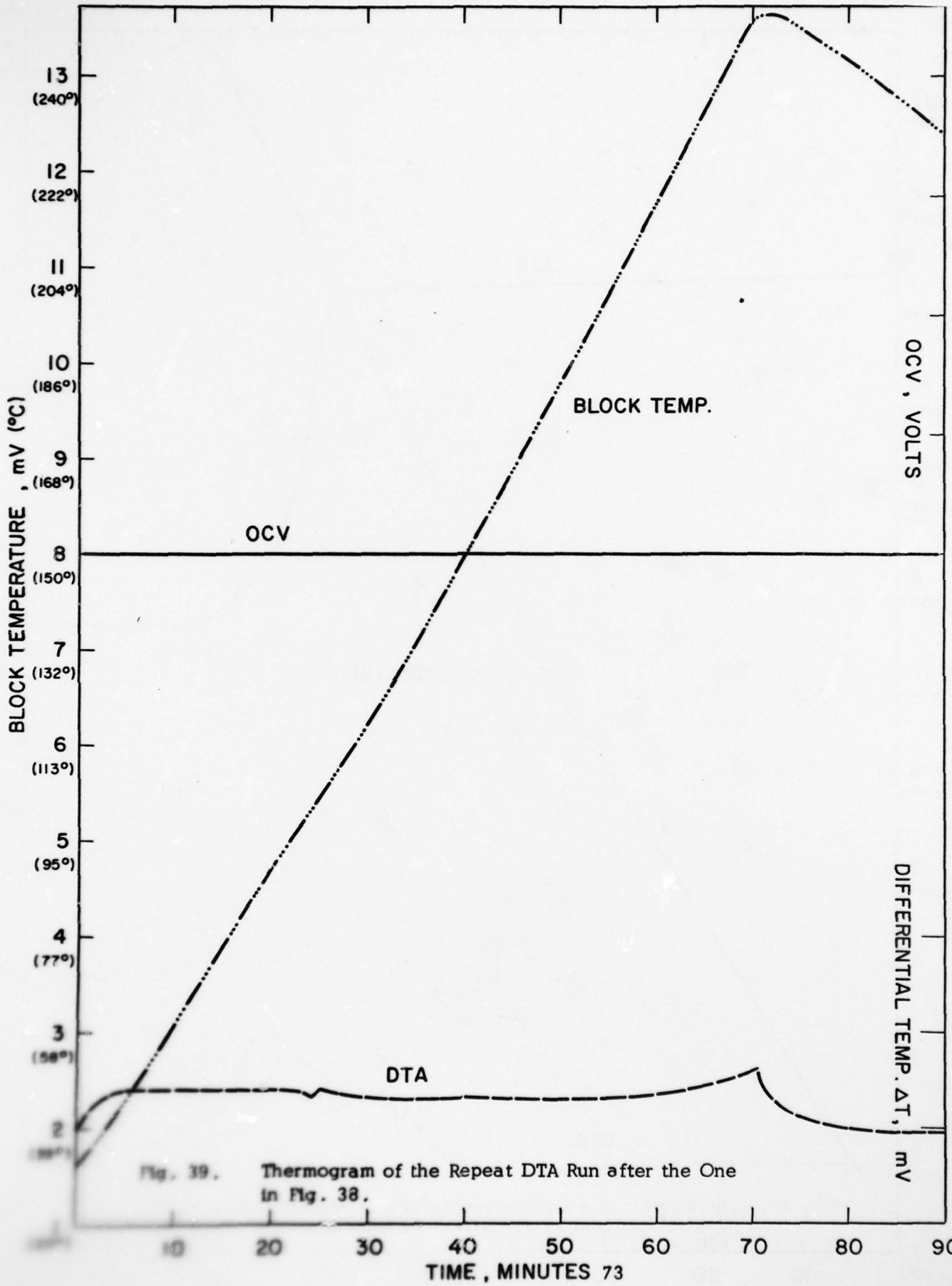

Fig. 39. Thermogram of the Repeat DTA Run after the One in Fig. 38.

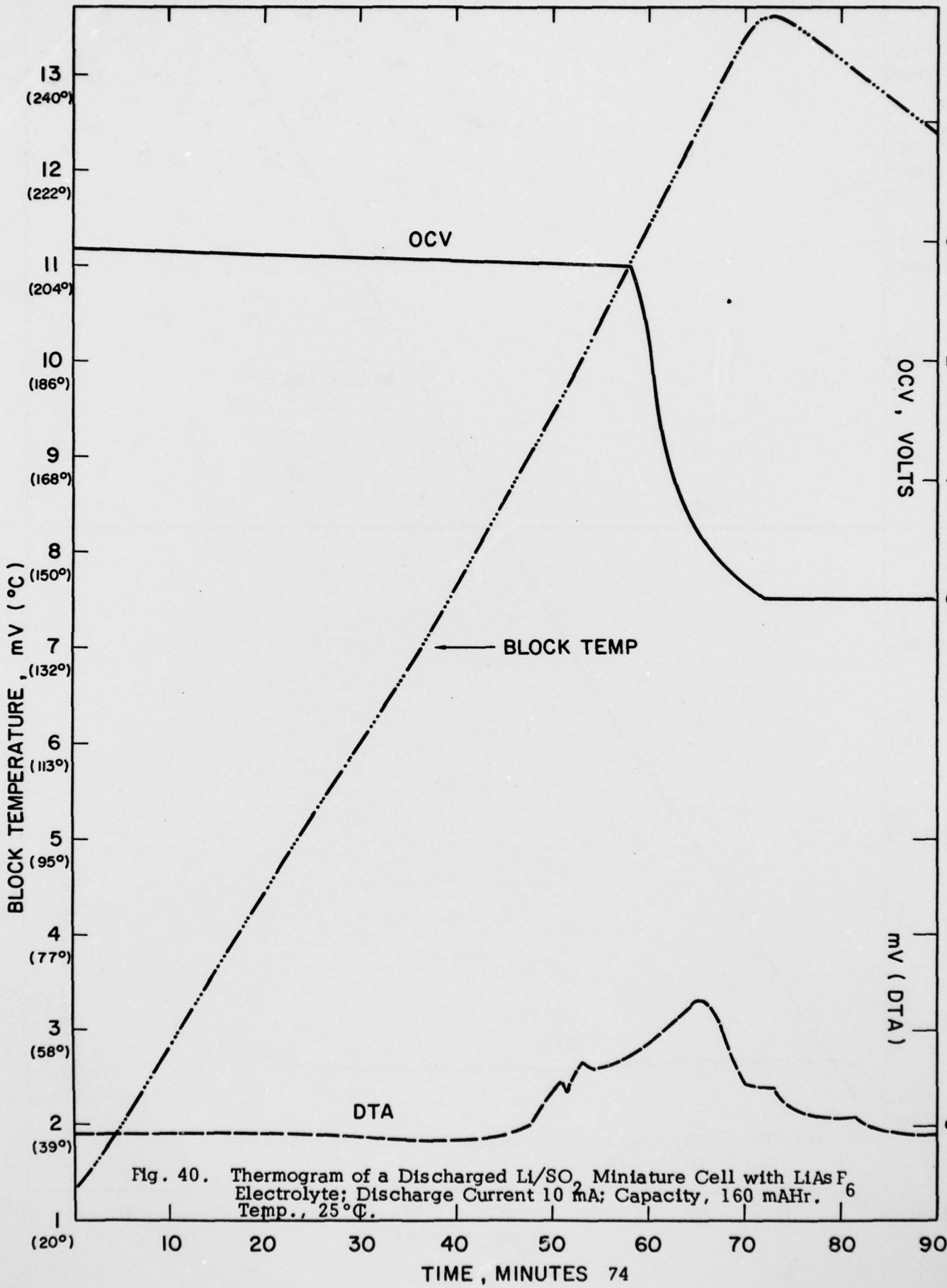

Fig. 40. Thermogram of a Discharged Li/SO_2 Miniature Cell with $LiAsF_6$ Electrolyte; Discharge Current 10 mA; Capacity, 160 mAHr. Temp., 25°C.

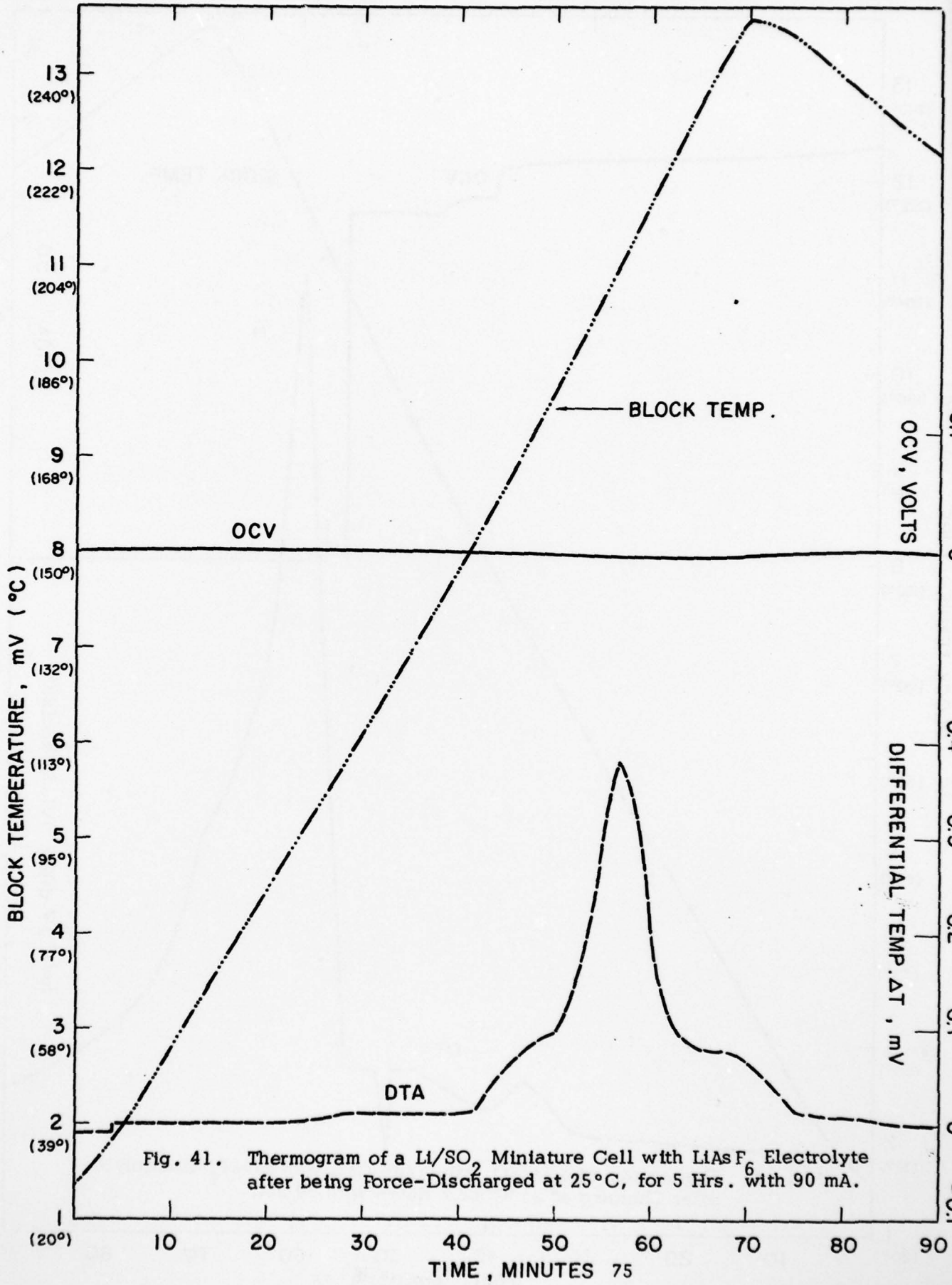

Fig. 41. Thermogram of a Li/SO_2 Miniature Cell with $LiAsF_6$ Electrolyte after being Force-Discharged at 25°C, for 5 Hrs. with 90 mA.

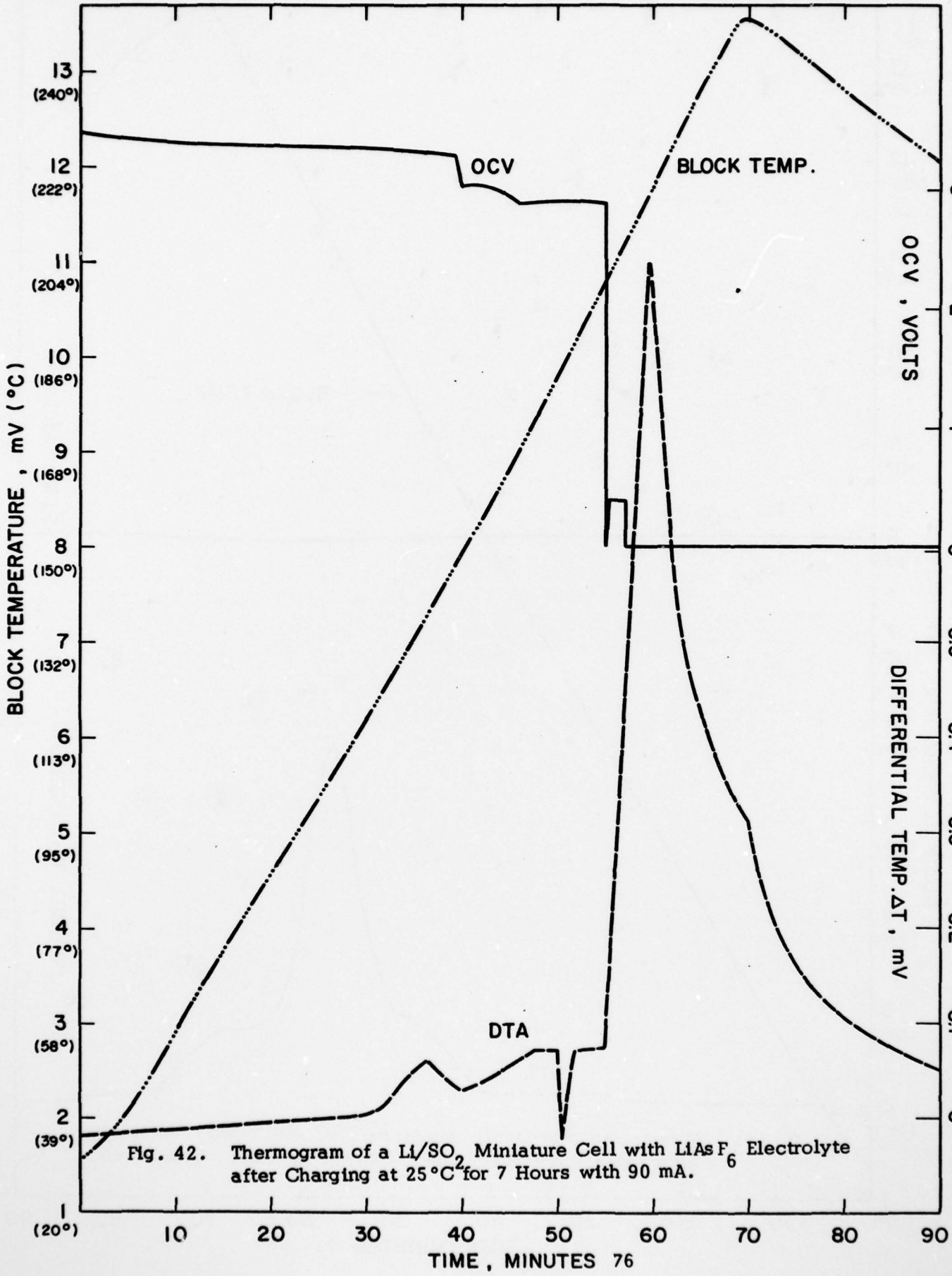

Fig. 42. Thermogram of a Li/SO_2 Miniature Cell with $LiAsF_6$ Electrolyte after Charging at 25°C for 7 Hours with 90 mA.

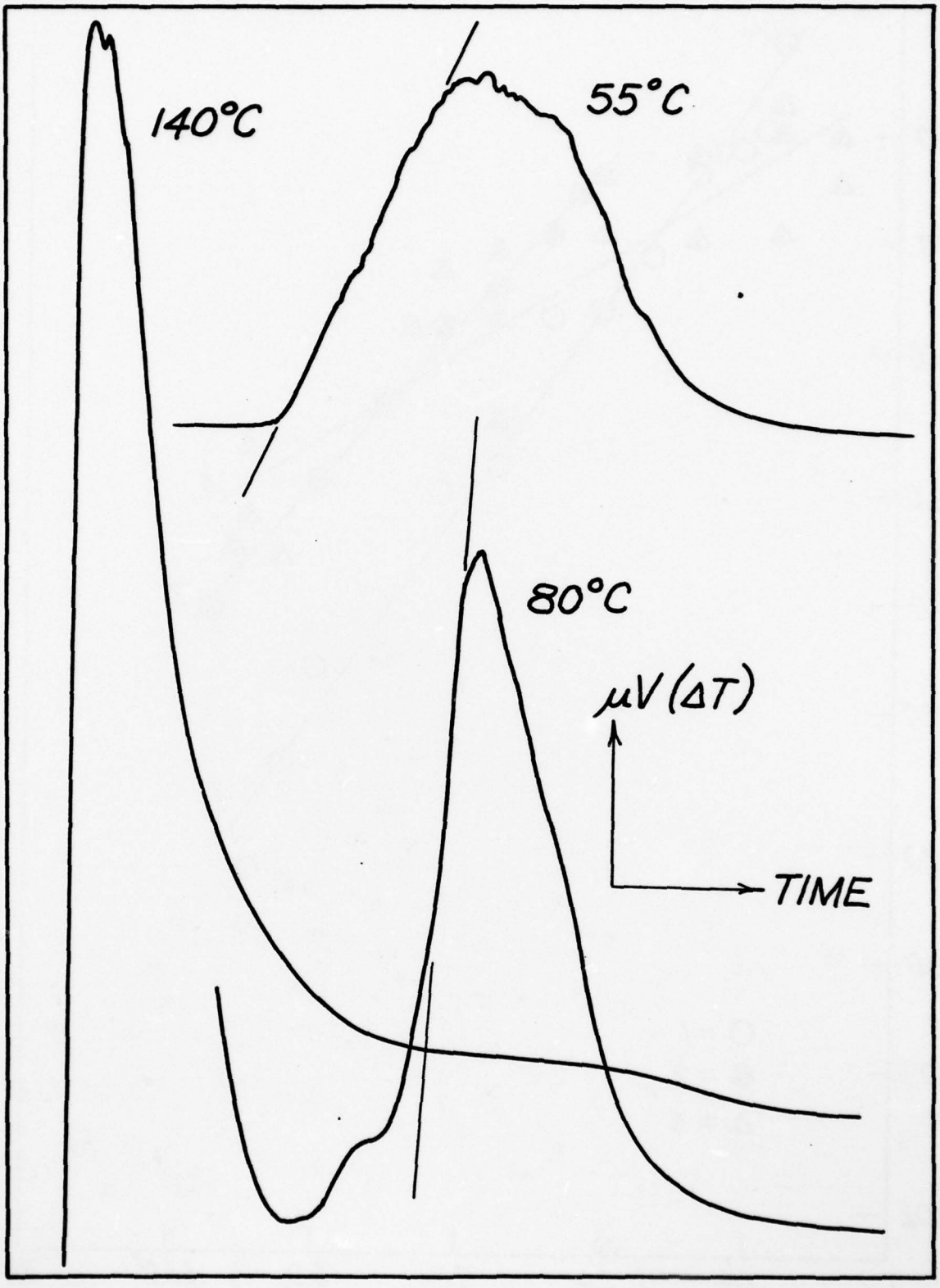

Fig. 43. Typical Isothermal DTA Thermograms of Li + AN System at Various Temperatures.

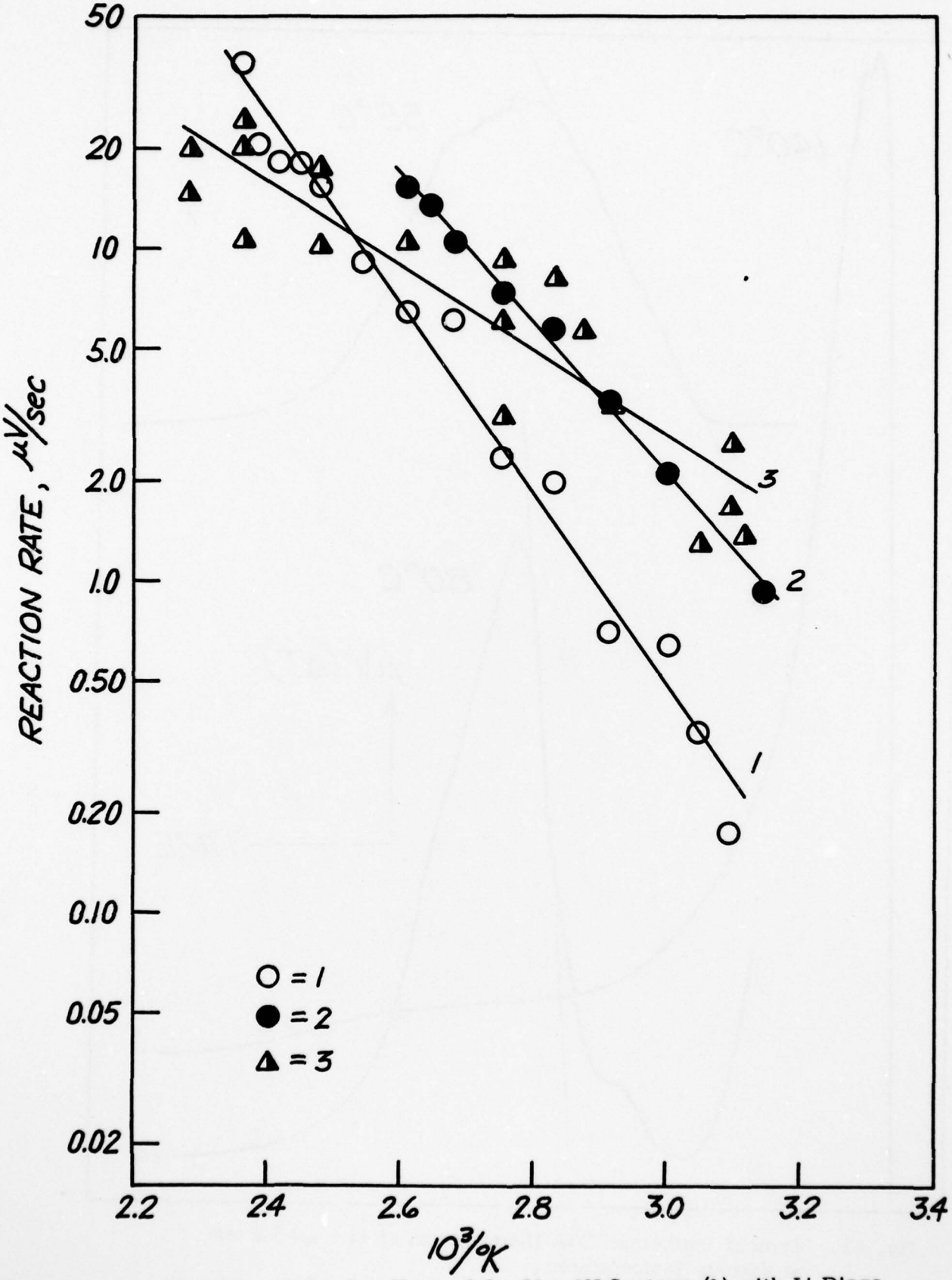

Fig. 44. Arrhenius Plots of the Li + AN System; (1) with Li Discs Aged in Dry Box, (2) Freshly Cut Li Discs (3) with 0.32 M LiBr in AN.

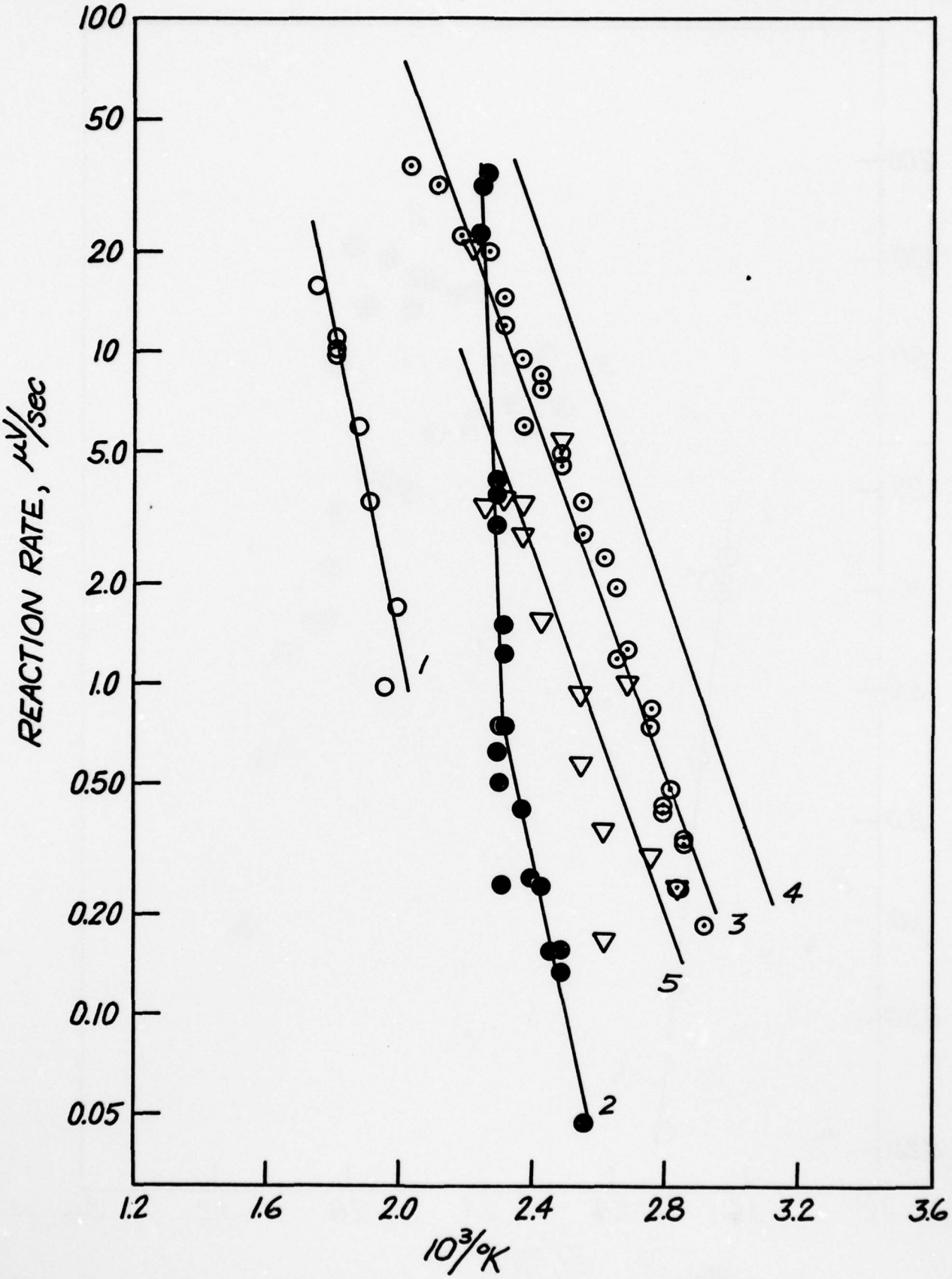

Fig. 45. Arrhenius Plots of the Li + AN + PC System; (1) 0% AN, (2) 50% AN, (3) 80% & 95% AN, (4) 100% AN, and (5) 0% PC and 3% SO_2. 79

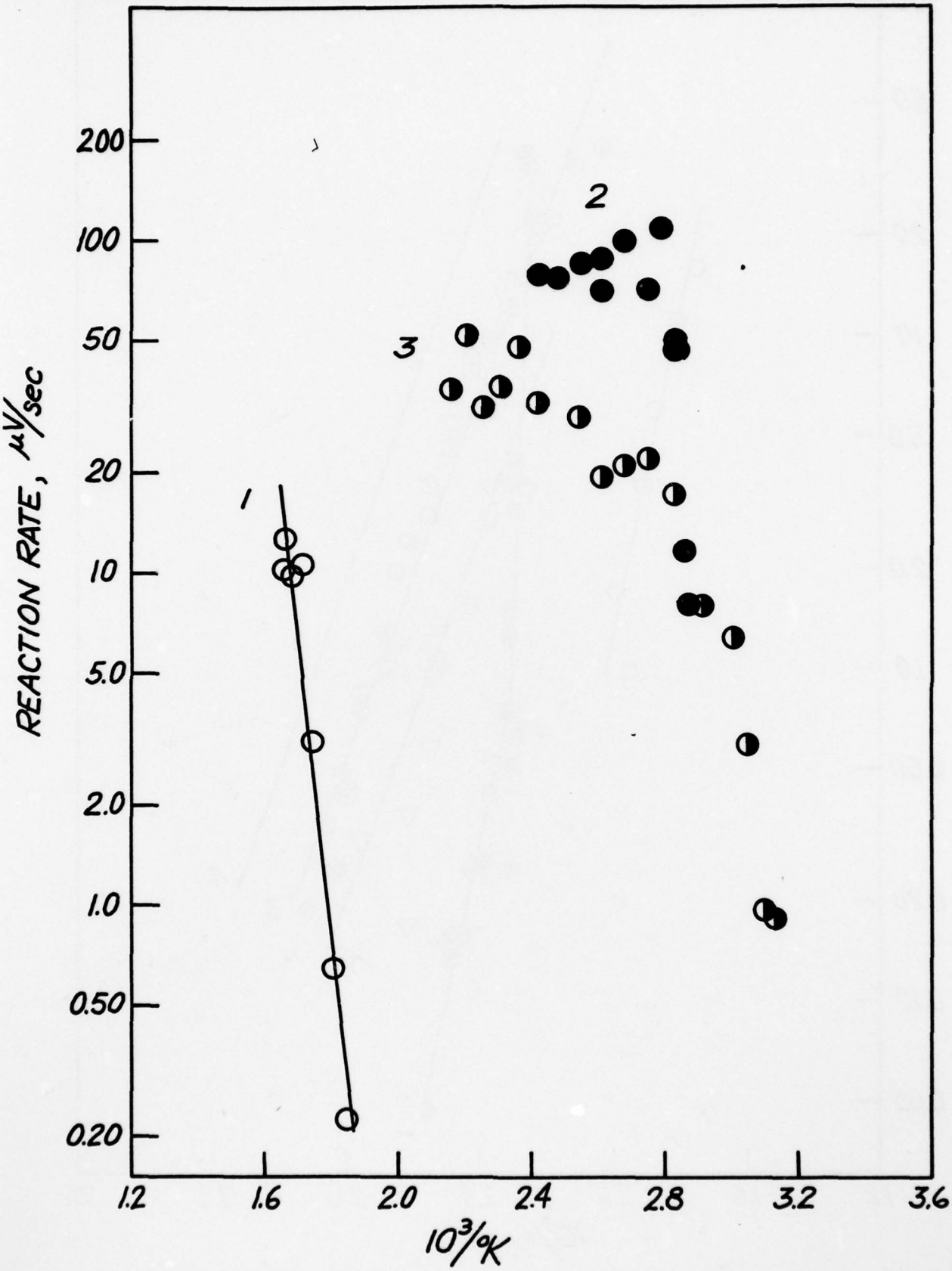

Fig. 46. Arrhenius Plots of Li + AN + MF System; (1) 0% AN, (2) 80% AN, and (3) 95% AN.

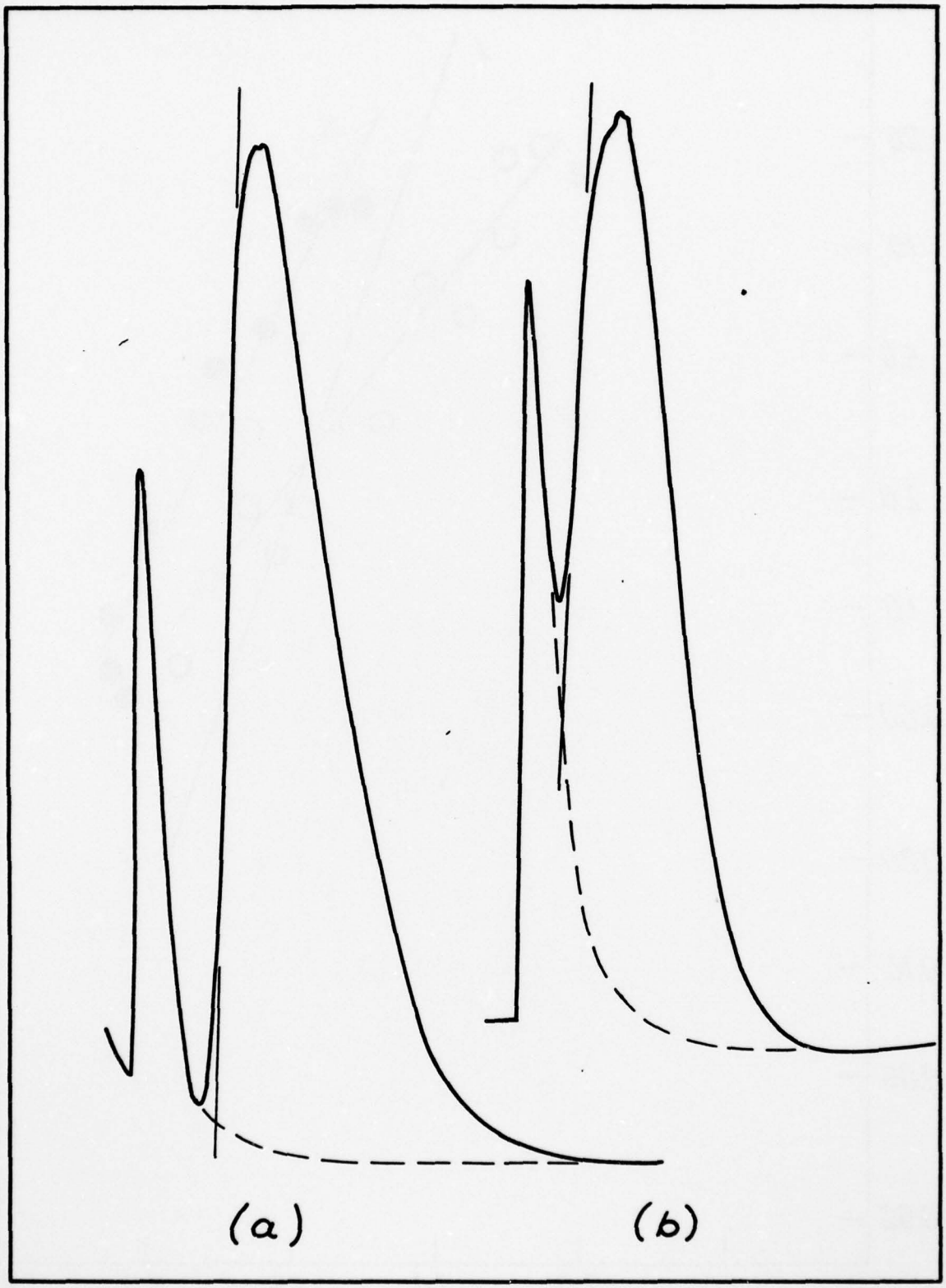

Fig. 47. Isothermal DTA Thermograms (a) Normal Runs, (b) for Reactions with Short Induction Periods as with Li + AN/MF (80/20).

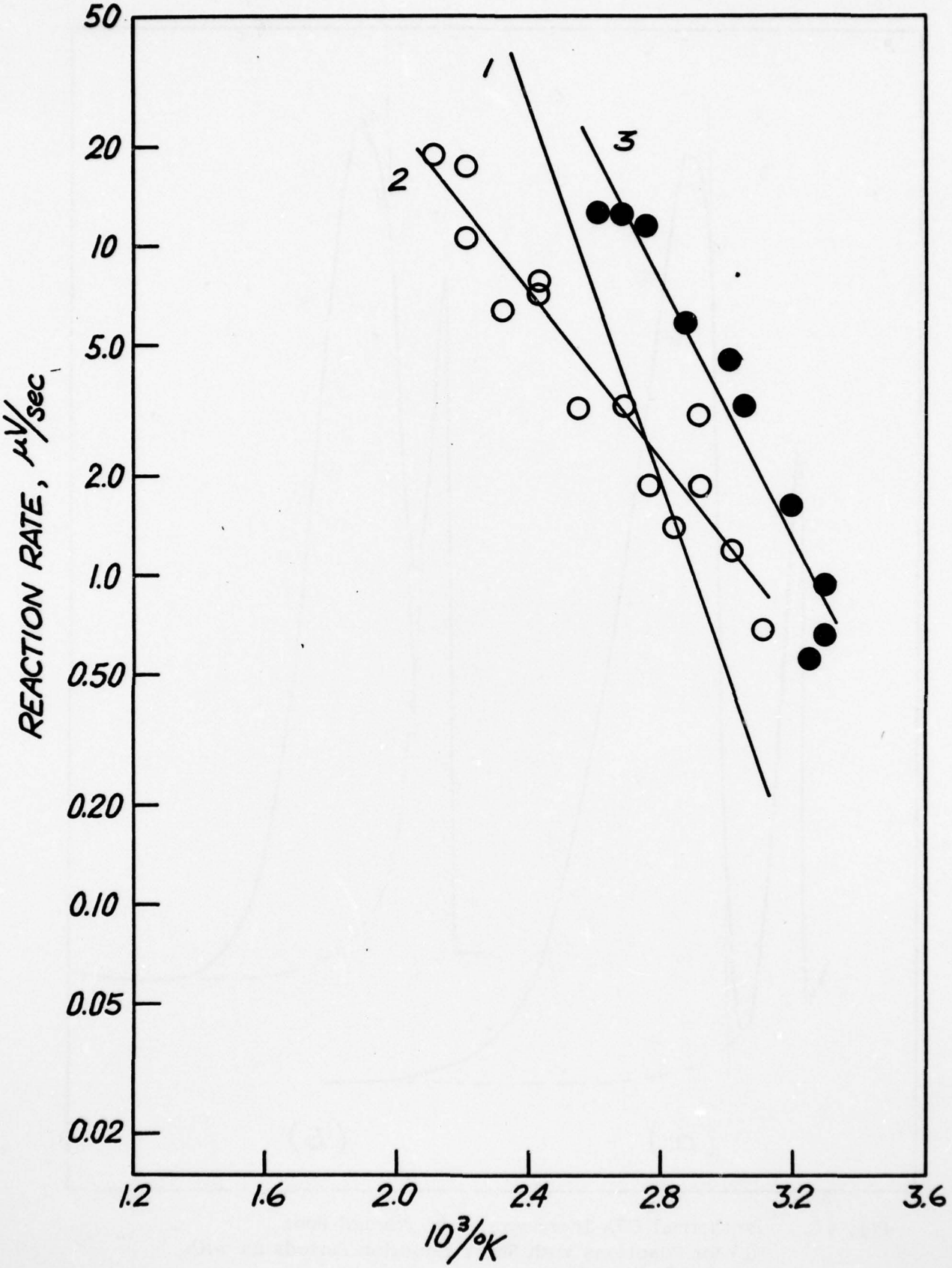

Fig. 48. Arrhenius Plots of Li + AN + DME System; (1) 0% DME, (2) 5% DME, and (3) 20% DME.

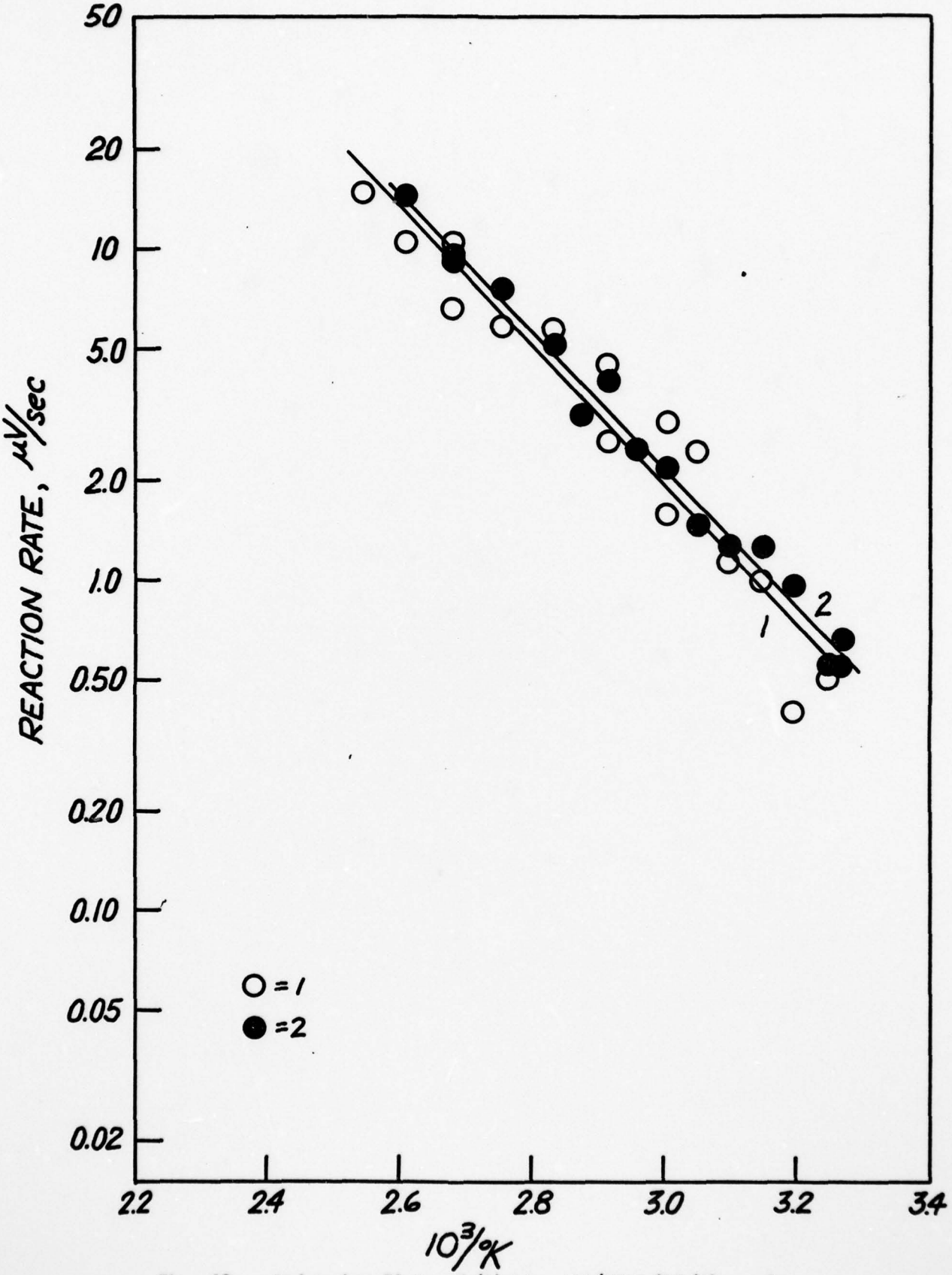

Fig. 49. Arrhenius Plots of (1) Li + AN/THF (95/5), and (2) Li + AN/DG (95/5) Systems.

DISTRIBUTION LIST

Defense Documentation Center (12)
Attn: DDC-TCA
Cameron Station (Bldg 5)
Alexandria, VA 22314

Commander (1)
Naval Electronics Laboratory Center
Attn: Library
San Diego, CA 92152

CDR, Naval Surface Weapons Center (1)
White Oak Laboratory
Attn: Library, Code WX-21
Silver Spring, MD 20910

Commandant, Marine Corps (2)
HQ, US Marine Corps
Attn: Code LMC
Washington, DC 20380

Rome Air Development Center (1)
Attn: Documents Library (TILD)
Griffiss AFB, NY 13441

AFGL/SuLL (1)
S-29
Hancom AFB
Bedford, MA 01731

HQDA (DAMA-ARZ-D) (1)
Dr. F. D. Verderame
Washington, DC 20310

CDR, Harry Diamond Laboratories (1)
Attn: Library
2800 Powder Mill Road
Adelphi, MD 20783

Director, US Army Material Systems (1)
Analysis Activity
Attn: DRXSY-MP
Aberdeen Proving Ground, MD 21105

CDR, US Army Research Office (1)
Attn: DRXRO-IP

PO Box 12211
Research Triangle Park, NC 07709

CDR, US Army Signals Warfare Lab (1)
Attn: DELSW-OS
Vent Hill
Forms Station
Warrentown, VA 22186

Commander
US Army Mobility EQP Res & (1)
Dev CMD
Attn: DRXFB-R
Fort Belvoir, VA 22060

Commander
US Army Electronics R&D Command
Fort Monmouth, NJ 07703

DELET-DD	(1)
DELET-DT	(2)
DELET-P	(1)
DELSD-L (Tech Lib)	(1)
DELET-PR (Sol Gilman)	(30)
DELSD-L-S	(2)
USMC-LNO	(1)

NASA Scientific & Tech Info (1)
Facility
Baltimore/Washington Intl Airport
P. O. Box 8757, MD 21240

Distribution List Continued

Transportation Systems Center (1)
Kendall Square
Cambridge, MA 02142
Attn: Dr. Norman Rosenberg

GTE Laboratories, Inc. (1)
40 Sylvan Road
Waltham, MA 02154

Foote Mineral Company (1)
Route 100
Exton, PA 19341
Attn: Dr. H. Grady

Honeywell, Inc. (1)
104 Rock Road
Horsham, PA 19044
Attn: C. Richard Walk

Sanders Associates, Inc. (1)
Sonobuoy Division
95 Canal Street
Nashua, N.H. 03060
Attn: Mr. David Dwyer

Eagle-Picher Industries, Inc. (1)
Electronics Division
Attn: Mr. Robert L. Higgins
P. O. Box 47
Joplin, Missouri 64801

Yardney Electric Company (1)
82 Mechanic Street
Pawcatuck, CT 02891
Attn: Mr. William E. Ryder

Exxon Research & Engineering Co. (1)
Corporate Research Laboratory
Linden, N.J. 07036
Attn: Dr. R. Hamlen

Argonne National Laboratories (1)
9700 South Cass
Argonne, IL 60439
Attn: Dr. E. C. Gay

GTE Sylvania, Inc. (1)
77 A Street
Needham Heights, MA 02194
Attn: Mr Richard Pabst

General Motors Corp. (1)
Research Laboratories
General Motors Technical Center
12 Mile and Mounds Roads
Warren, MI 48090
Attn: Dr. J. L. Hartman

Union Carbide Corporation (1)
Parma Research Center
P. O. Box 6116
Cleveland, OH 44101

P. R. Mallory & Co. Inc. (1)
South Broadway
Tarrytown, N.Y. 10591
Attn: J. Dalfonso

North American Rockwell Corp. (1)
Atomics International Division
Box 309
Canoga Park, CA 91304
Attn: Dr. L. Heredy

General Electric Research & (1)
Development Center
P. O. Box 8
Schenectady, N.Y. 12301
Attn: Dr. Stefan Mitoff

University of California (1)
Department of Science & Research
Santa Barbara, CA 93100
Attn: Dr. J. Kennedy

The Electric Storage Battery Co. (1)
Carl F. Norburg Research Center
19 W. College Avenue
Yardley, PA 19067
Attn: Dr. A. Salkind

Gulton Industries, Inc. (1)
Metuchen, N.J. 08840
Attn: Mr. S. Charlip

Electrochimica (1)
2485 Charleston Road
Mountain View, CA 94040
Attn: Dr. Eisenberg

Distribution List Continued

Dr. Hugh Barger (1)
P. O. Box 2232
Davidson, N.C. 28036

Energy Storage & Conversion Dept. (1)
T.R.W. Systems
One Space Park
Redondo Beach, CA 09278
Attn: Dr. H. P. Silverman

Sanders Associates, Inc. (1)
24 Simon Street
Mail Stop NSI-2208
Nashua, N.H. 03060
Attn: J. Marshali

Power Conversion, Inc. (1)
70 MacQuesten Pkwy
Mount Vernon, N.Y. 10550
Attn: Stuart Chodosh

Dr. D. Pouli (1)
Portfolio Manager
Hooker Chemicals & Plastics Corp.
M.P.O. Box 8
Niagara Falls, N.Y. 14302

Dr. Leonard Nanis (1)
G207
S.R.I.
Menlo Park, CA 94025

Dr. J. J. Auborn, Rm. 1A-317 (1)
Bell Laboratories
600 Mountain Avenue
Murray Hill, N.J. 07974

Frank Murphy/SB331 (1)
Naval Underwater Systems Center
Newport Laboratory
Newport, R.I. 02840

NASA Lewis Research Center (1)
Mail Stop 6-1
2100 Brookpark Road
Cleveland, OH 44101
Attn: Dr. Stuart Fordyce

Mr. Joe McCartney (1)
Naval Undersea Center
Code 608
San Diego, CA 92132

EIC, Inc. (1)
Attn: S. B. Brummer
Newton, MA 02158

Altus Corp. (1)
Attn: Douglas Glader
440 Page Mill Road
Palo Alto, CA 94306

J. Bene MS488 (1)
NASA Langley Research Center
Hampton, VA 23665

Mr. Eddie T. Seo (1)
Research and Development Division
The Gates Rubber Co.
999 S. Broadway
Denver, Colorado 80217

Mr. Sidney Gross (1)
Mail Stop 8C-62
Boeing Aerospace Company
P. O. Box 3999
Seattle, WA 98124

AD-A064 977 MALLORY (P R) AND CO INC BURLINGTON MASS LAB FOR PH--ETC F/G 10/3
ANALYSIS OF PRESSURE PRODUCING REACTIONS IN LITHIUM-SULFUR DIOX--ETC(U)
FEB 79 A N DEY, R W HOLMES DAAB07-77-C-0472

UNCLASSIFIED DELET-TR-77-0472-1 NL

2 OF 2
AD
A064 977

END
DATE
FILMED
4 -79
DDC

Mr. Donald
AF Aero Prop
Attn: AFAPL
Wright-Patt

Mr. Richard
Department
Hqs., US M
Code LMC 4
Washington,

Commander
Harry Diamo
Attn: DELHI
2800 Powder
Adelphi, MD

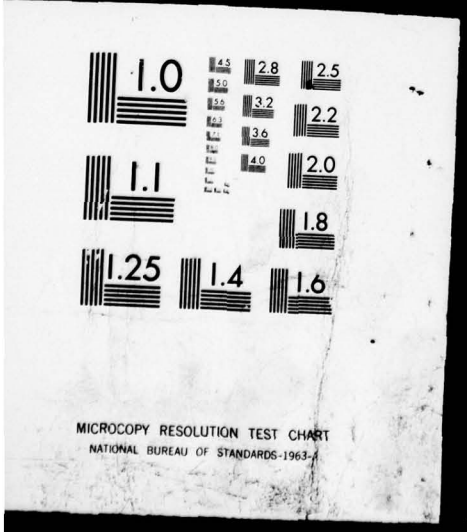

SUPPLEMENT TO DISTRIBUTION LIST

Other Recipients

Mr. Donald Mortel (1)
AF Aero Propulsion Lab.
Attn: AFAPL-POE-1
Wright-Patterson AFB, Ohio 45433

Mr. Richard E. Oderwald (1)
Department of the Navy
Hqs., US Marine Corps
Code LMC 4
Washington, DC 20380

Commander (1)
Harry Diamond Laboratories
Attn: DELHD-RDD (Mr. A. Benderly)
2800 Powder Mill Road
Adelphi, MD 20783